

FACULTY OF SCIENCE AND TECHNOLOGY

MASTER'S THESIS

Study program/Specialization:

M.Sc. Petroleum Geoscience

Spring Semester, 2019

Confidential

Author:

Ville August Aarseth



(Writer's signature)

University supervisor: **Professor Nestor Cardozo**

Company supervisors: **Hugh Anderson and Rodmar Ravnås**

Title of master's thesis:

Salt tectonics on the Cod Terrace and Sørvestlandet High, Central North Sea

Credits (ECTS): 30

Key words:

- Salt tectonics
- 2D Restorations
- Structural evolution
- Post-Jurassic structural rejuvenation

Number of Pages: 94
+ enclosures: 15 Pages

Stavanger, 15/06/2019

Copyright
by
Ville August Aarseth
2019

Salt tectonics on the Cod Terrace and Sørvestlandet High, Central North Sea

By

Ville August Aarseth

MSc Thesis

Presented to the Faculty of Science and Technology

University of Stavanger

2019

Acknowledgements

This thesis has been carried out at the Department of Energy Resources, University of Stavanger, and marks the completion of a Master`s degree in Petroleum Geosciences.

I would like to express my gratitude to my university supervisor, Nestor Cardozo, for providing valuable feedback and discussions, both during the thesis and my studies. I thank my second supervisor, Rodmar Ravnås, for helping me define the thesis problem and reflect on my seismic interpretations. Also, a special thanks to Luis Alberto Rojo, for introducing me to salt tectonics, which led me to this thesis.

I would like to thank Anders Rosslund for giving me the opportunity to collaborate with AkerBP this thesis semester. At AkerBP, I especially would like to thank my company supervisor, Hugh Anderson, who guided me with the restorations and was a great person to discuss challenges throughout the thesis. Also, I thank Petroleum Geo-Services (PGS) for their seismic data.

Last but not least, I would like to thank all of my fellow students, friends, family and girlfriend for their support during the last 5 years.

Salt tectonics on the Cod Terrace and Sørvestlandet High, Central North Sea

Ville August Aarseth^{1,*} Nestor Cardozo^{1,*} Hugh Anderson^{2,*} Rodmar Ravnås^{2,*}

1: Department of Energy Resources, University of Stavanger, 4036 Stavanger, Norway

2: AkerBP, Jåttåvågveien 10, 4020 Stavanger, Norway

Abstract

Four high- to moderate-quality 3D seismic surveys and public well data were used to define the structural framework and understand the Mesozoic and Cenozoic structural evolution of the salt diapirs on the Cod Terrace and the Sørvestlandet High. The salt is part of the Late Permian Zechstein Group, and is composed of mobile halite and less mobile anhydrites, carbonates and siliciclastics. Structural restorations of four salt structures on the Cod Terrace and Sørvestlandet High are used in order to understand their development. The results are broadly consistent with the “pod-interpod” model, where Late Jurassic extension led to diapir collapse, generating sediment accommodation above the diapirs. However, this does not apply to the evolution of all diapirs in the area, nor does it include Cenozoic salt remobilization. Based on their present-day geometries and associated sediment growth, the studied diapirs are classified as: buried diapirs; collapsed diapirs; reactivated diapirs; salt walls and rollers; and salt stocks. The collapsed and reactivated diapirs on the Cod Terrace and Sørvestlandet High are the focus of this study. The collapsed diapirs (e.g. Ula structure) experienced collapse and salt withdrawal during Jurassic – Early Cretaceous and structural rejuvenation in the Late Cretaceous – Early Paleogene, followed by Cenozoic burial. The reactivated diapirs (e.g. Oda structure) underwent minor collapse during Jurassic – Early Cretaceous and major structural rejuvenation during Cenozoic shortening. The deformation caused by salt movement in these diapirs influence the petroleum system by facilitating (1) the accommodation of Jurassic sediments (reservoir units) above the diapirs during salt withdrawal, and (2) the formation of anticlines immediately after Jurassic deposition, or the uplift of sediments on the diapir flanks (traps). Risks related to reservoir presence and trap failure are higher in the reactivated diapirs (i.e. on the Sørvestlandet High), due to minor Jurassic salt withdrawal and extensive Cenozoic deformation. This study shows that the interpretation of high-quality 3D seismic data together with structural restorations, increases the understanding of the link between salt movement and sedimentation in this area.

Table of Contents

Acknowledgements	iv
Abstract	v
1 Introduction.....	1
1.1 Area and Challenges	1
1.2 Objectives	3
1.2.1 (i) Structural Framework	3
1.2.2 (ii) Evolutionary Model.....	3
1.3 Salt Tectonics	6
1.3.1 Introduction	6
1.3.2 Salt characteristics.....	6
1.3.3 Diapir formation processes.....	7
1.3.4 Diapir growth	8
1.3.5 Turtle-structure.....	12
1.3.6 Implications for the Petroleum system.....	13
1.4 2D Kinematic Restorations.....	14
1.4.1 2D Decompaction.....	14
1.4.2 2D Unfolding.....	16
1.4.3 Move-on-fault.....	17
2 Geological Setting.....	18
2.1 The Central North Sea	18
2.1.1 Permian – Triassic rifting	18
2.1.2 Middle Jurassic thermal doming	20
2.1.3 Upper Jurassic-Early Cretaceous rifting	21
2.1.4 Early Cretaceous: Early post-rift.....	21
2.1.5 Late Cretaceous: Late post-rift & CNS inversion	22
2.1.6 Paleogene and Neogene: Intra-cratonic basin w/inversion	22
2.1.7 Quaternary: Subsidence, sediment loading and halokinesis	22
3 Database and Methodology	23
3.1 Approach	23
3.2 Dataset	23
3.2.1 Seismic data.....	23
3.2.2 Well log data	23
3.2.3 Seismic well ties.....	24
3.3 Interpretation workflow	28

3.3.1	Semi-regional interpretations	28
3.3.2	Local seismic interpretations.....	32
3.4	Restoration workflow	33
4	Results	37
4.1	Semi-regional (Structural Framework).....	37
4.1.1	Permian.....	37
4.1.2	Triassic and Jurassic	42
4.1.3	Base Cretaceous Unconformity (BCU).....	44
4.1.4	Cretaceous	47
4.1.5	Cenozoic.....	51
4.2	Local analysis	56
4.2.1	Ula Structure	57
4.2.2	Oda Structure.....	60
4.2.3	NE-SW trending diapir.....	63
4.2.4	NW-SE trending diapir.....	66
5	Discussion.....	69
5.1	Structural Styles.....	69
5.1.1	Diapir classification.....	69
5.1.2	Structural distribution.....	72
5.1.3	Salt composition	74
5.2	Structural evolution	77
5.2.1	Permian.....	77
5.2.2	Triassic	78
5.2.3	Jurassic	81
5.2.4	Cretaceous	82
5.2.5	Cenozoic.....	85
5.3	Implications for the petroleum system	88
5.3.1	Reservoir	88
5.3.2	Trap types and timing.....	88
6	Conclusions.....	90
7	Recommendations for further work.....	91
8	References	92
9	Appendix I	95
10	Appendix II.....	96

List of figures

Figure 1. Tectonic framework of the north western Europe. Approximate locations of figures 2, 4 and 16, cross-section A-A', are shown. Modified after Coward 1990.....	1
Figure 2. Structural elements in the Central North Sea and approximate span of study area defined by the dashed red polygon. Map location shown in Figure 1.....	4
Figure 3. Pod-interpod model, illustrating supra-salt sediment distribution during extension and diapir collapse. (modified from Mannie et al., 2014, after Hodgson et al., 1992).....	5
Figure 4. Seismic stratigraphy and deformation related to a pod-interpod setting from the West Central Graben, UK-sector (modified from Karlo et. al., 2014). Approximate location of seismic section in Fig.1. Seismic is in time.....	5
Figure 5. Overview of various salt geometries. (from Fossen, 2010).....	6
Figure 6. Sandbox model illustrating salt growth during a reactive diapir stage (from Jackson and Hudec, 2017).....	9
Figure 7. Conceptual model of salt growth during an active diapir stage with associated deformation (from Jackson and Hudec, 2017, after Jackson et al. 1994).....	10
Figure 8. Conceptual model of several growth stages during passive diapirism. (From Hudec and Jackson, 2011).....	11
Figure 9. The Turtle structures evolution described through four steps: (a) deposition of the prekinematic unit; (b) primary peripheral sink and initial salt movement; (c) secondary peripheral sink and renewed salt movement; and (d) tertiary peripheral sink and renewed salt movement, with associated inversion of the primary peripheral sink (from Hudec and Jackson 2017, after Trusheim 1957,1960).....	12
Figure 10. Conceptual model with two different types of salt structures and their implications to the petroleum system. (from Jackson and Hudec, 2017).....	13
Figure 11. Restoration cartoon. A: areas of extension, salt withdrawal and diapirism are shown. B: salt and supra-salt layers are adjusted to the regional, salt is added, and extension removed. (from Rowan, 1993).....	14
Figure 12. Porosity-depth curves available in Move. Red dots are the digitized points which make the kaolinite curve (SC_1)......	15
Figure 13. Nordland Group removed, underlying sediments decompacted using two separate compaction curves, A: decompaction using compaction curve for kaolinite-rich clays. B: decompaction using compaction curve from Sclater & Christie (1980)......	15
Figure 14. A: Simple shear principle. B: Flexural slip principle. (from Move manual, 2019).....	17
Figure 15. Two forward models: (I) Simple shear with a shear angle of 60 degrees; (II) Elliptical Fault Flow with the largest displacement at the fault centre. (from Move manual, 2019)......	17
Figure 16. Regional cross section across the Central North Sea. Location of the section is shown in figure 1 (A-A'). (from Zanella and Coward 2003; and Mannie et. al. 2014).....	18
Figure 17. Lithostratigraphic chart with regional tectonic events in the Central North Sea (modified from NPD fact pages and Tvedt et. al. 2013).....	19
Figure 18. Triassic rift fault patterns of the North Sea. (from Zanella and Coward, 2003)....	20
Figure 19. Jurassic to Early Cretaceous extension phases; Left map: Callovian to early Kimmeridgian extension, Right map: Early Kimmeridgian to Volgian extension. (after Erratt et al. 1999).....	21
Figure 20. Provided dataset, (A) Seismic coverage; (B) Well database and composite lines. Red dots are the selected wells. The table shows the well-tie information for these wells.....	25

Figure 21. Seismic well-tie for well 8/4-1 in the MC3D-Q8-2008 seismic survey. A Ricker inverse wavelet and a 25ms bulk shift were applied.	26
Figure 22. Seismic well-tie for well 8/4-1 in the MC3D-Q8-2008 seismic survey. A Ricker inverse wavelet and a 25ms bulk shift were applied. Resampled acoustic impedance (resampled AI) is shown together with measured acoustic impedance (AI).	27
Figure 23. E-W cross-section across the PGS16008CGR cube, including the main horizons and faults. Section VE = 5. Location of the section is shown on the map.	31
Figure 24. Multi-Z interpretation (light blue lines) with the triangulated mesh surface (pink) showing salt distribution on the Sørvestlandet High and basin margin salt stocks. From MC3D-Q8-2008 seismic cube. VE = 3.	32
Figure 25. Top salt surface mapped in Petrel and imported into move. The four restored cross sections are shown. VE = 2.5	35
Figure 26. Sequential restoration workflow. Made after Rowan (1993) and steps from the move manual.	35
Figure 27. Flexural isostasy workflow, shown through three steps. In the uppermost section nothing is removed, while in the middle section the upper part of Hordaland Group is removed. Isostasy is not included until the lowermost figure. Here, the dashed line represents no flexural relief after removal of the top load.	36
Figure 28. Two-pin unfolding procedure, using flexural slip. The layers on each side of the structural crest are rotated around their assigned pin. (pin 1 = left side, pin 2 = right side)....	36
Figure 29. Top Rotliegend Group configuration: (A) Variance map. Dark to red areas indicate structures; (B) Main sub-salt normal faults. (BB) = Breiflabb Basin; (CT) = Cod Terrace; (HH) = Hidra High; (JH) = Jæren High; (NDB) = Norwegian-Danish Basin; and (SVLH) = Sørvestlandet High); and (C) Structure map.	38
Figure 30. Top Zechstein interpretation with structural trends, showing three tall diapirs aligned on the eastern flank. Overlying fields and discoveries are included.	40
Figure 31. Top Zechstein Group interpretation, including main salt structures (pink).	40
Figure 32. Sub-salt normal faults interpreted on top Rotliegend Group with overlying salt structures, field and discoveries. Structural elements include the (BB) = Breiflabb Basin; (CT) = Cod Terrace; (HH) = Hidra High; (JH) = Jæren High; (NDB) = Norwegian-Danish Basin; and (SVLH) = Sørvestlandet High).	41
Figure 33. Top intra-Triassic interpretation. The surface is merged with the top Zechstein Group where $Z_{\text{Triassic}} \leq Z_{\text{Zechstein}}$. This means that the interpreted top intra-Triassic surface follows the interpreted top Zechstein Group surface where the elevation of the top intra-Triassic is lower than the top Zechstein Group.	42
Figure 34. Time-thickness maps. (A) Top Zechstein Group - Intra-Triassic reflector; (B) Intra-Triassic reflector – BCU: Transparent polygon shows the position of a depocenter during Early Triassic (A) and the arrow illustrates how this depocenter shifted during Late Triassic - Jurassic.	43
Figure 35. SW-NE cross-section within the PGS16008CGR cube (Inline 26658), including supra-salt fault families F1 and F2. Location of the section is shown on the map.	45
Figure 36. Base Cretaceous Unconformity configuration: (A) Variance map. Dark to red areas indicate structures; (B) Structural trends, including main salt bodies, supra-salt normal faults and fields and discoveries. (BB) = Breiflabb Basin; (CT) = Cod Terrace; (HH) = Hidra High; (JH) = Jæren High; (NDB) = Norwegian-Danish Basin; and (SVLH) = Sørvestlandet High); and (C) Structure map.	46

Figure 37. Cromer Knoll Group configuration: (A) Variance map. Dark to red areas indicate structures. Blue dashed lines represent approximate structural element boundaries: (BB) = Breiflabb Basin; (CT) = Cod Terrace; (HH) = Hidra High; (JH) = Jæren High; (NDB) = Norwegian-Danish Basin; and (SVLH) = Sørvestlandet High); (B) Structure map; and (C) Time-thickness map.	48
Figure 38. Shetland Group configuration: (A) Variance map. Dark to red areas indicate structures. Blue dashed lines represent approximate structural element boundaries: (BB) = Breiflabb Basin; (CT) = Cod Terrace; (HH) = Hidra High; (JH) = Jæren High; (NDB) = Norwegian-Danish Basin; and (SVLH) = Sørvestlandet High); (B) Structure map; and (C) Time-thickness map.	50
Figure 39. Rogaland Group configuration: (A) Variance map. Dark to red areas indicate structures. Blue dashed lines represent approximate structural element boundaries: (BB) = Breiflabb Basin; (CT) = Cod Terrace; (HH) = Hidra High; (JH) = Jæren High; (NDB) = Norwegian-Danish Basin; and (SVLH) = Sørvestlandet High); (B) Structure map; and (C) Time-thickness map.	52
Figure 40. Hordaland Group configuration: (A) Variance map. Dark to red areas indicate structures. Blue dashed lines represent approximate structural element boundaries: (BB) = Breiflabb Basin; (CT) = Cod Terrace; (HH) = Hidra High; (JH) = Jæren High; (NDB) = Norwegian-Danish Basin; and (SVLH) = Sørvestlandet High); (B) Structure map; and (C) Time-thickness map.	53
Figure 41. Time-thickness maps. (T1) Top Rogaland Group - Intra-Hordaland Group reflector; (T2) Intra-Hordaland Group reflector - Top Hordaland Group. The intra-Hordaland Group reflector is identified on the cross-section in Figure 23.	54
Figure 42. Nordland Group time-thickness map. Black dashed lines represent approximate structural element boundaries: (BB) = Breiflabb Basin; (CT) = Cod Terrace; (HH) = Hidra High; (JH) = Jæren High; (NDB) = Norwegian-Danish Basin; and (SVLH) = Sørvestlandet High).....	55
Figure 43. Top Zechstein Group interpretation highlighting a set of diapirs. The restored cross-sections are shown by the yellow lines: B-B' = Ula structure C-C' = Oda structure; D-D' = NE-SW salt diapir and E-E' = NW-SE trending salt diapir.....	56
Figure 44. WSW-ENE cross-section across the PGS16008CGR cube, including bedding relationships near the studied salt diapir or Ula Structure. The location of the section is shown in Figure 43 (B-B`.).....	57
Figure 45. Restored and unfolded sections of the Ula structure, collapsed diapir, from the present to the top Zechstein Group. The location of the section is shown on the three-dimensional surface, displayed with a VE = 2.5. Additionally, a variance map covering the structure is included. (See Appendix II).....	59
Figure 46. SW-NE cross-section in the PGS16008CGR and CE1202R15 cubes, including bedding relationships near the addressed salt diapir, Oda Structure. Location of the section is shown in Figure 43 (C-C`.)	60
Figure 47. Restored and unfolded sections of the Oda structure, a reactivated diapir, from the present to the top Zechstein Group. The location of the section is shown on the three-dimensional surface, displayed with a VE = 2.5. Additionally, a variance map covering the structure is included. (See Appendix II).....	62
Figure 48. NNW-SSE cross-section in the CE1202R15 cube, including bedding relationships near the NE-SW trending diapir. Location of the section is shown in Figure 43 (D-D`.)	63

Figure 49. Restored and unfolded sections of a NE-SW trending reactivated diapir from the present to top the Zechstein Group. The location of the section is shown on the three-dimensional surface, displayed with a VE = 2.5. Additionally, a variance map covering the structure is included. (See Appendix II).....	65
Figure 50. SSW-NNE cross-section in the PGS16008CGR cube, including bedding relationships near the addressed salt diapir, north of Oda. Location of the section is shown in Figure 43 (E-E').	66
Figure 51. Restored and unfolded sections of a NW-SE trending reactivated diapir from the present to the top Zechstein Group. The location of the section is shown on the three-dimensional surface, displayed with a VE = 2.5. Additionally, a variance map covering the structure is included. (See Appendix II).....	68
Figure 52. Diapir classification by Hudec and Jackson (2017), made after Jackson and Talbot (1986).	71
Figure 53. Interpretation of the different diapir types in the top Zechstein Group map. Structural elements included are the (BB)=Breiflabb Basin; (CT)=Cod Terrace; (HH)=Hidra High; (JH) = Jæren High; (NDB)=Norwegian-Danish Basin and (SVLH)=Sørvestlandet High.	72
Figure 54. Salt classification plot. X-axis provides position in terms of structural element. Y-axis is the relative abundance of the selected structure within the study area. Vertical exaggeration = 3	73
Figure 55. Sub-salt normal faults interpreted on the top Rotliegend Group with overlying salt structures, field and discoveries. Structural elements included are the (BB)=Breiflabb Basin; (CT)=Cod Terrace; (HH)=Hidra High; (JH) = Jæren High; (NDB)=Norwegian-Danish Basin and (SVLH)=Sørvestlandet High.	74
Figure 56. NW-SE cross-sections: upper section from original PGS seismic; lower section generated by using the “outcrop attribute”.....	76
Figure 57. Salt composition from the basin-centre towards the basin margins, defined by four zones (from Jackson et al., 2019). Proposed ranges within study area are displayed; CT = Cod Terrace, JH = Jæren High, SVLH = Sørvestlandet High and NDB = Norwegian-Danish Basin.	76
Figure 58. E-W cross-section across the PGS16008CGR cube, including a sub-salt interval and faults.....	77
Figure 59. W-E cross section illustrating intra-Triassic reflector geometries covering the collapsed diapir, Ula Structure: (A) present-day section of the collapsed Ula structure; (B) present-day strata-terminations; and (C) Intra-Triassic restored section with strata-terminations. VE = 1	79
Figure 60. W-E cross section illustrating intra-Triassic reflector geometries covering the collapsed diapir, Ula Structure: (A) present-day section; (B) a present-day turtle structure observed east of the Ula Structure, where green arrows represent the first growth package, and the blue arrows mark a shift in the depocenter towards the east; and (C) Intra-Triassic restored section with the turtle structure still present. VE =1	80
Figure 61. W-E restored BCU cross section for (A): Collapsed diapir, Ula structure; and (B): NW-SE trending reactivated diapir. VE = 1	82
Figure 62. W-E restored Cromer Knoll Group cross-section for (A): Collapsed diapir, Ula structure; and (B): NW-SE trending reactivated diapir. VE = 1	83
Figure 63. W-E cross-section capturing the Oda structure. (A): Present-day geometries. R2 and R3 are regional levels for top Cromer Knoll Group and top Hordaland Group, respectively; (B): Restored Shetland Group. R2 is the regional level for the top Cromer Knoll Group; and (C):	

Restored Cromer Knoll Group. R1 is the regional level for the near top Jurassic (BCU). VE = 1	85
Figure 64. W-E cross-section capturing the Oda structure. (A): Restored top Hordaland Group. R3 is the regional level for the top intra-Hordaland Group; (B): Restored intra-Hordaland Group. R2 is the regional level for the top Rogaland Group; and (C): Restored Rogaland Group. R1 is the regional level for the top Shetland Group. VE = 1	87
Figure 65. W-E restored top Hordaland Group cross-section capturing the Ula structure. R3 is the regional level for the top intra-Hordaland Group. VE = 1	88

List of tables

Table 1. Physical properties of Halite, Quartz and Ice. (from Jackson and Hudec, 2017).....	7
Table 2. Properties and seismic character of the interpreted reflectors.	30
Table 3. Lithological units and their assigned properties.	33

1 Introduction

1.1 Area and Challenges

The Central North Sea (CNS) is located in the southern part of the Norwegian Continental Shelf (Fig. 1). The area has undergone multiple stages of deformation, often accommodated by salt mobilization (Stewart, 2007; Stewart and Coward, 1995; Harding and Huuse, 2015). These stages have added complexity to the basin and have implications for the petroleum systems. Major oil and gas discoveries both in Norway (e.g. Valhall, Ekofisk, Gyda, Tambar and Ula) and in the UK (e.g. Machar, Mirren and Mungo) are situated within this region, with many fields located in association with salt structures. The principal reservoir intervals lie within Upper Jurassic marine sandstone reservoirs (e.g. Ula, Oda, Tambar and Gyda – Fig. 2) or Upper Cretaceous chalk reservoirs (e.g. Ekofisk, Vallhal, Tor, Eldfisk), and show different degree of salt influence on structure/trap and reservoir development. Despite extensive exploration in the area, specific salt structures on the Cod Terrace and Sørvestlandet High can be understood further by implementing new workflows. These structures will be the focus of this study.

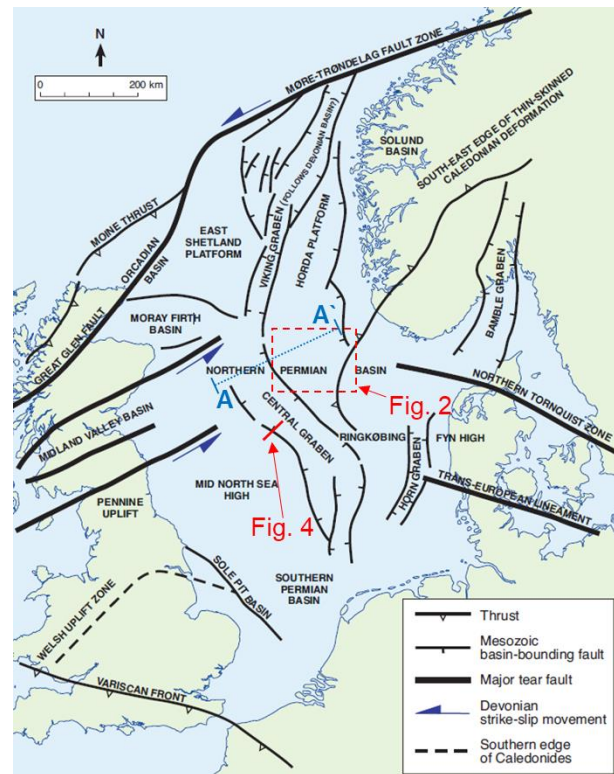


Figure 1. Tectonic framework of the north western Europe. Approximate locations of figures 2, 4 and 16, cross-section A-A', are shown. Modified after Coward 1990.

The salt is contained in the Zechstein Group, which was deposited during the Late Permian. A pre-salt extension phase formed a network of normal faults, which influenced later salt deposition and salt tectonics (Ge et al., 2017). Mesozoic extension and contraction, in combination with sediment infill, re-distributed the salt to its current state. This resulted in a broad range of structures, previously attributed to a combination of tectonic regimes including strike-slip, extensional and compressional tectonics (Sears et al., 1993; Karlo et al., 2014). The early-stage structural evolution may be masked beneath more recent events. Therefore, present-day geometries must be analyzed carefully.

Studies from the 1990`s describe the structural styles and the relationship between extensional tectonics and salt behaviour in the area (Penge et al., 1993; Sears et al., 1993; Stewart and Coward, 1995). These studies mainly use 2D data and some 3D seismic datasets of poor quality compared to the 3D seismic datasets available today. Seismic interpretation is challenging because the Central North Sea has undergone salt remobilization and deformation caused by polyphase extension and subsequent inversion, which generated complex structures that are challenging to image in seismic. Additionally, weak acoustic impedance contrasts between the post-salt Triassic sediments and the Zechstein salt, and strong multiples produced by the base chalk and the base Cretaceous Unconformity, make the interpretation of internal Triassic and Jurassic seismic geometries difficult. Within the Triassic, seismic amplitudes are variable, with strong continuous reflectors in some sections and weak discontinuous reflectors in others. Moreover, most wells have target units shallower than Triassic and Permian, providing poor control on the top Triassic and top salt (Zechstein Gp).

Despite limitations in the seismic data, various authors have proposed a “pod-interpod” model to describe Jurassic reservoir development within supra-salt minibasins in the Central North Sea (Hodgson et al., 1992; Karlo et al., 2014; Mannie et al., 2014). These supra-salt minibasins are referred to as interpods and they are separated by thick Triassic minibasins (pods) (Fig. 3). In Figure 4, these geometries have been best imaged in the UK-sector by Karlo et al. (2014). Here, the top salt pick is well recognized on the structural highs with a strong reflector, while it is less certain along the diapir flanks. Internal pod geometries within the Triassic succession are well imaged. Karlo et al. (2014)`s analysis from the UK-sector enables early-stage salt movement to be unraveled. Similar seismic observations on the Cod Terrace and Sørvestlandet High have been made based on a modern high-quality 3D seismic dataset (in courtesy of Petroleum Geo-Services).

On the Cod Terrace, the evolution of a “pod-interpod” structure has been studied by Mannie et al. (2014), but information regarding the structural evolution during the Cenozoic is lacking. Now, access to state-of-art high-quality seismic datasets gives the opportunity to study the Mesozoic salt development and the post-Jurassic structural evolution in greater detail. This is the motivation for this thesis.

1.2 Objectives

A high-quality 3D seismic reflection dataset extending beyond the study area and covering the Cod Terrace and Sørvestlandet High (red polygon, Fig. 2), enables detailed seismic analysis near salt structures. The aim of this study is to investigate the evolution of four salt structures and their driving mechanisms of mobilization, with focus on diapirs that show multiple stages of growth. This provides a better understanding of the effect of salt movement on trap formation, reservoir distribution, and hydrocarbon potential. A parallel MSc project carried out by Andrea Trollsås Liverød on the interaction between Triassic fluvial systems and early-stage salt tectonics complements this study.

The focus of this study goes from semi-regional scale interpretation, to restoration of specific salt structures in order to unravel their evolution. To achieve this, two main objectives have been proposed:

1.2.1 (i) Structural Framework

The purpose is to gain better understanding of the structural framework in the study area and to provide a classification of salt-related structures from the platform to the basin areas. This goal can be subdivided in the following objectives:

- determine the semi-regional distribution of Zechstein salt and its thickness, as well as classify structures based on their geometry (i.e. salt stocks, salt rollers, buried diapirs, collapsed diapirs and reactivated diapirs), and sediment growth patterns in minibasins adjacent to and on top of salt structures;
- address the relationship between pre-existing faults (i.e. Permo-Triassic faults), salt distribution, and salt related structures; and
- investigate Mesozoic and Cenozoic deformation in relation to underlying and adjacent salt structures, with emphasis on salt movement.

1.2.2 (ii) Evolutionary Model

Propose an evolutionary model based on sequential restorations of four diapirs located on the Cod Terrace and Sørvestlandet High. For all structures, the timing of supra-salt fault movement, salt mobilization, impact on the petroleum system, and if possible, the effect of sub-salt fault movement are investigated. Specific objectives include:

- determining timing and controlling factors on initial salt mobilization and later salt remobilization;

- comparison of the timing of salt mobilization between all four structures;
- comparison of proposed models with previous models of the Central North Sea and assessment of the additional information on salt mobilization provided by this study; and
- identifying thickness of stratigraphic units near salt structures.

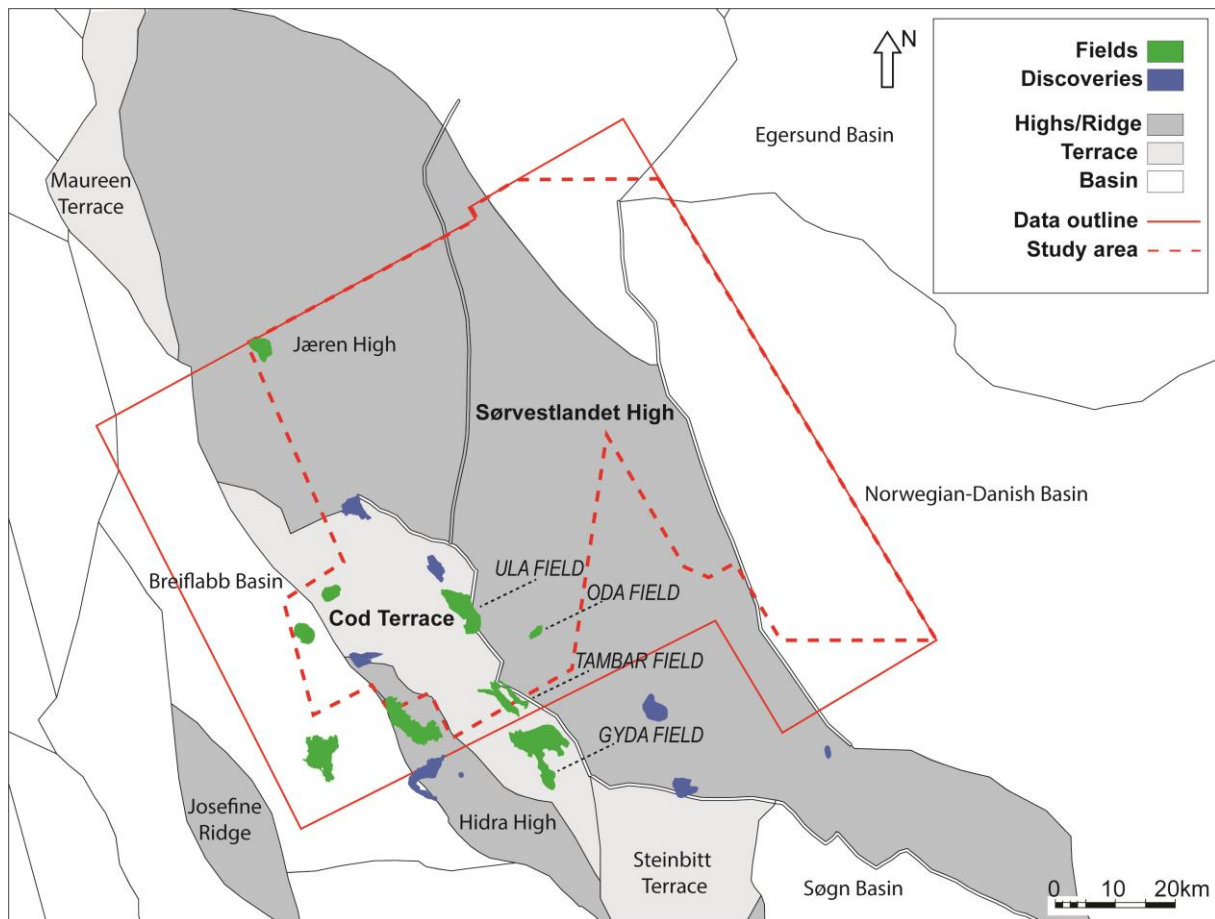


Figure 2. Structural elements in the Central North Sea and approximate span of study area defined by the dashed red polygon. Map location shown in Figure 1.

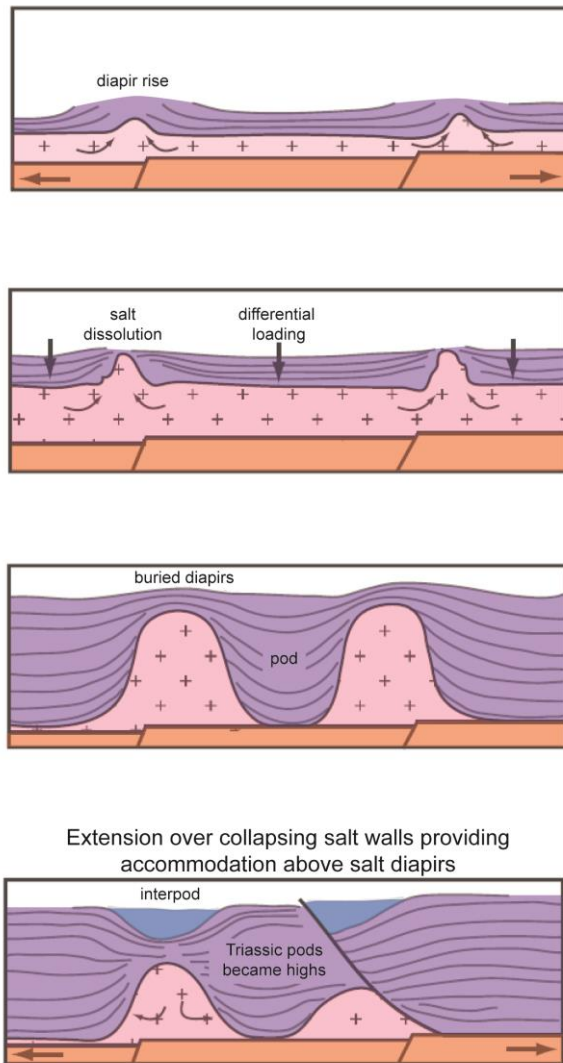


Figure 3. Pod-interpod model, illustrating supra-salt sediment distribution during extension and diapir collapse. (modified from Mannie et al., 2014, after Hodgson et al., 1992)

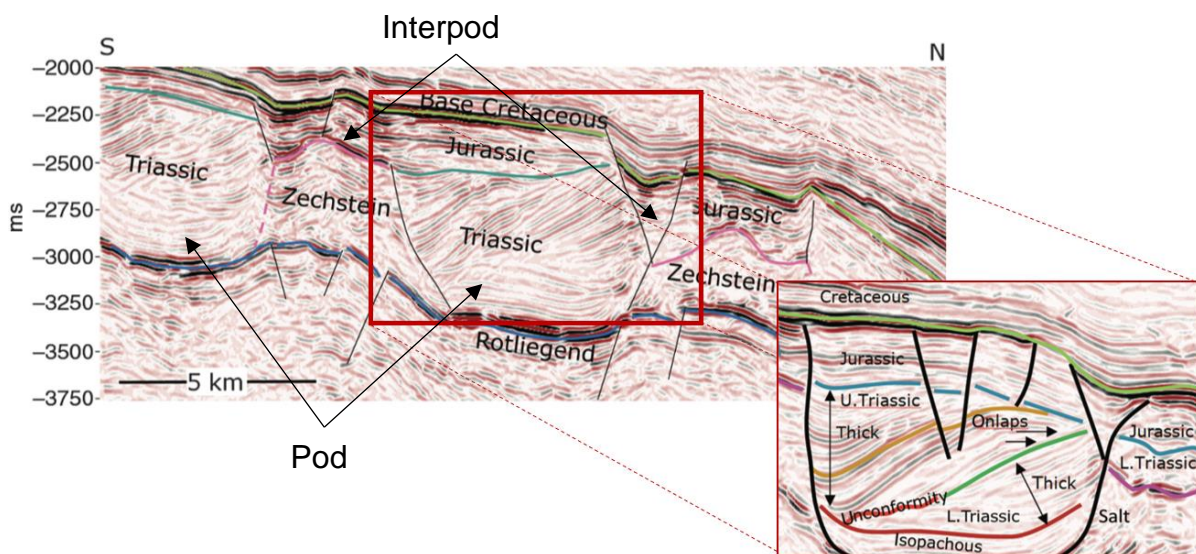


Figure 4. Seismic stratigraphy and deformation related to a pod-interpod setting from the West Central Graben, UK-sector (modified from Karlo et al., 2014). Approximate location of seismic section in Fig.1. Seismic is in time.

1.3 Salt Tectonics

1.3.1 Introduction

Salt has the ability to take a large variety of geometries through time. The main shapes of salt bodies are elongated structures, such as salt walls, anticlines and rollers, whereas tall isolated structures are often recognized as salt stocks (Fig.5). When it comes to describing salt structures the term *diapir* is commonly used. This term refers to salt structures which have been flowing upward, piercing through its overburden, during a process called diapirism (Fossen, 2010).

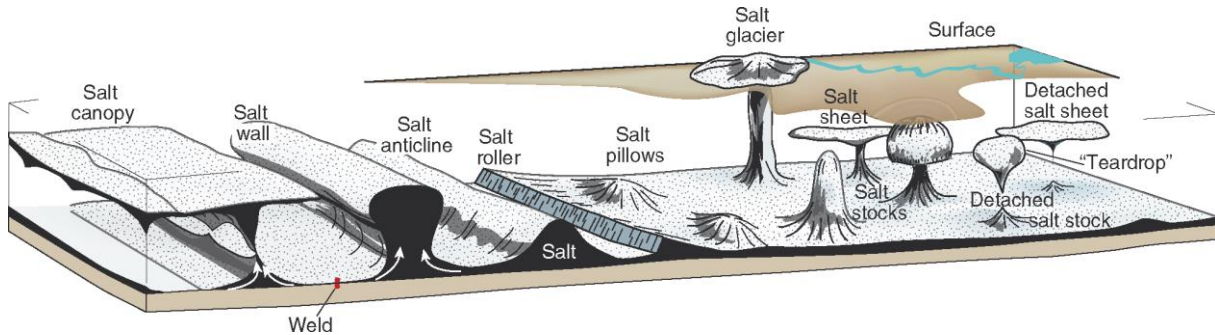


Figure 5. Overview of various salt geometries. (from Fossen, 2010)

1.3.2 Salt characteristics

Salt is often referred to as one specific material, with known and homogeneous properties, but this is rarely the case. Heterogeneity within what we refer to as salt, includes evaporites, halite, gypsum and anhydrite (hydrated from gypsum), and non-evaporitic rocks including carbonates and siliciclastics. Halite is the most common, weakest and easily deformed rock material, while gypsum and anhydrite deform about 10^5 and 10^7 times slower than halite, respectively (Williams-Stroud and Paul, 1977). Therefore, some areas of a salt body may be less ductile and produce different deformation patterns. For post-salt sediment deposition and structural evolution, the abundance and composition of evaporites play a fundamental role in the basin development (Jackson et al., 2019). For example, sediment loading and tectonic events can deform the salt body less where anhydrite and gypsum are present (Jackson and Hudec, 2017).

Through geological time scales, salt movement is described as a fluid which flows, while the overburden is strong and brittle. Halite is almost incompressible and has a high thermal expansivity factor (Table.1), which results in a slight expansion with burial. The average density of salt is about 2.2 g/cm^3 and it barely varies with depth. Due to its stable and lower density in comparison to surrounding sediments, early studies suggest that salt movement is driven purely by buoyancy effects with upward movement resembling a lava lamp. Today, differential loading is understood to be the main process driving salt flow (Jackson and Hudec, 2017).

Table 1. Physical properties of Halite, Quartz and Ice. (from Jackson and Hudec, 2017)

Property	Halite	Quartz	Ice
Density	2.160 g/cm ³	2.650 g/cm ³	0.920 g/cm ³
Bulk modulus	22 GPa	37 GPa	9 GPa
Young`s modulus	29 GPa	72 GPa	9 GPa
Rigidity (shear) modulus	11 GPa	38 GPa	4GPa
Poisson`s ratio	0.31	0.17	0.33
Compressive strength	24 MPa	1100 MPa	4 MPa
Tensile strength	2 MPa	50 MPa	1 MPa
P-wave acoustic velocity	4200 m/s	5800 m/s	3800 m/s
S-wave acoustic velocity	2400 m/s	3750 m/s	3100 m/s
Thermal conductivity	6.7 W/m.K	1.4 W/m.K	2.2 W/m.K
Thermal diffusivity	3.6 x 10 ⁻⁶ m ² /K	0.9 x 10 ⁻⁶ m ² /K	1.3 x 10 ⁻⁶ m ² /K
Thermal expansivity	42 x 10 ⁻⁶ /K	0.6 x 10 ⁻⁶ /K	23 x 10 ⁻⁶ /K

1.3.3 Diapir formation processes

Three mechanisms drive salt growth: (i) gravitational (vertical) loading, (ii) displacement (tectonic) loading, and (iii) thermal loading (Jackson and Hudec, 2017).

- (i) Gravitational loading is related to the load from the weight of the overburden. The lateral gradient of the vertical force from the overburden displaces the salt laterally into nearby diapirs or form new diapirs at an early stage. The flow of salt caused by differential loading is referred to as “salt withdrawal” or “salt expulsion”.
- (ii) Displacement loading is initiated either from compression or extension. Tectonic events are commonly not the initial trigger, but rather a secondary driving mechanism that transports salt into active structures.
- (iii) Thermal loading is a result of a volume increase or decrease due to temperature changes. The thermal expansivity of salt is high (Table.1) which leads to a rapid increase in volume relative to the surrounding rocks. Expanding salt increases the stress and can have an impact on adjacent salt deformation.

Forces resisting salt flow

The mentioned mechanisms related to salt growth need to overcome the strength of the host rock for the salt to flow. Salt on its own is highly mobile, but when trapped between dense rocks, gravitational loading must act together with other events (e.g. tectonic events) for the salt to pierce through the overlying layers. The strength of the overburden prevents the salt to move, even with high differential stresses present. The strength of sedimentary rocks is several orders

of magnitude larger than that of salt, making the process of salt movement challenging (Jackson and Hudec, 2017).

1.3.4 Diapir growth

Diapiric growth for salt stocks and salt walls was described by Vendeville and Jackson (1992) using three stages: reactive-, active-, and passive- growth. Sediment growth may gradually evolve from one stage to the other and back again depending on a set of variables.

Reactive diapirism

Extension of the overburden causes faults and grabens, which result in differential loading (i.e. depressions have a higher sediment load than highs and will compact more). Tectonic stress weakens the overburden by fracturing and faulting. Salt walls pressurized by a load adjacent to the diapir flanks begin to rise above the thinned overburden. This occurs during regional extension where grabens form, as gravitational loading on its own will only produce an evenly distributed overburden where salt remains stable. The diapir does not form as a forceful intrusion, but continued extension and faulting enables the salt to rise as a triangular diapir (Fig. 6). An analogue to reactive diapirism is Airy isostasy, in which blocks of equal density float at different elevations depending on their thickness (Bowie, 1927).

Reactive diapirism is mainly controlled by extension, if extension stops the diapir does not rise and renewed extension results on reactivated diapir growth. Hence, extension also controls the overall shape of the diapirs, which appear as elongated salt structures. Additionally, syn-kinematic sedimentation contributes to this process. The infill of sediments within the graben area above the salt depends on the depositional systems; if there is a high sedimentation rate, the salt will rise less and vice versa. In this way, growth-strata play an important part in controlling diapir growth. However, sediment filling the graben does not entirely stop salt growth even if the available space is completely filled with sediments, because young sediments are unconsolidated and can be less dense than salt. The structures related to reactive diapirism are mostly symmetrical salt walls and asymmetrical salt rollers, with a narrowing upward shape (Fig.6).

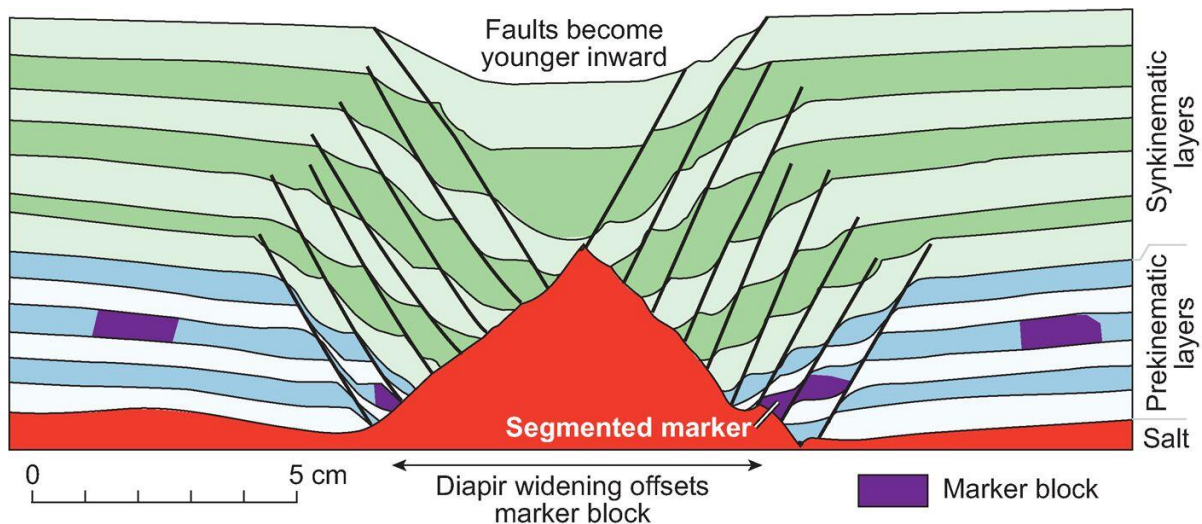


Figure 6. Sandbox model illustrating salt growth during a reactive diapir stage (from Jackson and Hudec, 2017)

Active diapirism

Active diapirism occurs when a salt body pierces through its roof during active rise, producing salt arches, uplifts or shoulders aside its overburden (i.e. salt pushes actively upwards). Active rise is driven by halokinetic processes or contraction (contractional rise).

For active diapirism, it is buoyancy or surface topography which enables salt movement. Under these conditions, salt is driven by the load of the overburden acting on the adjoining salt source layers, and with sediment densities significantly higher than salt, buoyancy can alone move the salt. For the salt to rise, the threshold thickness, which is the thickness of the roof where buoyancy forces are balanced, must be breached. Halokinetic rise either takes place during increase in the driving force (sediment load), decrease in resisting forces (faulting and/or thinning of the overburden) or both. Sediment density, roof strength and anisotropy, and salt lithology and geometry influence the magnitude of salt movement during halokinetic active rise (Jackson and Hudec, 2017).

Contractional rise differs from halokinetic rise since the stresses applied are generally much larger. Thus, a diapir which was stable can begin to rise under these conditions. Contractional rise is triggered by shortening in two ways:

- (i) Shortening adds a compressive load to the gravitational load, resulting in the convergence of the diapir flanks and narrowing of the diapir. Narrowing of the diapir pushes salt upwards, arching the roof faster than with halokinesis alone. During shortening, the salt is also forced downwards in areas where the source layer is thick.

However, in areas where salt has evacuated, and supra- and sub-salt sediments are welded, it is difficult to establish a new salt source layer.

- (ii) Shortening can buckle the overburden, causing it to rise into an anticlinal structure, even without being pushed by pressurized salt.

The most distinctive structure in active diapirism is the arched roof with radial fault patterns (Fig. 7), but here it is important to not overinterpret stratigraphic observations near the diapir. Both compaction and active diapirism will result in a gradual upward decrease in structural relief of an arched roof. Arched roofs can also be generated by drape compaction or differential compaction, as sediments compact with depth and salt expands when heated. However, if the structural relief is more than a few hundred meters above the regional, which is the maximum relief caused by compaction, active diapirism should be considered. Folds, reverse faults and other signs of shortening above or adjacent to salt structures are additional support for active diapirism.

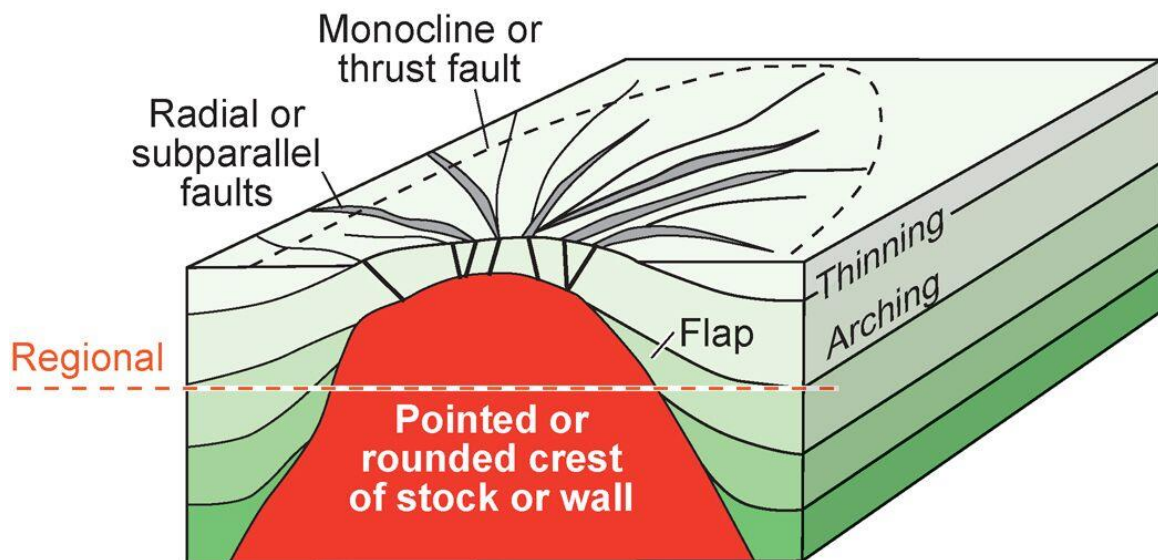


Figure 7. Conceptual model of salt growth during an active diapir stage with associated deformation (from Jackson and Hudec, 2017, after Jackson et al. 1994)

Passive diapirism

A commonly used term for passive diapirism is “downbuilding” (Barton, 1933). This defines the process by which the diapir subsides together with the surrounding sediments. The main characteristic of this process is that salt is emergent at surface level (Fig. 8), which causes problems in terms of upbuilding and space. Downbuilding solves this issue, by creating accommodation space above the diapir, but not enough to create a permanent roof.

Salt can grow as a passive diapir in any tectonic setting where salt reaches the surface. Generally, this occurs after deposition as the diapir breaches the overburden and emerges to the surface, but it may also initiate at an early stage. However, the salt usually reaches the surface after long periods of reactive diapirism followed by active diapirism. Extension can establish a load gradient and weaken the roof, making upward salt movement possible if the pressure acting on the salt body is enough.

Passive diapirism has generated most of the world’s largest salt stocks and walls, with mild deformation of adjacent rock. The deformation is often observed from subtle thickness changes in the overburden and upturned strata near the diapir contact. Salt domes which have grown as a passive diapir over long periods show multiple phases of growth. Each phase comprising a set of tilted beds near the diapir flanks, referred to as a halokinetic sequence. One episode of burial, breakout and downbuilding is recorded within a halokinetic sequence (Jackson and Hudec, 2017).

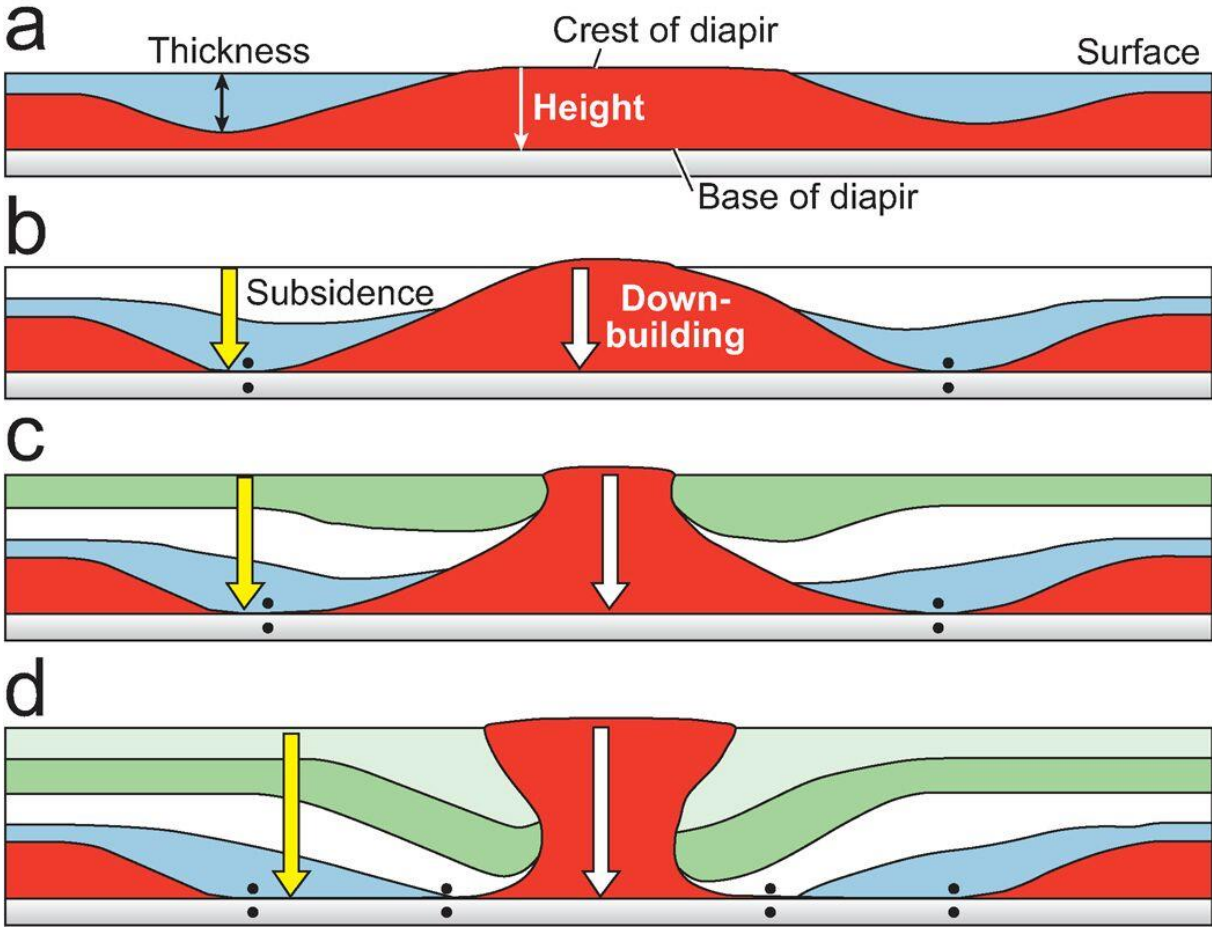


Figure 8. Conceptual model of several growth stages during passive diapirism. (From Hudec and Jackson, 2011)

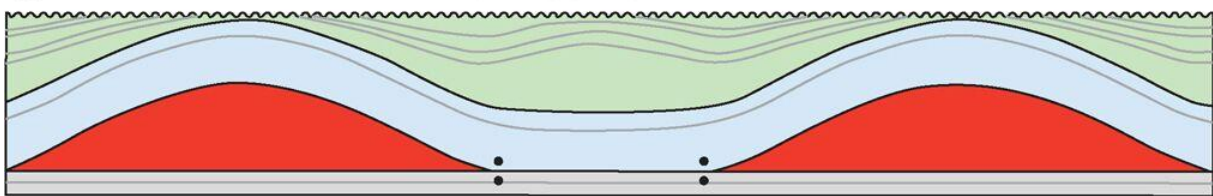
1.3.5 Turtle-structure

Trusheim (1957, 1960) introduced the term *Turtle-structure*. This structure forms after focussed deposition with salt withdrawal until it is completely depleted (Fig. 9, primary peripheral sink), followed by a lateral shift in the depocenter as salt withdraws from new areas. The renewed salt movement and deposition inverts the primary peripheral sink and is referred to as a *Turtle-structure* (Fig.9).

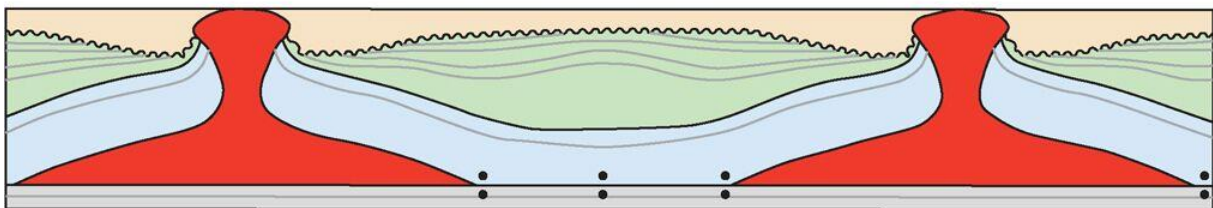
a End Muschelkalk



b Lower Cretaceous (Dogger)



c End Lower Cretaceous



d End Cenozoic

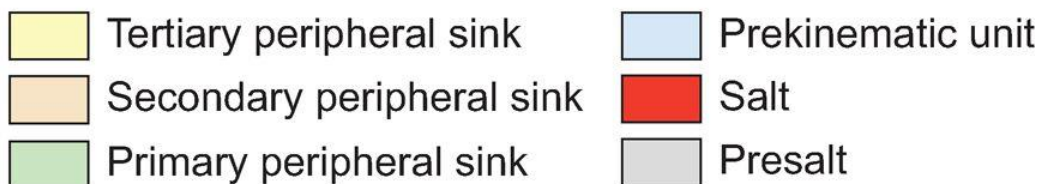
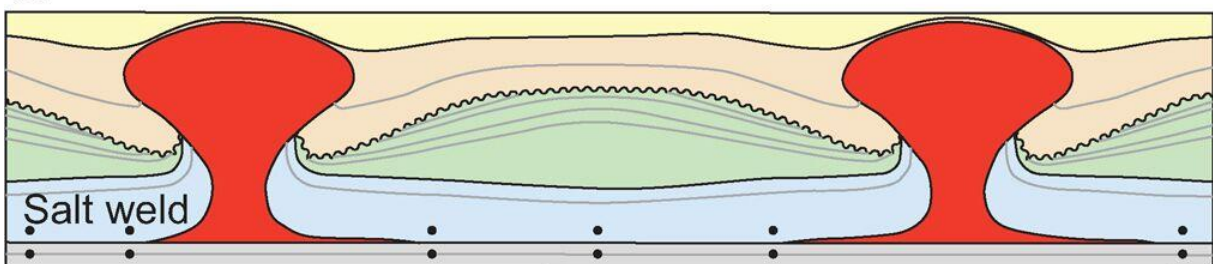


Figure 9. The Turtle structures evolution described through four steps: (a) deposition of the prekinematic unit; (b) primary peripheral sink and initial salt movement; (c) secondary peripheral sink and renewed salt movement; and (d) tertiary peripheral sink and renewed salt movement, with associated inversion of the primary peripheral sink (from Hudec and Jackson 2017, after Trusheim 1957,1960)

1.3.6 Implications for the Petroleum system

Salt has implications for all aspects of the petroleum system (Fig. 10). The high thermal conductivity of salt can potentially mature a shallow source rock above the salt, or it can cool down sub-salt reservoirs which otherwise would have been overmatured and with reduced reservoir properties. For migration, salt tectonics can create (1) topography, (2) folding, (3) faulting, (4) rise of salt stock and walls, (5) salt sheets and canopies, and (6) welding, which may generate or restrict migration pathways (Jackson and Hudec, 2017). Salt may also set controls on depositional systems, where salt movement can change the basin geometry and thereby reservoir distribution (Mannie et al., 2014; McKie, 2014). Additionally, salt movement can generate several structure types which can work as traps, and salt can act as an excellent seal where salt overhang or canopies are covering sediments (Jackson and Hudec, 2017).

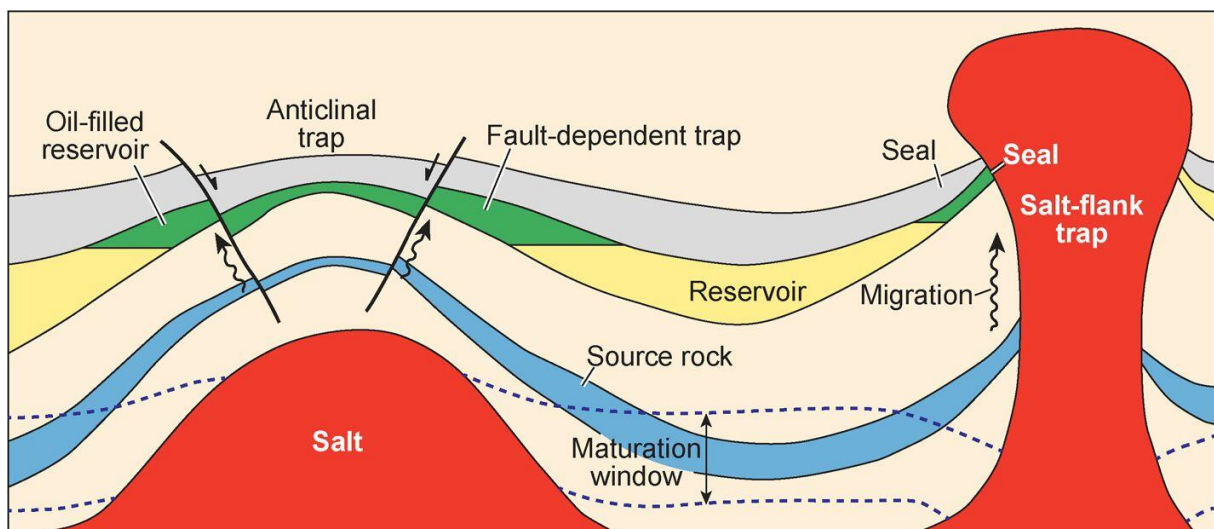


Figure 10. Conceptual model with two different types of salt structures and their implications to the petroleum system. (from Jackson and Hudec, 2017)

1.4 2D Kinematic Restorations

Structural restorations are often used to constrain pre-deformational geometries in salt provinces. Restorations were performed in a software (e.g. Move by Petroleum Experts) following restoration steps by Rowan (1993) and an established restoration workflow from the Butch discovery, now Oda field (Fig. 26). These restorations were carried out on a basin formed during extension of salt and post-salt successions, without sub-salt deformation impacting salt re-mobilization. Still, the methods and principles regarding salt movement extracted from the restorations are useful.

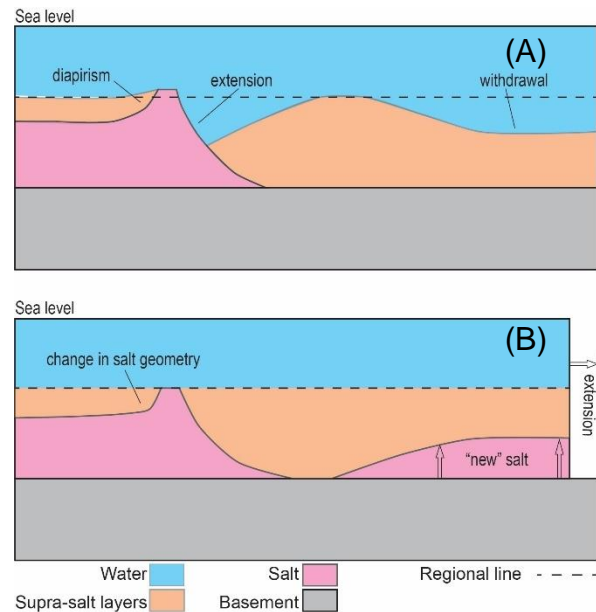


Figure 11. Restoration cartoon. A: areas of extension, salt withdrawal and diapirism are shown. B: salt and supra-salt layers are adjusted to the regional, salt is added, and extension removed. (from Rowan, 1993)

Restoring salt in a two-dimensional section is described as a three-dimensional procedure, where salt flows in and out of the section (Fig. 11). The deformation modifying the basin geometry is caused by: (1) sedimentation, (2) compaction, (3) eustasy, (4) fault-related deformation, (5) salt movement, (6) isostasy, or/and (7) thermal subsidence. These factors need to be considered during the restoration steps and implemented to ensure that the available information is used (e.g. stratigraphic properties, sea-level and timing of rifting).

For the purpose of this study, thermal subsidence and water depth are not handled in great detail. Thermal subsidence is related to the volume change during crustal cooling and would have an impact on the basin. Sea-level curves from Jurassic to the present show water depth changes from 25-75 m during the Cretaceous and 250-1500 m during the Palaeocene-Eocene (Gradstein and Båström, 1996). These water depth changes have not been considered in the restorations. The errors related to excluding these factors will be discussed later.

1.4.1 2D Decompaction

Decompaction removes the uppermost layer and adjusts the underlying layers following porosity-depth curves. The default settings for decompaction are from work on the North Sea by Sclater and Christie (1980), where they assume an exponential decrease of porosity with

increasing depth. There are also two other compaction curves available, the Baldwin-Butler curve and the Dickinson curve (Fig.12). Additionally, compaction curves can be added for specific lithologies. The compaction curve for shale was updated based on studies by Marcussen et al. (2010) (black curve, Fig. 12). In this study, decompaction of smectite-rich and kaolinite-rich mudstones are compared, with porosities at shallow depths near 40% and 20%, respectively. From these, the kaolinite curve has a rapid porosity decrease during initial burial stages, until porosity remains fixed at 13% below 4000m (black curve, Fig. 12). This curve shows a reasonable fit with well data in the uppermost and lowermost sections. The difference in initial versus buried porosities are lower compared to Sclater and Christie`s curve, such that applying the black curve to the claystones, produces a better fit in the initial decompaction step (Fig. 13).

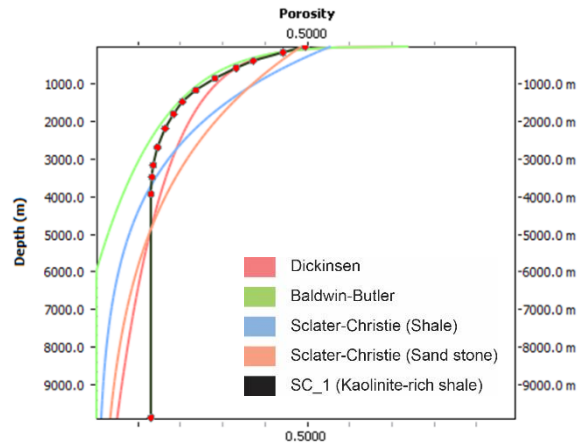


Figure 12. Porosity-depth curves available in Move. Red dots are the digitized points which make the kaolinite curve (SC_1).

Salt does not change density during burial, while the surrounding and overlying sediments do. The effect of this is shown in figure 13B. In this figure, there is strata uplift on the diapir flank, while areas above salt are lower. This is due to the large difference in initial versus buried compaction for the Sclater and Christie (1980) clay curve. For this reason and the fact that Marcussen et al. (2010) mentions large lateral variability in Cenozoic shale properties in the North Sea, the kaolinite curve was used in the restorations.

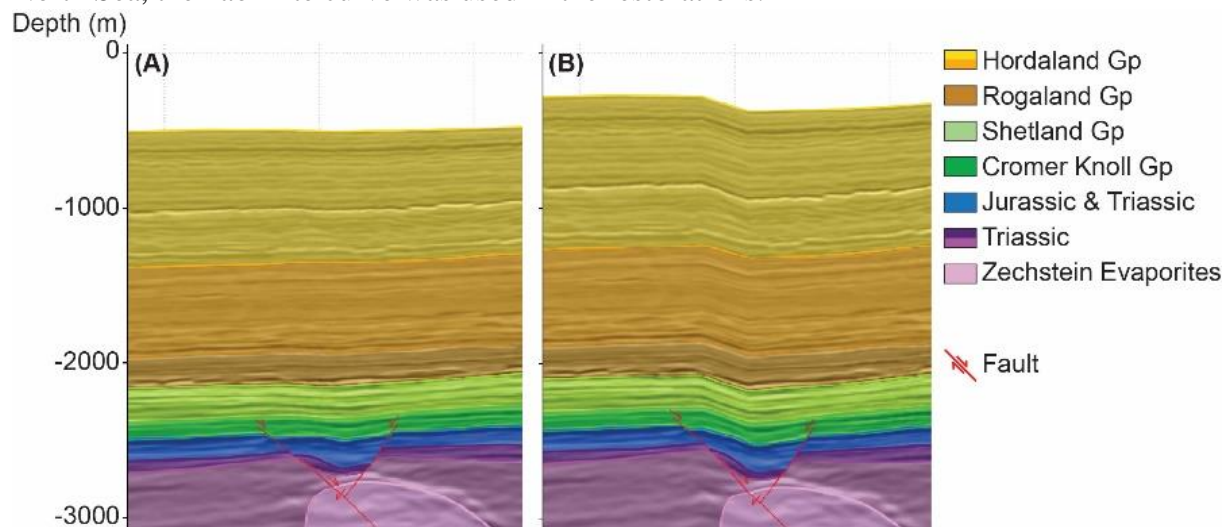


Figure 13. Nordland Group removed, underlying sediments decompacted using two separate compaction curves, A: decompaction using compaction curve for kaolinite-rich clays. B: decompaction using compaction curve from Sclater & Christie (1980).

Another important element considered in the decompaction process, is isostatic response. This is calculated during removal of the sediments. Two options can be used to account for the removed load, *Airy Isostasy* and *Flexural Isostasy*. Airy isostasy assumes that the crust is supported by a fluid layer, similarly to ice cubes floating in water. Flexural isostasy on the other hand assumes that the crust is supported by an elastic plate of a determined thickness. An elastic thickness of 1.5 km was used by Roberts et al. (2019) in 3D backstripping of the Northern North Sea. The same value was used for this study. However, this value was calibrated for the syn-rift/ early-post-rift history, when stratigraphic loads had a short wavelength and results in a value almost equal to Airy isostasy. Late post-rift loads have long wavelength deformation, which is better represented by larger elastic thickness. Despite the elastic thickness being too low, the short length of the section means there is a limited effect on the restored geometries, where the relative relationship between stratigraphic units is key.

1.4.2 2D Unfolding

Two options are available to unfold a section in Move: *simple shear and flexural slip*. The unfolding option allows interpreted horizons to be restored to a pre-deformed stage, assuming horizontal sedimentation infill at the time of deposition.

Simple shear enables vertical or inclined unfolding of horizons (Fig.14A). The method uses an algorithm which is best suited for flattening a gentle dipping regional surface. Unfortunately, line length is not preserved with this algorithm, hence area is neither preserved. To preserve line length and area, *flexural slip* is more useful (Fig.14B). *Flexural slip* rotates the limbs of a fold on each side of a pin located at the fold hinge to a specified regional level. Then, layer-parallel shear is applied to the fold limbs in order to remove the effects of the flexural slip component of folding. The process maintains bed thickness, unlike simple shear. The *flexural slip unfolding* method is often used when there are complex deformations present, such as in thrust belts or areas of extensive salt structures (Move manual, 2019).

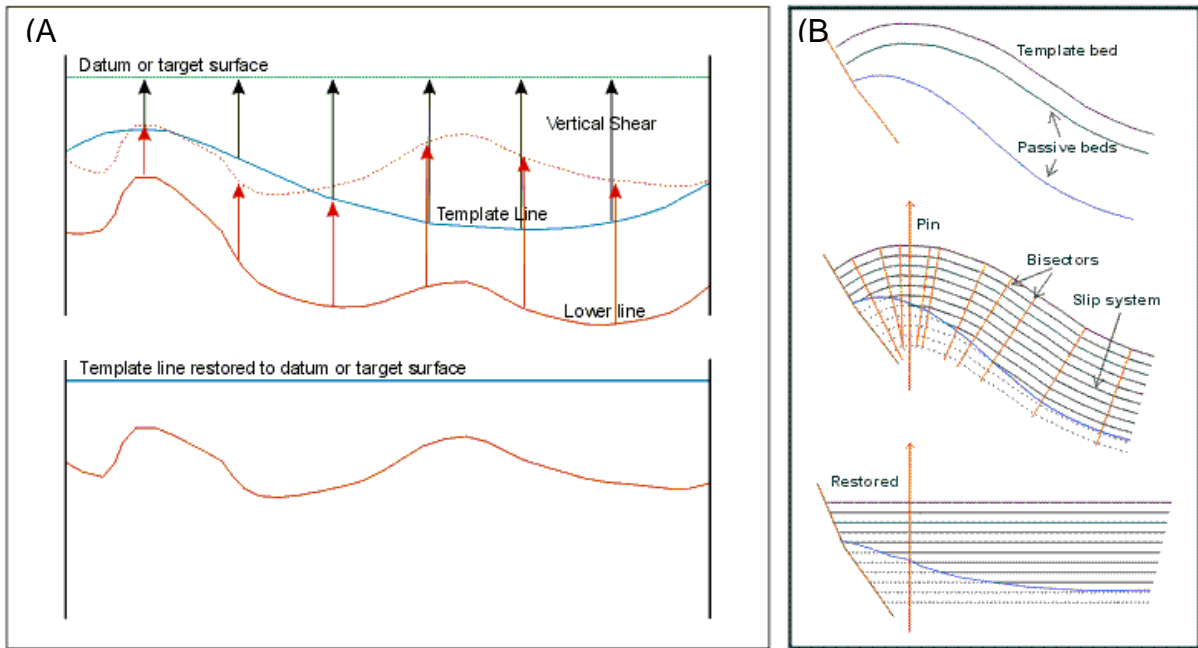


Figure 14. A: Simple shear principle. B: Flexural slip principle. (from Move manual, 2019)

1.4.3 Move-on-fault

Fault restoration was done with the *2D Move-on-fault* tool in Move, which provides several methods to control the deformation along the fault. For extensional regimes, where rollover anticline structures develop on listric normal faults, the *simple shear* algorithm is the most suitable.

Another method which was used is *elliptical fault flow*. This algorithm allows to interactively change fault displacement with time. This helps validate interpretations and restore faults with variable displacement. Standard methods require fault offsets to remain constant or increase with depth, while *elliptical fault flow* generates a variable displacement profile along the fault plane which can be adjusted by the user (Fig. 15).

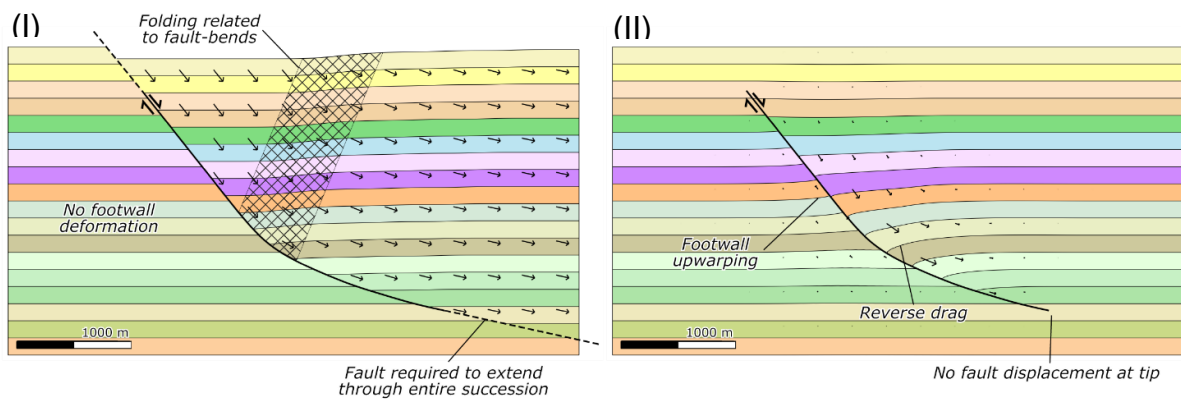


Figure 15. Two forward models: (I) Simple shear with a shear angle of 60 degrees; (II) Elliptical Fault Flow with the largest displacement at the fault centre. (from Move manual, 2019)

2 Geological Setting

2.1 The Central North Sea

The Central North Sea is located over the central part of the North Sea rift system and has the overall characteristic of a symmetric graben (Fig.16). The basin was formed by two main episodes of extension, the Permian-Triassic and the Late Jurassic-Early Cretaceous rifting. Salt movement, basin subsidence and post Jurassic to Paleogene inversion later reorganized the basin (Fig.17).

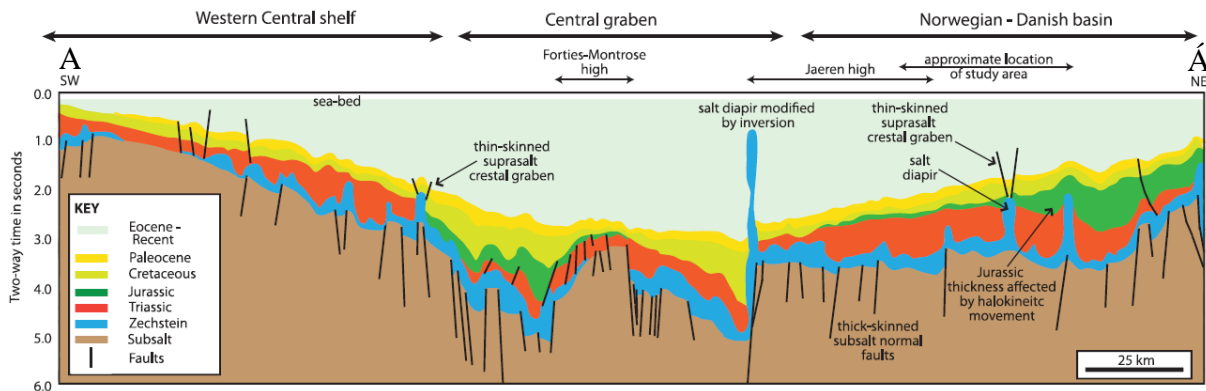


Figure 16. Regional cross section across the Central North Sea. Location of the section is shown in figure 1 (A-A'). (from Zanella and Coward 2003; and Mannie et. al. 2014)

2.1.1 Permian – Triassic rifting

The Permo-Triassic faults generated in the Central North Sea were produced by reactivation of pre-existing structures and generation of intra-Triassic faults (Fig 18). During the NE-SW trending Early Permian rifting phase, non-marine sediments of the Rotliegend Group were deposited under arid conditions in a laterally extensive basin, the North Permian Basin, which was located to the north of the Caledonian mid-North Sea High. Rifting was accompanied by subsidence, marine flooding and deposition of thick Zechstein evaporites (Ziegler, 1990). These evaporites mostly consist of gypsum and halite (salt), but they can also contain denser rock types. Carbonates formed at the basin margins and more halite-prone sediments were deposited towards the basin center.

The Triassic basin-fill consists of the shale-prone Smith Bank Formation and the overlying sandier succession of the Skagerrak Formation. The control of sediment input by salt structures are reflected by the sediment pathways within the Lower Triassic. Here, sediments are observed to accumulate in minibasins where salt evacuated (McKie, 2014). These Triassic intervals experienced thin-skinned deformation, where normal faults detached from the top salt interface

near the basin center. At the basin-margins, NW-SE orientated soft-link deformation offsetting the Zechstein evaporites was common (Zanella and Coward, 2003).

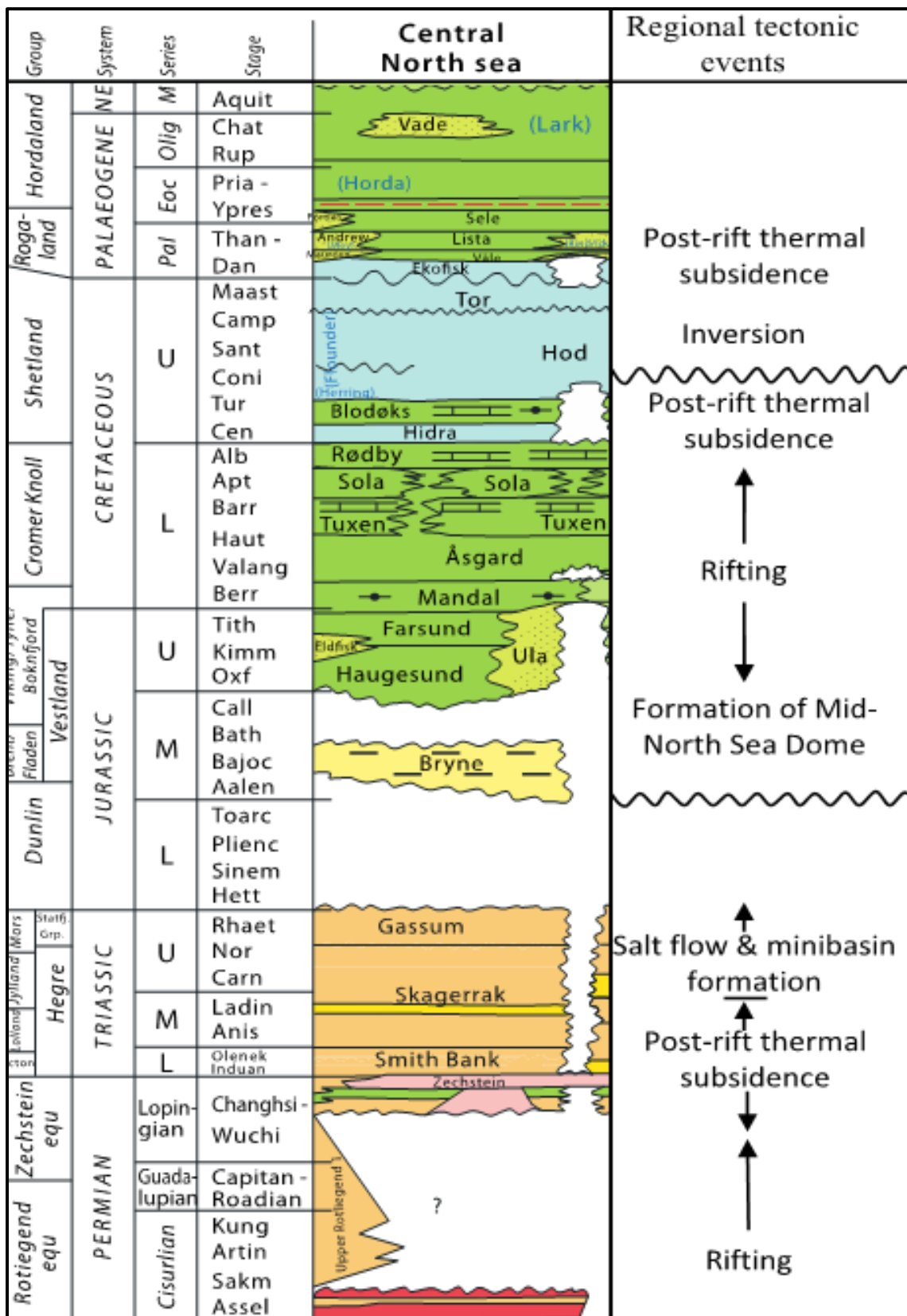


Figure 17. Lithostratigraphic chart with regional tectonic events in the Central North Sea (modified from NPD fact pages and Tvedt et. al. 2013)

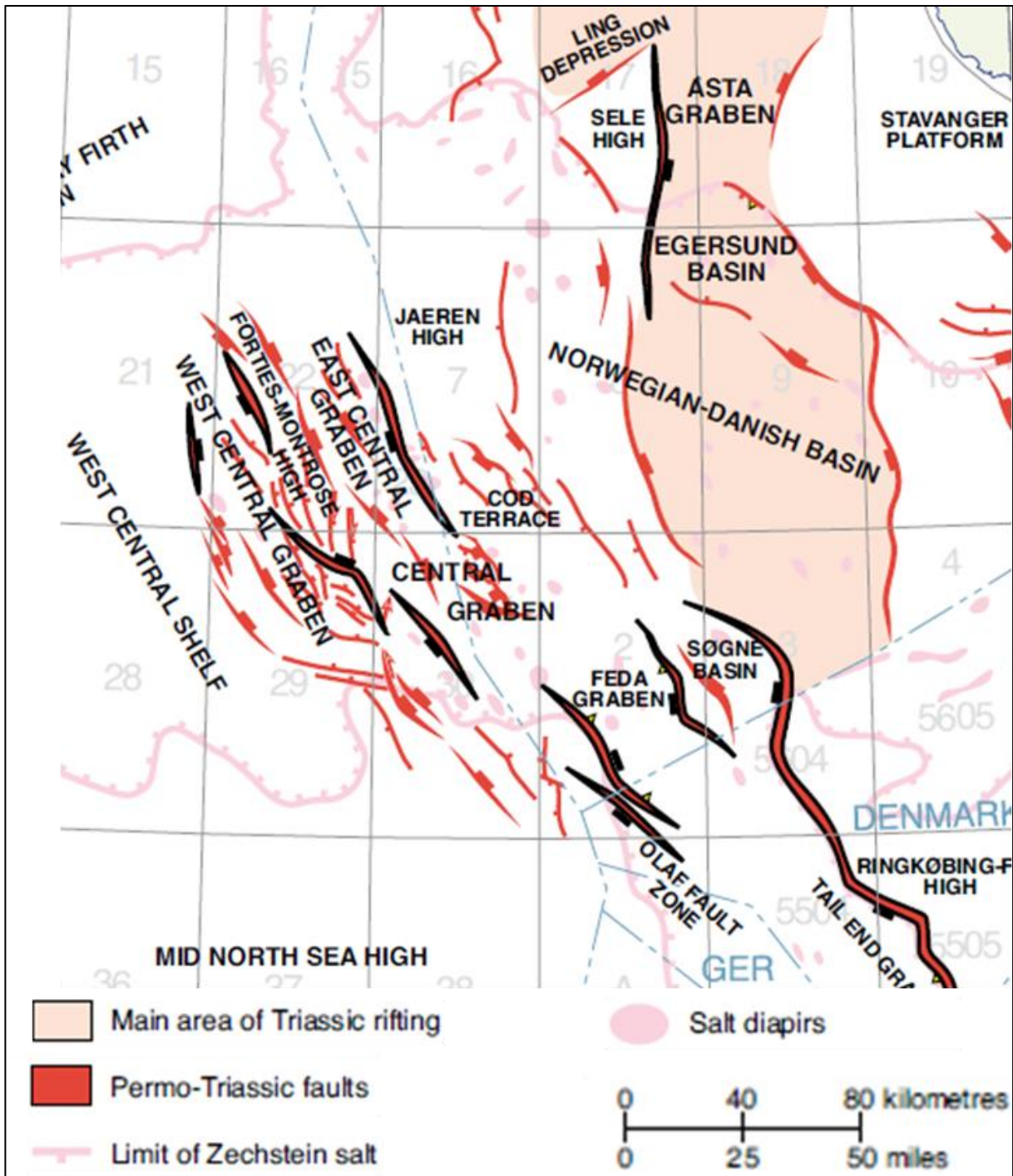


Figure 18. Triassic rift fault patterns of the North Sea. (from Zanella and Coward, 2003)

2.1.2 Middle Jurassic thermal doming

The Middle Jurassic was predominantly a period of tectonic quiescence. However, stratigraphic gaps are present in the southern parts of the North Sea. This is explained by uplift from thermal doming of the North Sea, which resulted in poorly preserved stratigraphic units from the Lower and Middle Jurassic and possibly erosion of the uppermost Triassic and emergent Zechstein evaporites (Zanella and Coward, 2003; Mannie et al., 2014).

2.1.3 Upper Jurassic-Early Cretaceous rifting

Rifting during the Late Jurassic was initially oblique to the Triassic fault system with E-W extension (Fig.19). Later in the Jurassic – Early Cretaceous, an anticlockwise rotation of the rift axis was established, changing the rift direction to ENE-WSW (Fig. 19) (Erratt et al., 1999). Extension caused renewed growth of basement-involved faults, tilting of fault blocks and faulting of the supra-salt sediments. Topographic highs bounded by large faults, enabled salt flow and diapir growth (Jackson and Larsen, 2009; Lewis et al., 2013; Tvedt et al., 2013; Jackson and Lewis, 2016). Highs were a source for sediment to be deposited in the adjacent basins, while less pronounced footwalls provided less sediment. The extension was separated by periods of tectonic quiescence, which influenced sediment influx (Coward et al., 2003). Additionally, extension could have triggered collapse of some diapirs generating local depocenters (Karlo et al., 2014; Mannie et al., 2014). On a regional scale, this second extensional phase led to subsidence with related transgression and deposition of syn-rift shallow marine sediments in the basin (Stewart, 2007).

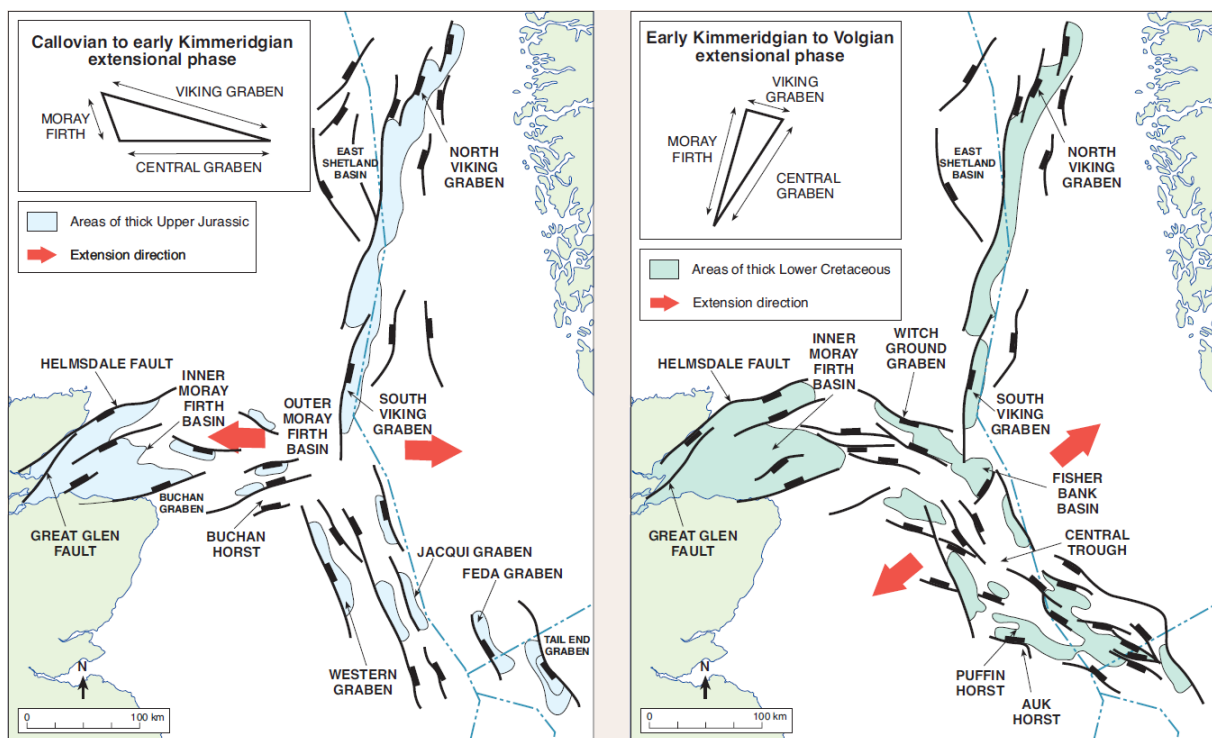


Figure 19. Jurassic to Early Cretaceous extension phases; Left map: Callovian to early Kimmeridgian extension, Right map: Early Kimmeridgian to Volgian extension. (after Erratt et al. 1999)

2.1.4 Early Cretaceous: Early post-rift

The Upper Jurassic shallow marine sandstones were sealed by deeper marine sediments of the Upper Jurassic-Early Cretaceous organic-rich Kimmeridge Clay Formation. This occurred as rifting ceased and sea level rose with the onset of passive thermal subsidence (Coward et al.,

2003). The Kimmeridge Clay does not only act as a seal, but it is the main source rock in the North Sea (Eriksen et al., 2003). Sediments continued to fill the basins onlapping and covering uplifts, with additional salt-controlled fault reactivation in the Early Cretaceous. These basins were later overprinted by renewed salt growth and tectono-eustatic events (Coward et al., 2003).

2.1.5 Late Cretaceous: Late post-rift & CNS inversion

During the Late Cretaceous, laterally extensive chalk was deposited throughout the North Sea. The chalk is observed to thin against the crest of major salt structures and re-deposit away from structural highs due to gravity sliding, as the salt structures grow with sediment deposition (Hodgson et al., 1992).

Diapir growth can be linked to compressional pulses. The Alpine orogeny and the opening of the North Atlantic during the Late Cretaceous – Paleogene, led to inversion and reactivation of basin-bounding normal faults (e.g. Growers et al. (1993); Ziegler (1990)) and the rejuvenation of pre-existing salt structures (Stewart, 2007). This event formed salt-cored anticlines. An additional explanation for shortening can be linked to the onset of the Africa-Iberia-Europe convergence, which is unrelated to the early Alpine orogeny (Kley and Voigt, 2008).

2.1.6 Paleogene and Neogene: Intra-cratonic basin w/inversion

During the transition Paleocene-Eocene, continental break-up and initiation of the Norwegian Sea began as Greenland drifted from the Norwegian margin. This introduced a new stress field to the entire region as seafloor spreading continued and oceanic crust formed. Compressional deformation from this period has been identified in the northern and mid North Sea (Coward et al., 2003). Additionally, the area experienced contraction in the late Eocene to Oligocene related to the Pyrenean – Saviian tectonic phase (Knox et al., 2010).

2.1.7 Quaternary: Subsidence, sediment loading and halokinesis

The Late Cenozoic was a period of steady subsidence, combined with a large amount of sediments from the uplifted basin margins, which led to thick sediment accumulations. High sedimentation rates drove available mobile salt (halite) towards established structures, similar to Harding et. al. (2015) in the Netherlands and the southern North Sea.

3 Database and Methodology

3.1 Approach

This thesis comprises several interpretation and seismic analysis steps. First, the focus is directed to a semi-regional scale covering the entire study area. In this step the integration between seismic data, well data and regional geological knowledge is important. Before interpreting, it is necessary to evaluate which horizons and fault families are of geological importance to accomplish the established objectives. A set of stratigraphic intervals was chosen and interpreted over large parts of the data (Fig. 20A). These were selected based on regional significance and quality of reflectors. Secondly, to investigate the local impact of salt tectonics, four structures were selected based on their structural style and structural evolution. This work required the use of the geological modelling software Move, which allowed restoration of the structures to illustrate and test models for their evolution.

3.2 Dataset

AkerBP ASA provided access to well data and seismic surveys (courtesy of Petroleum-Geo Services, PGS), covering the study area.

3.2.1 Seismic data

The seismic data for this thesis consists of four 3D seismic surveys of high- to moderate-quality; PGS16008CGR, MC3D-JHUN99-R09, MC3D-Q8-2008 and CE1202R15 (Fig. 20A). All of the surveys are in time. PGS16008CGR is a full-stack dataset which was processed to remove multiples. This is helpful in many areas; however, it can also weaken primary reflections in the Triassic interval. For this thesis the data quality of the Triassic interval is less critical than in the post Triassic successions, as these successions are the main focus. Also, this cube has a better image of the reflectors near the diapir flanks and has a vertical resolution between 20 and 40 m in the Mesozoic interval. MC3D-JHUN99-R09 and MC3D-Q8-2008, do not have the same quality. In these datasets, there is a higher abundance of multiples and generally more noise. For the fourth survey, CE1202R15, there are major pull-up effects related to salt. In areas where the salt has a large thickness, the sub-salt is pulled up generating artificial anticlines.

3.2.2 Well log data

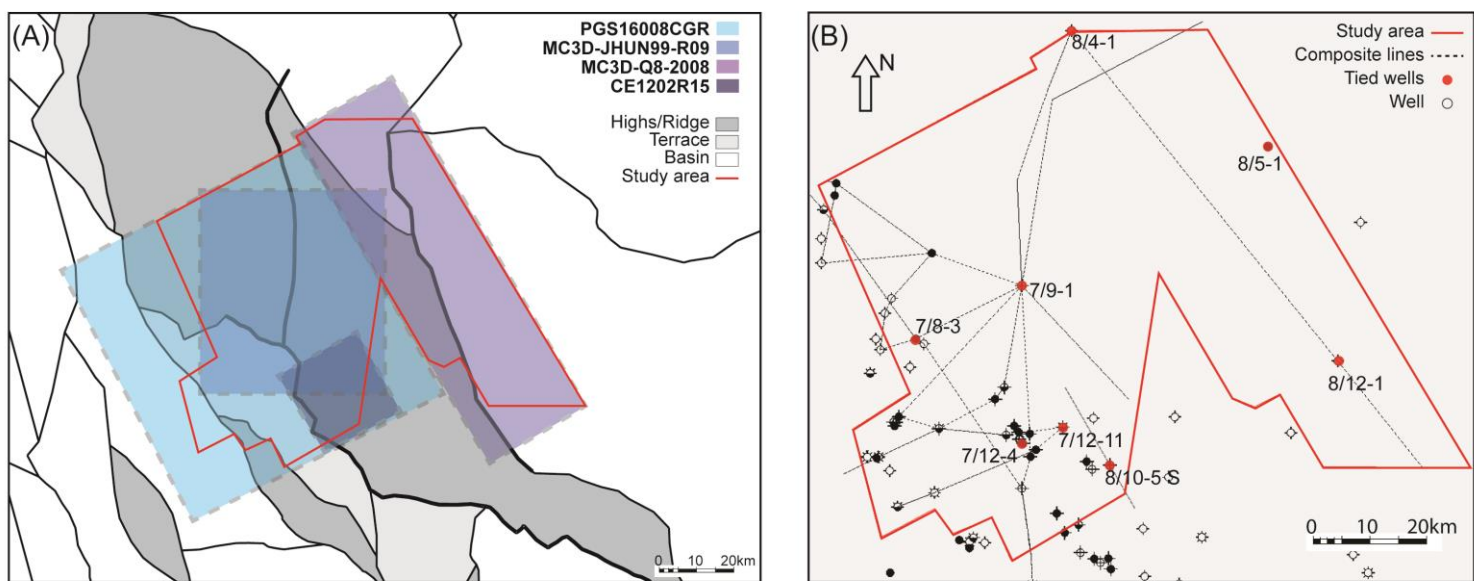
The available well database contains all public well data (wells drilled more than two years ago) within the study area and proximal to the outer boundary. This information includes well

reports, time-depth relationships (checkshots), wells logs (e.g. gamma ray (GR), sonic (DT), spontaneous potential (SP), density (RHOB), neutron (NEU), resistivity (RES) and caliper (CALI), and well-tops from NPD and internal AkerBP reports. Eight wells were selected based on their drilled depth and encountered intervals (Fig. 20B, red dots). These wells have available checkshots (time-depth relationship) The information from these wells was used to identify seismic stratigraphic levels. In addition, other wells were used to roughly QC interpretations throughout the seismic data. This was often done to validate the Top Zechstein (salt) pick.

3.2.3 Seismic well ties

All seismic surveys were tied to the selected wells, which ensure that the horizons were interpreted with consistency over the study area. For the chosen wells, a synthetic seismic section was generated based on a resampled acoustic impedance from the sonic log and the density log, together with a wavelet representing the character of the seismic survey (table in Fig.20). The wavelet was computed with a period of 128ms, sample rate of 2ms and central frequency of 25Hz (Ricker wavelet) symmetric about time zero, and zero-phase. For the MC3D-Q8-2008 dataset, a phase rotation of 180° was applied to match the SEG Y reverse polarity of the seismic.

Figures 21 and 22 show the well-tie result for well 8/4-1. This well is in the northern part of the study area in the MC3D-Q8-2008 seismic survey. For this well, a bulk shift of 25ms was applied, providing a reasonable correlation between the synthetic and the seismic reflection data.



Well name	Seismic survey	Polarity (SEG Y reverse or normal)	Seismic well-tie	Align points	Bulk shift	Stratigraphic interval (tied interval)	Drilled to
7/8-3	PGS16008CGR	SEG Y normal	Yes	Yes	---	Hordaland Gp - Zechstein Gp	Zechstein Gp (TVD=4320m)
7/9-1	PGS16008CGR	SEG Y normal	Yes	Yes	---	Shetland Gp Fm - Zechstein Gp	Zechstein Gp (MD=2931m)
7/12-4	PGS16008CGR	SEG Y normal	Yes	---	Yes, 20ms	Mandal Fm - Skagerrak Fm	Skagerrak Fm (TVD=3623m)
7/12-11	PGS16008CGR	SEG Y normal	Yes	---	Yes, 91ms (uploaded CKS had a shift that needed to be adjusted)	Balder Fm - Ula Fm	Skagerrak Fm (TVD=3864m)
8/4-1	MC3D-Q8-2008	SEG Y reverse	Yes	---	Yes, 25ms	Balder Fm - Zechstein Gp	Zechstein Gp (TVD=2631m)
8/5-1	MC3D-Q8-2008	SEG Y reverse	Yes	Yes	---	Balder Fm - Smith Bank Fm	Smith Bank Fm (TVD=2404m)
8/10-5S	CE1202R15	SEG Y normal	Yes	Yes	---	Hordaland Gp - Zechstein Gp	Zechstein Gp (TVD=2796m)
8/12-1	MC3D-Q8-2008	SEG Y reverse	Yes	Yes	---	Shetland Gp - Skagerrak Gp	Skagerrak Fm (MD=2875m)

Figure 20. Provided dataset, (A) Seismic coverage; (B) Well database and composite lines. Red dots are the selected wells. The table shows the well-tie information for these wells.

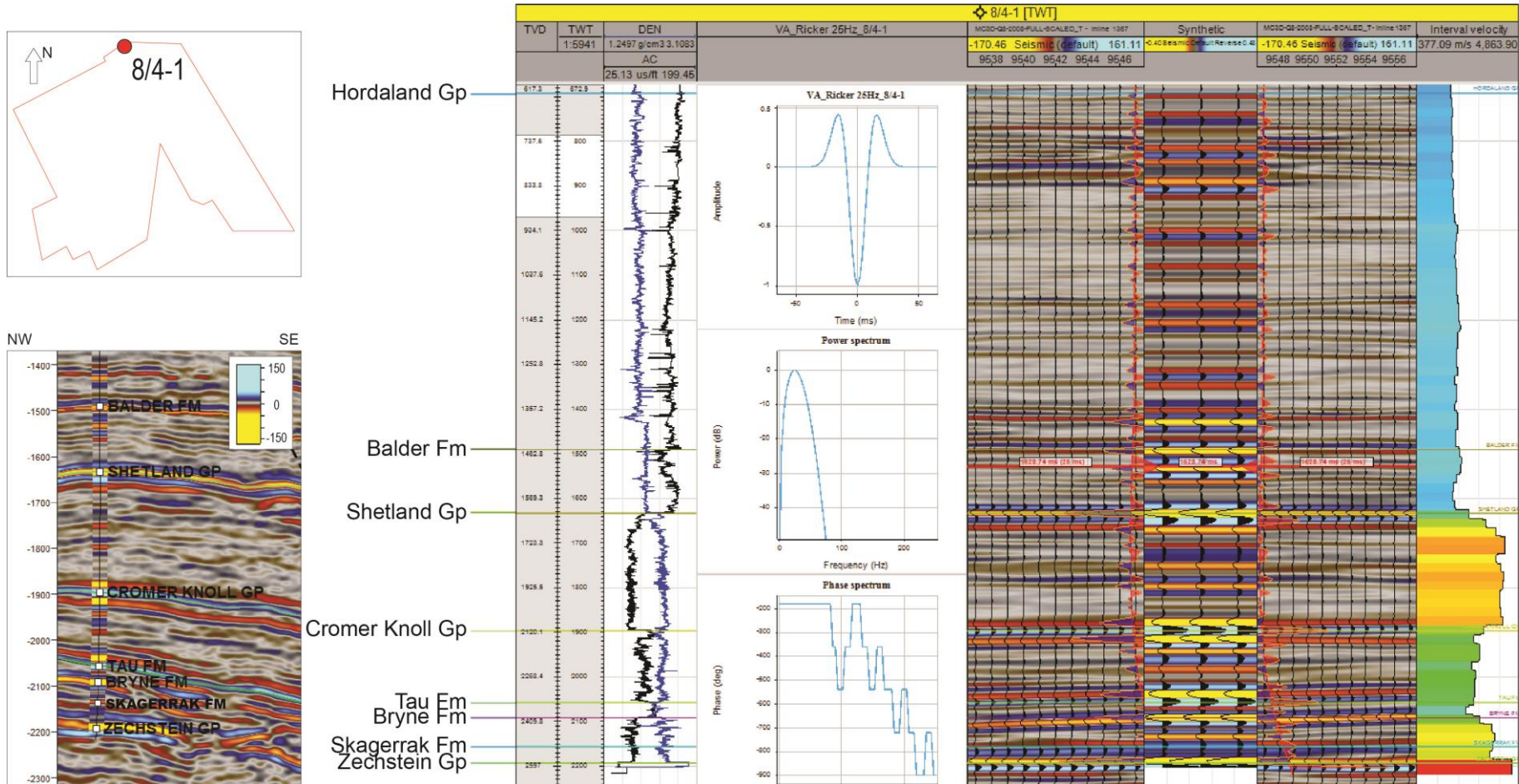


Figure 21. Seismic well-tie for well 8/4-1 in the MC3D-Q8-2008 seismic survey. A Ricker inverse wavelet and a 25ms bulk shift were applied.

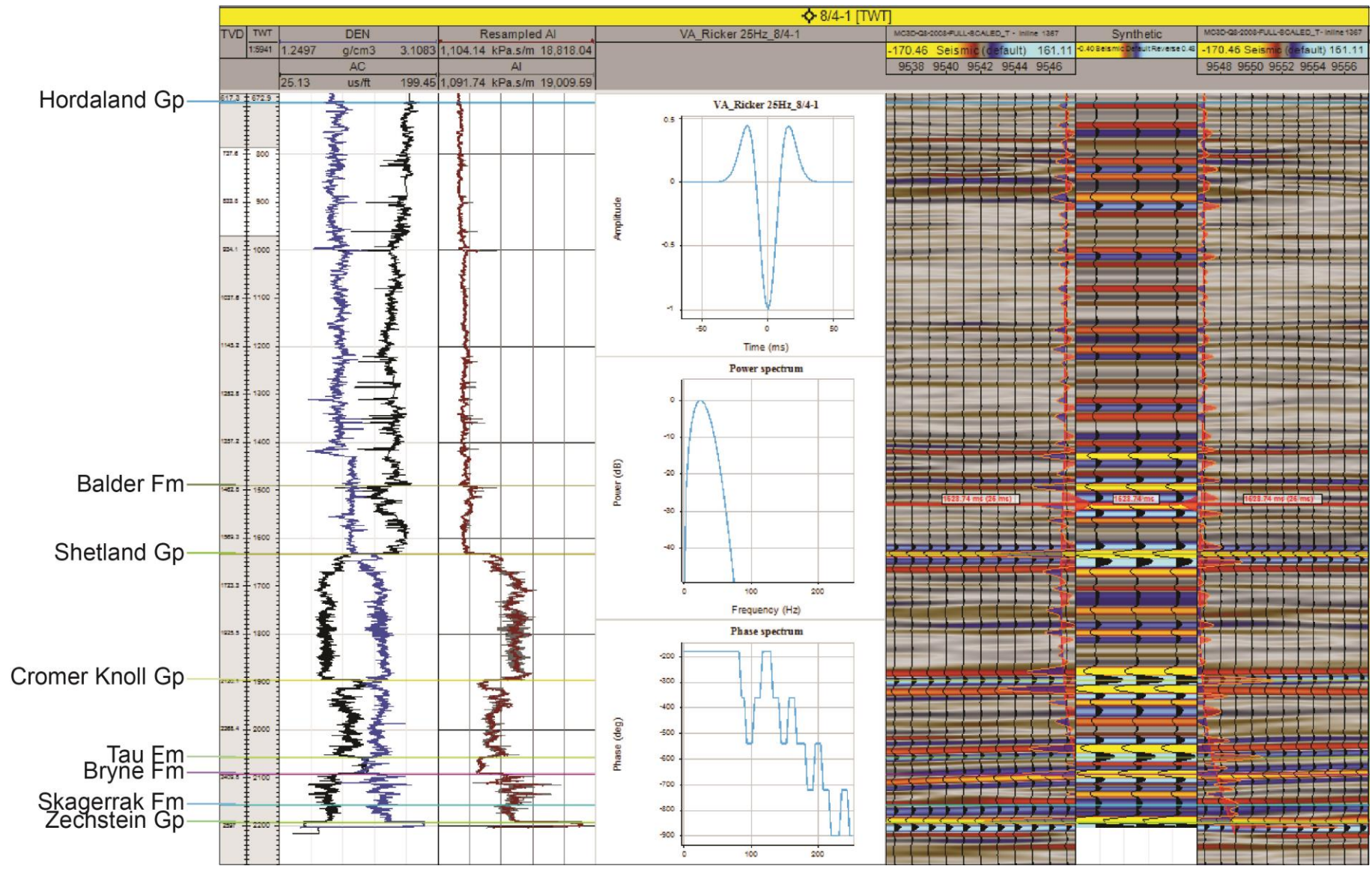


Figure 22. Seismic well-tie for well 8/4-1 in the MC3D-Q8-2008 seismic survey. A Ricker inverse wavelet and a 25ms bulk shift were applied. Resampled acoustic impedance (resampled AI) is shown together with measured acoustic impedance (AI).

3.3 Interpretation workflow

3.3.1 Semi-regional interpretations

Horizons

The 3D seismic reflection datasets were used to generate the structural framework by interpreting key horizons, sub-salt deformation and supra-salt deformation over a semi-regional area (Table. 2). The key horizons are confined to the Mesozoic and Cenozoic successions, but also contain the top and base salt, which are the Permian Zechstein Group and Rotliegend Group tops, respectively. The interpreted horizons and faults are highlighted in a representative cross-section across the PGS cube (Fig. 23). Here, the sub-salt deformation below the Top Rotliegend Group, salt distribution, Triassic minibasin geometries, and supra-salt structural relationships are shown.

Strategically positioned composite lines (cross-sections) were used to control the interpretations within and between seismic surveys (lines of sections are shown in Fig. 20B). However, there are few wells placed in the Triassic minibasins (pods) or drilled to top Zechstein Group. The interpretations of Intra-Triassic, Top Zechstein Group and Top Rotliegend Group, are therefore dependent on the seismic character of their reflectors. Table 2 shows the seismic character that was used for the interpretation of these reflectors. It is also important to emphasize that the Top Zechstein Group has a highly variable top pick, changing from a continuous strong amplitude on an increasing acoustic impedance reflector, to a shift in polarity, and further to a chaotic response near the diapir flanks. The seismic character of this reflector is linked to the physical properties within the salt body, which can vary in terms of mineral composition, as well as deformation caused by salt movement.

Faults

Sub-salt faults and supra-salt faults were mapped in 3D. The structures were first mapped roughly on seismic inlines and crosslines by generating coarse-gridded fault planes. Then, detailed mapping of each fault was done to make sure the fault traces were correctly aligned. After the faults were mapped out, polygons (cutoffs) for each fault were generated for the Top Rotliegend Group and Base Cretaceous Unconformity. This was not done for the overlying horizons. Instead, maps illustrating the magnitude of supra-salt deformation during the Cenozoic are provided.

Attributes

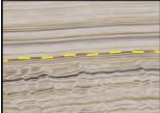
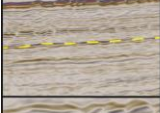
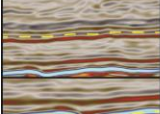
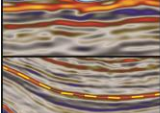

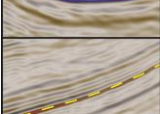
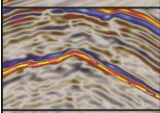


To highlight the impact of supra-salt deformation, the variance attribute was applied to the top Rogaland Group and the top Hordaland Group. The variance attribute is used to investigate the lateral similarity/continuity of waveforms or traces along an interpreted horizon. Variance is defined as one minus correlation (100% correlation = 0), which means that areas where the reflector is continuous will plot close to zero, while a break in the reflector will plot closer to one. These values are illustrated on maps, where white is close to zero (good lateral reflector continuity) and black to red is closer to one (poor lateral reflector continuity). The areas showing poor lateral continuity (high variance) are linked to deformation of the reflector due to faulting, folding or salt movement.

Generation of Time-Structural and Time-Thickness Maps

Structure maps are generated based on interpretations of the key horizons in time. These maps include fault gaps and structural relief of each interpreted horizon. For the Top Rotliegend Group and Base Cretaceous Unconformity, a variance attribute was applied. This enhances the sub-salt and supra-salt- deformation, making it easier to adjust and control fault polygons.

The structural maps made from the interpretations define the spatial relationship between pre-salt- and supra-salt- deformation and post-rift structures. Thickness maps between key horizons illustrate the tectono-stratigraphic evolution, based on lateral shifts of depocenters and thinning and thickening trends through time.

Table 2. Properties and seismic character of the interpreted reflectors.

Seismic character (PGS16008CGR SEGY-normal)	Horizon pick	Reflector strength & character <i>AI = acoustic impedance</i>	Presence near salt structures	Geological character <i>Lithostratigraphic Unit</i>	Seismic coverage
	Top Hordaland Group (Late Eocene ~ 14Ma)	Strong (AI increase), Continuous	Not present above major salt structures in the east	Post-rift High sediment infill, transport direction NE-SW	PGS16008CGR, MC3D-JHUN99-R09, MC3D-Q8-2008, CE1202R15
	Intra-Hordaland (Mid Eocene ~ 34Ma)	Medium (AI increase), Semi-continuous	Not present above major salt structures	Post-rift High sediment infill, transport direction NE-SW	PGS16008CGR
	Top Rogaland Group (Early Eocene ~ 56Ma)	Medium to strong (AI increase), Semi-continuous with polygonal faults	Not present above major salt structures	Post-rift Thin and variable group thickness	PGS16008CGR, MC3D-JHUN99-R09, MC3D-Q8-2008, CE1202R15
	Top Shetland Group (Early Paleocene ~ 61Ma)	Strong (AI increase), Semi-continuous with supra-salt normal faults	Group thinning above diapir crests - mass transport from highs	Post-rift, Top chalk group, change in depositional setting	PGS16008CGR, MC3D-JHUN99-R09, MC3D-Q8-2008, CE1202R15
	Top Cromer Knoll Group (Early Cretaceous ~ 100Ma)	Strong to medium (AI decrease) Semi-continuous with supra-salt normal faults	Group thinning above diapir crests	Early post-rift Siliciclastic deposition, onlapping and covering highs and filling local basins	PGS16008CGR, MC3D-JHUN99-R09, MC3D-Q8-2008, CE1202R15
	Base Cretaceous Unconformity (~ 145Ma)	Strong (AI decrease) Continuous, base post-rift, with supra-salt normal faults	Variable thickness above diapir crests	Intra-syn-rift Kimmeridge Clays: main North Sea source rock	PGS16008CGR, MC3D-JHUN99-R09, MC3D-Q8-2008, CE1202R15
	Intra-Triassic (~ 200Ma)	Medium to weak (AI decrease) Semi-continuous with rift related normal faults	Not present or very thin above salt structures	Early salt movement, focussed infill with minibasin geometries	PGS16008CGR
	Top Zechstein Group (Late Permian ~ 251Ma)	Variable, AI increase and decrease (Strong to weak)	---	Widespread evaporite deposition, contains clastics and carbonates, top salt interpretation	PGS16008CGR, MC3D-JHUN99-R09, MC3D-Q8-2008, CE1202R15
	Top Rotliegend Group (Late Permian ~ 265Ma)	Strong to medium (AI increase) Semi-continuous with sub-salt normal faults	Continuous, with pull-up effect below thick salt sequences	Pre-rift Sub-salt basin geometries	PGS16008CGR, MC3D-JHUN99-R09, MC3D-Q8-2008, CE1202R15

Salt interpretation; multi-directional tool

Traditionally, seismic interpretation is driven by acoustic impedance contrasts between stacked units as waves propagate into the Earth's interior. The top salt horizon is interpreted with a multi-directional tool (multi-Z) in Petrel, which fully captures the salt geometry (e.g. diapir overhangs). This approach is necessary due to variable top salt reflections, highly deformed strata surrounding the salt bodies, and the physical properties of salt. Therefore, the top salt interpretation was made by “freehand”, not following a continuous reflector, but rather along a likely top salt surface. The interpretation was converted to an *Editable triangle mesh*, which was adjusted and further reconstructed to a triangulated mesh surface (Fig. 24). Unfortunately, Petrel does not create contours on a triangle mesh surface. To solve this issue, the mesh was transferred Move, which enables a more illustrative way to present the top salt interpretation (Fig. 25). The three-dimensional top salt surface was used on a semi-regional scale to classify structures within the study area, as described in the first set of objectives.

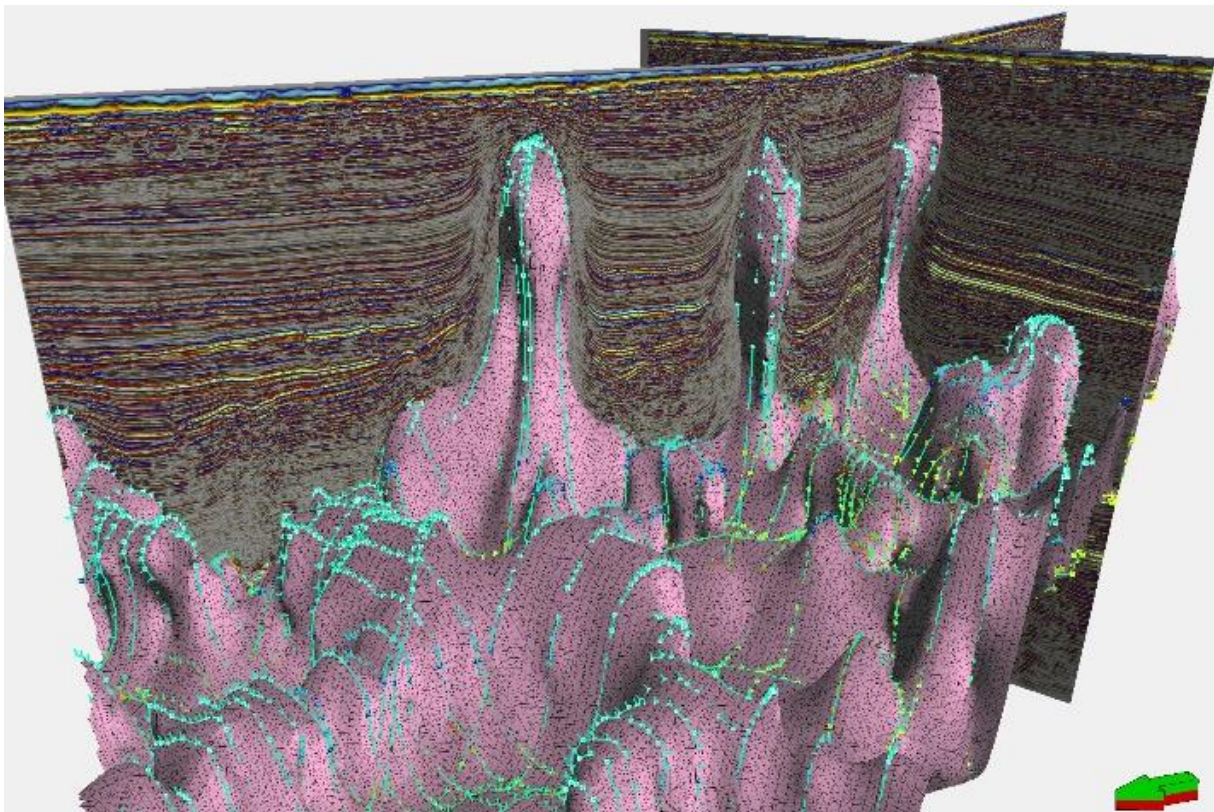


Figure 24. Multi-Z interpretation (light blue lines) with the triangulated mesh surface (pink) showing salt distribution on the Sørvestlandet High and basin margin salt stocks. From MC3D-Q8-2008 seismic cube. VE = 3

3.3.2 Local seismic interpretations

The second part of this thesis, (ii) *Evolutionary Model*, was carried out after interpretations of four key cross-sections (Fig. 25). Here, the semi-regional framework was adjusted where

necessary, and additional horizons and faults were interpreted on the sections. Also, strata-terminations were interpreted on the sections to get an idea of the main lithostratigraphic interval-characteristics. Onlaps, toplaps, truncations and thickness variations were the observations made during this step. This provides insight to the structural evolution before performing the restorations.

3.4 Restoration workflow

Figure 26 summarizes the restoration workflow. The interpretations were transferred from Petrel using the *Move Link for Petrel* tool, which moves the seismic sections, wells, horizons, triangle mesh and faults directly into Move. A stratigraphic framework was established with rock properties (Table 3) and compaction curves representative of the area (see Appendix).

Table 3. Lithological units and their assigned properties.

Lithological unit	Colour	Assigned lithology	Approx. Age (Ma)	Sst %	Shale %	Limest. %	Initial Porosity	Depth coefficient (1/km)
Seabed	Yellow	ShalySand	0	5	95	0	0.56	0.39
Hordaland Gp	Orange	Shale	14	0	100	0	0.63	0.51
Intra Hordaland Gp	Light Orange	Shale	34	0	100	0	0.63	0.51
Balder Fm	Dark Orange	Shale	56	0	100	0	0.63	0.51
Ekofisk fm	Light Green	Limestone	66	0	0	100	0.41	0.40
Cromer Knoll Gp	Green	Shale	100	0	100	0	0.63	0.51
BCU	Blue	Shale	145	0	100	0	0.63	0.51
Top Res	Dark Blue	Sandstone	146	100	0	0	0.49	0.27
Base Res_Near Top Trias	Purple	ShalySand	201	5	95	0	0.56	0.39
Base Res	Light Purple	ShalySand	230	5	95	0	0.56	0.39
Salt	Pink	Salt	251	-	-	-	0	N/A
Rotliegendes	Brown	Default	265	5	95	0	0.56	0.39

The next step was to collect the surfaces and faults intersecting the seismic section, this generates fault sticks and polylines attached to the section. These fault sticks and polylines were checked for errors in the interpretation, and adjustments were made where needed. Then, the polylines were resampled at 50 m interval and polygons were constructed. Once the section was filled with the interpretations, it was converted to depth following the time-to-depth relationship for the 7/12-13S well and lowermost part of the 2/1-7 (see Appendix I). This last well was drilled through 752 m of Zechstein evaporites, providing information on velocities in the deeper part of the basin. The depth-conversion can also be done using interval velocities assigned to their respective polygons (e.g. applying a constant velocity for the salt polygon). However, this did not provide a good result and therefore the simplest depth-conversion method using checkshots was used. After the seismic section and interpretations were converted to depth, each polygon was assigned to their correct stratigraphic units before starting the restorations.

The first step of the restoration process was to restore the compaction the units have undergone during burial. This was done as the uppermost layer is removed from the section and the underlying units expand, with a magnitude depending on their assigned compaction curve. All decompaction steps were run with flexural isostasy through two possible workflows: (1) compensating for flexural isostasy simultaneously with sediment removal and decompaction, or (2) calculating flexural isostasy for the load to be removed, then applying the isostatic response through a simple shear unfolding procedure after the sediments are removed and decompacted (Fig. 27). This second option is useful when the load of a specific interval cannot be removed in one operation but requires several decompaction steps.

The next step was to unfold the horizons below after the topmost horizon was removed. Unfolding was done with the flexural slip method, with a pin placed at the crest of the diapir or with two pins placed on the diapir flanks (Fig.28). The horizons were unfolded to their uppermost regional level. The regional level was dependent on the post-salt and sub-salt basin configuration. For instance, if the layers above the salt welds show no thickness variations, resembling a horizontal layer-cake model, the regional was placed along the top of the horizons. On the other hand, layers with thickening trends are linked to depletion of the underlying salt while sediments fill the basin. In this case, the chosen regional level was placed along a time-equivalent structural high, higher than the top growth horizons. The space generated beneath unfolded layer was filled with salt (e.g. Fig. 11B, “new” salt). Decompaction of the topmost layer and unfolding to the uppermost regional of the horizons below was run step by step until the deepest horizon was brought to its regional.

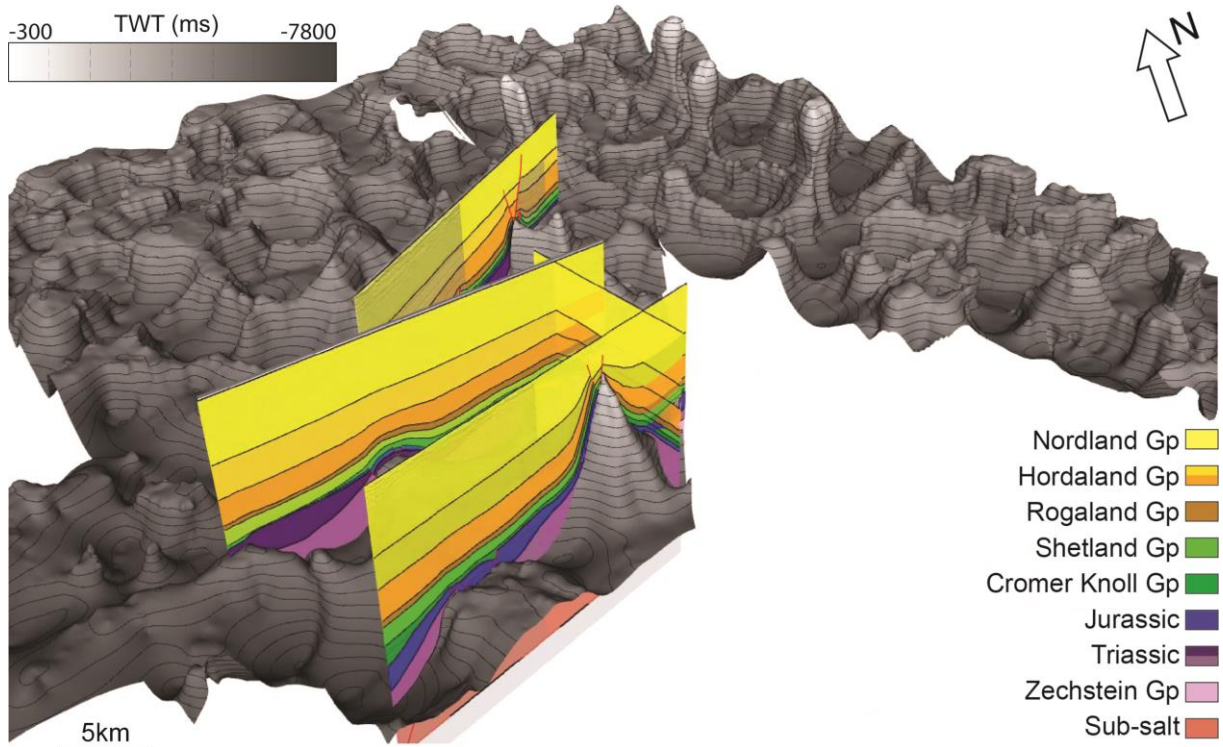


Figure 25. Top salt surface mapped in Petrel and imported into move. The four restored cross sections are shown. VE = 2.5

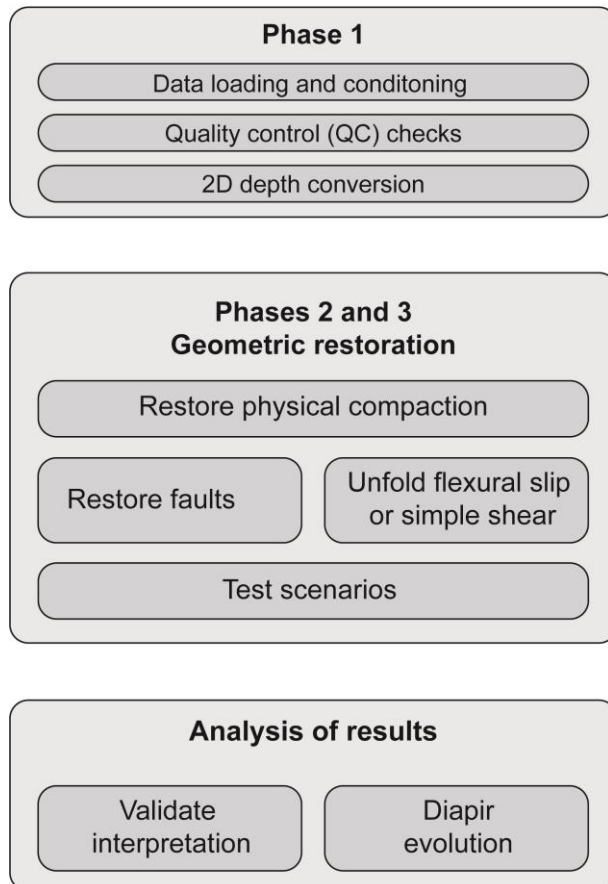


Figure 26. Sequential restoration workflow. Made after Rowan (1993) and steps from the move manual.

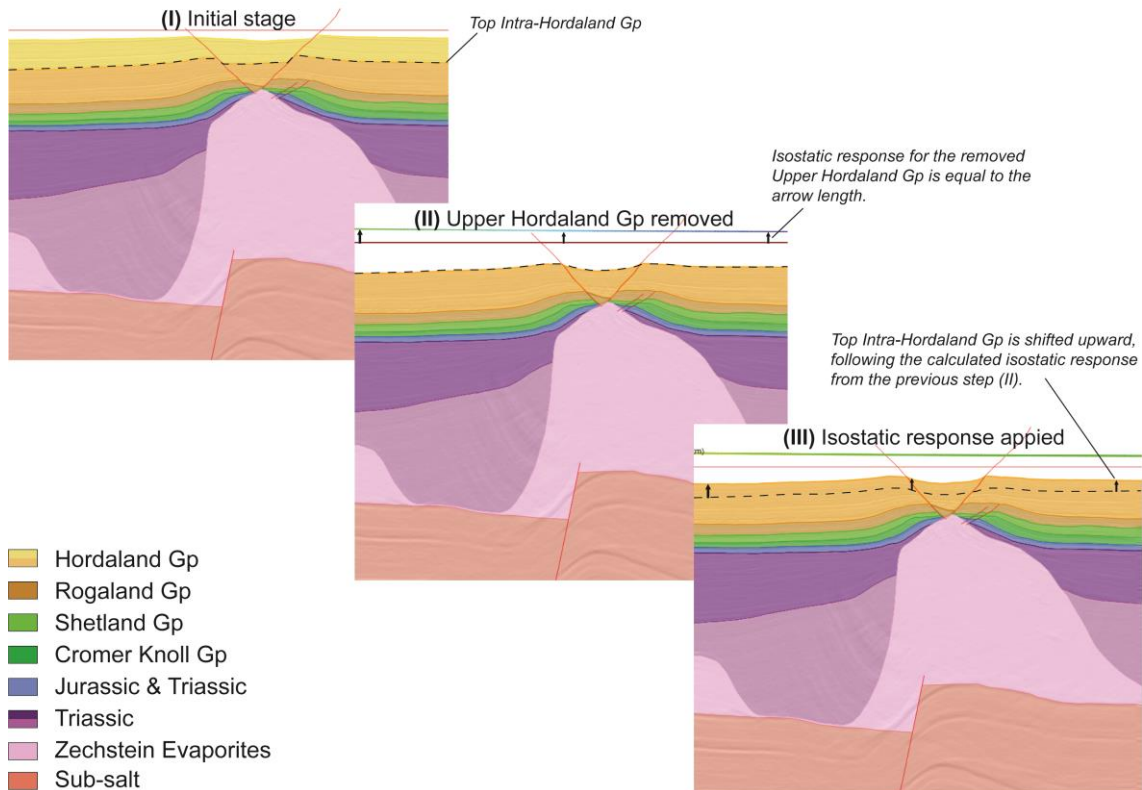


Figure 27. Flexural isostasy workflow, shown through three steps. In the uppermost section nothing is removed, while in the middle section the upper part of Hordaland Group is removed. Isostasy is not included until the lowermost figure. Here, the dashed line represents no flexural relief after removal of the top load.

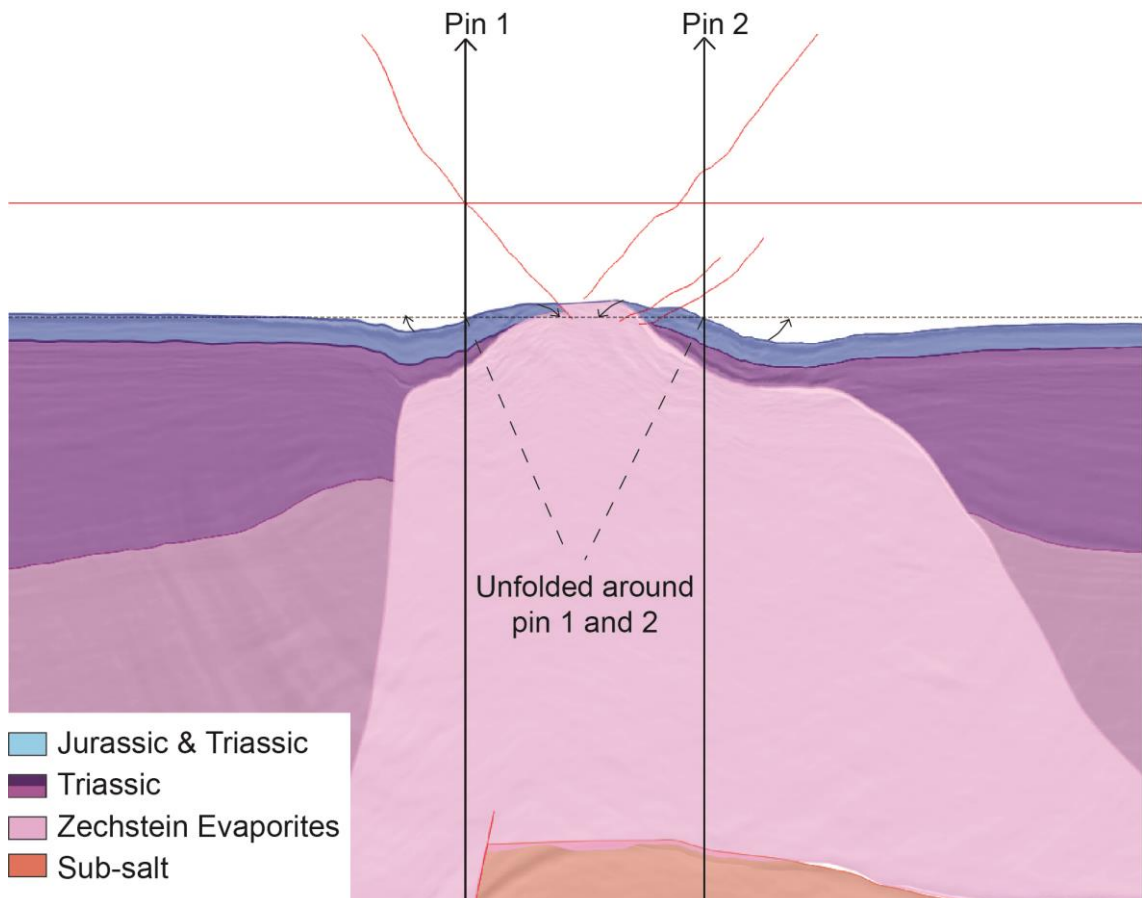


Figure 28. Two-pin unfolding procedure, using flexural slip. The layers on each side of the structural crest are rotated around their assigned pin. (pin 1 = left side, pin 2 = right side)

4 Results

4.1 Semi-regional (Structural Framework)

This chapter describes the semi regional structural elements included in Figure 2: (BB) = Breiflabb Basin; (CT) = Cod Terrace; (HH) = Hidra High; (JH) = Jæren High; (NDB) = Norwegian-Danish Basin; and (SVLH) = Sørvestlandet High.

4.1.1 Permian

Rotliegend Group (265Ma)

Structural styles

In Figure 23, the top Rotliegend reflector lies directly above an evenly thick layer, with little to no thickening near the fault planes, and beneath a variable thickness cover of Upper Permian Zechstein evaporites. The top Rotliegend reflector has a strong continuous response with seismic “pull-ups”, commonly present where the Zechstein evaporites are thick. Therefore, the reflector has artificial topographic highs beneath the salt structures (Fig. 23).

The variance attribute map shows major structures trending NNW-SSE and minor NE-SW trends (Fig. 29A). These observations are simplified in figure 29B where the faults intersecting the base salt surface are mapped. The top Rotliegend Group is gradually deepening to the SW, but also has local deepening in the eastern and central part of the study area (Fig. 29C).

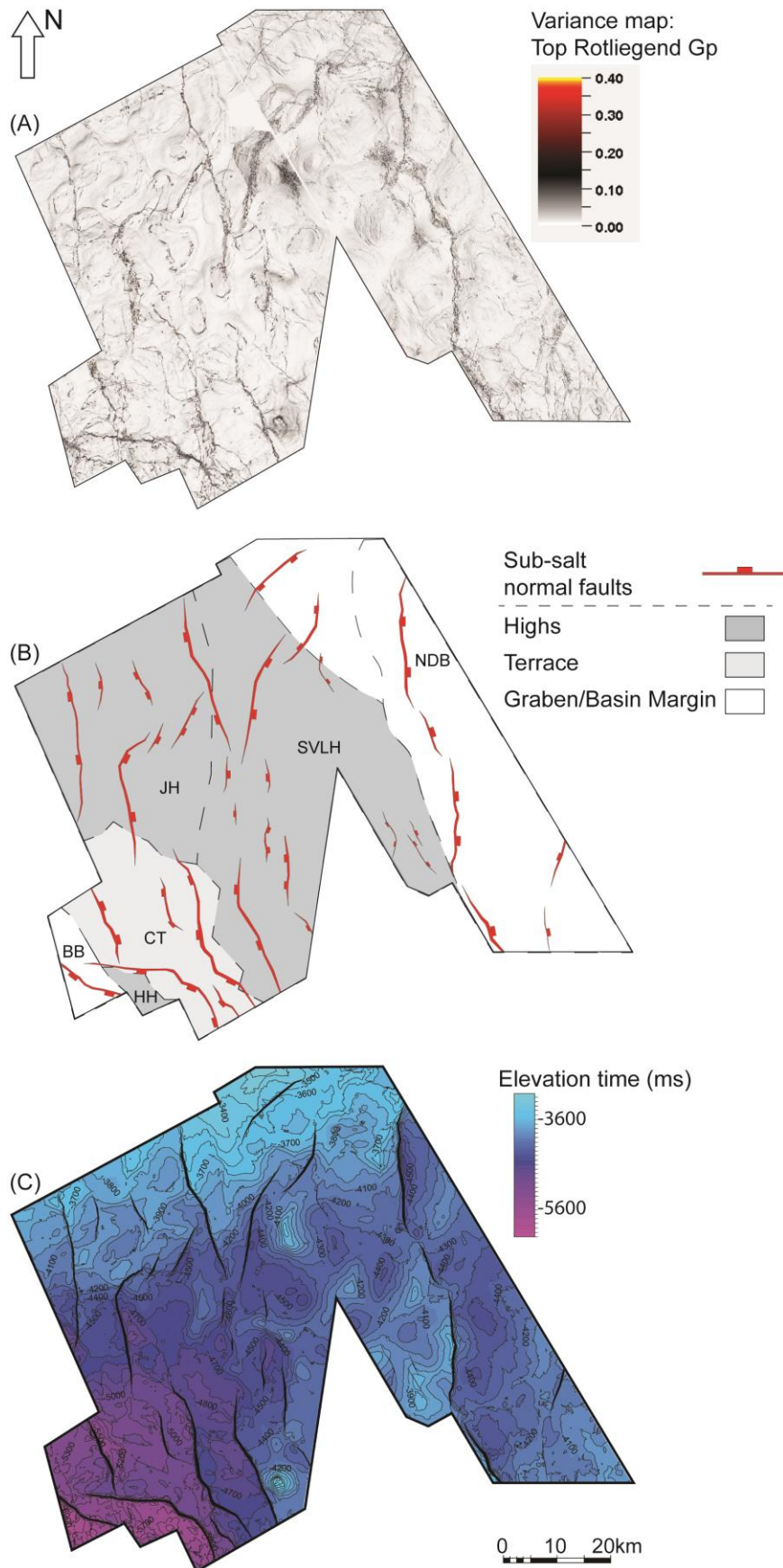


Figure 29. Top Rotliegend Group configuration: (A) Variance map. Dark to red areas indicate structures; (B) Main sub-salt normal faults. (BB) = Breiflabb Basin; (CT) = Cod Terrace; (HH) = Hidra High; (JH) = Jæren High; (NDB) = Norwegian-Danish Basin; and (SVLH) = Sørvestlandet High; and (C) Structure map.

Zechstein Group (251Ma)

Structural styles

The Zechstein evaporites are laterally connected, with exceptions of a few tall isolated salt structures (Fig. 30). Diapir overhangs are observed near these tall structures and a diapir north of the Oda structure (Fig. 30). This is illustrated on the E-W cross-section in Figure 23, where the tall diapir is almost pinched. In the following sections the distribution of salt across the basin will be described.

Eastern basin margin and highs

At the eastern boundary of the study area, i.e. NDB margin, elongated salt structures have a NE-SW trend towards the SVLH (Fig. 30, Zechstein trends). The minibasins adjacent to these salt structures follow this trend until reaching the three tall salt diapirs (Fig. 30). These diapirs are positioned on the footwall, west of the sub-salt normal faults, and almost pierce the seafloor (Fig. 32). They are linked together by narrow salt ridges and located on the transition between the NDB and SVLH. West from these structures, the diapirs and minibasins have a more random distribution, defining a new pattern of salt and minibasin geometries. However, the NE-SW trending salt structure intersecting the southern tall diapir continues with the same trend.

The structures on the SVLH are laterally connected with gentler and more symmetrically dipping diapir flanks. On the SVLH and JH, circular-shaped structures are also aligned N-S (Fig. 30, Zechstein trends). Their associated minibasins, directly north of Oda and Ula, are isolated by the N-S circular-shaped diapirs (Fig. 30). Across the northern limit of the study area, diapirs with steeply dipping flanks and semi-isolated minibasins are present (Fig. 30).

Terrace and southwestern basin margin

In this area, there is a structural shift from the JH and SVLH to the CT, observed by the change of salt structures with gentler dipping flanks. Salt does not pierce far into the overlying strata and the structures are buried deeper compared to the northern and eastern diapirs. To the southwest, along the hanging wall of the NW-SE striking sub-salt normal fault west of Tambar (Fig. 32), the top Zechstein Group increases in depth (Fig. 31).

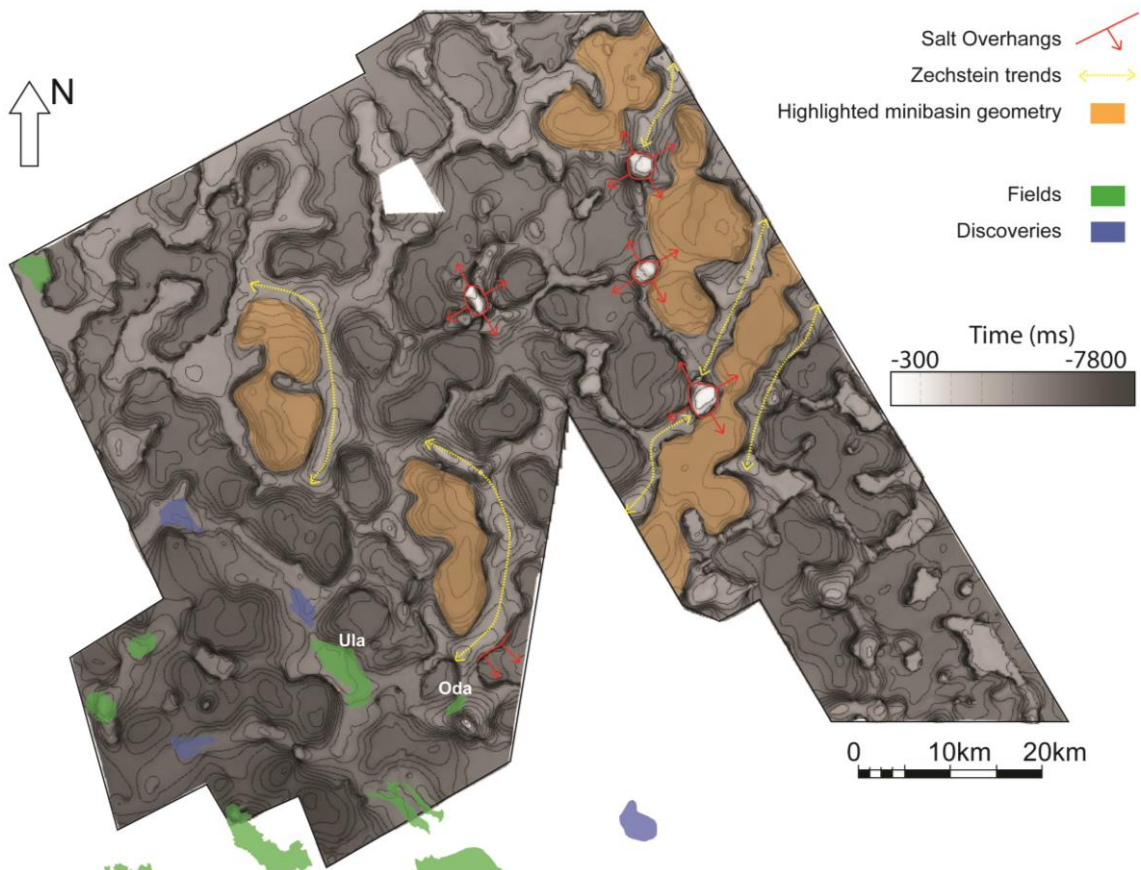


Figure 30. Top Zechstein interpretation with structural trends, showing three tall diapirs aligned on the eastern flank. Overlying fields and discoveries are included.

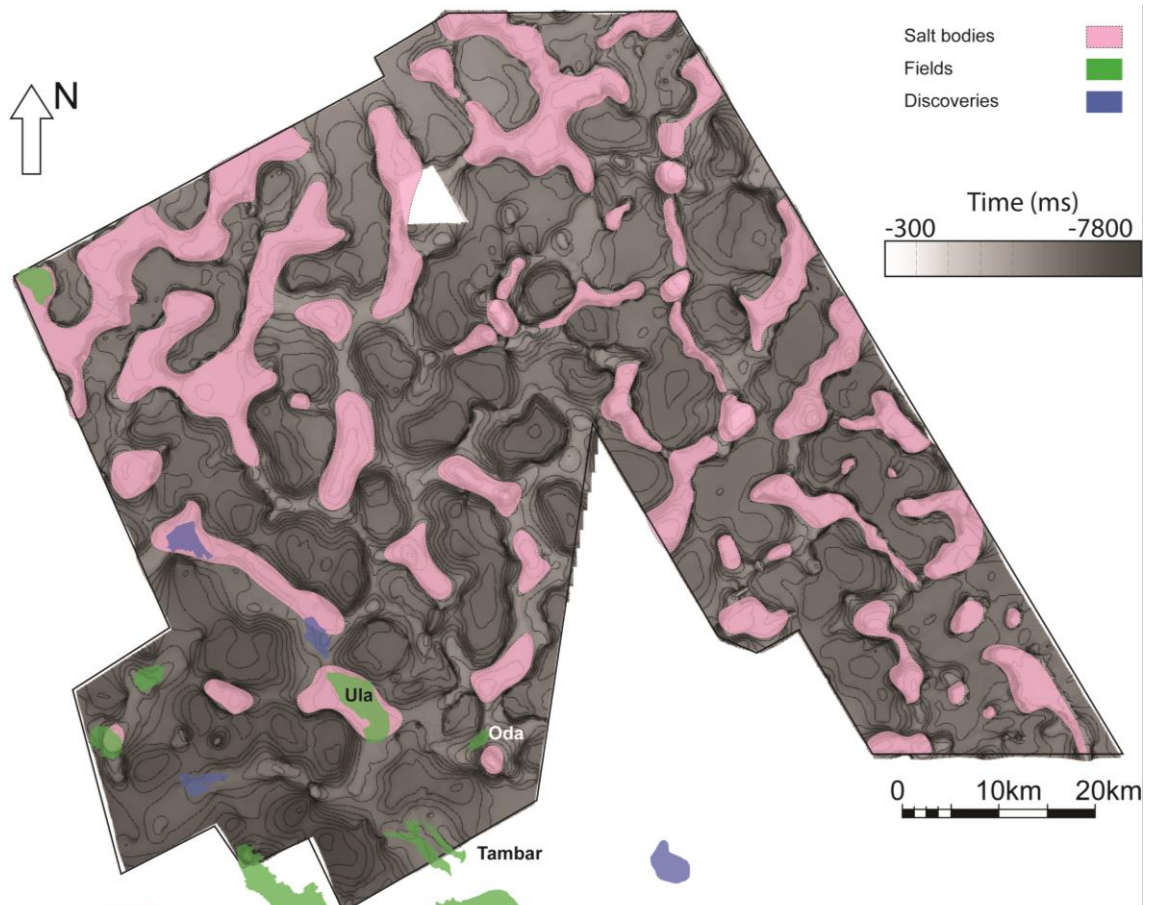


Figure 31. Top Zechstein Group interpretation, including main salt structures (pink).

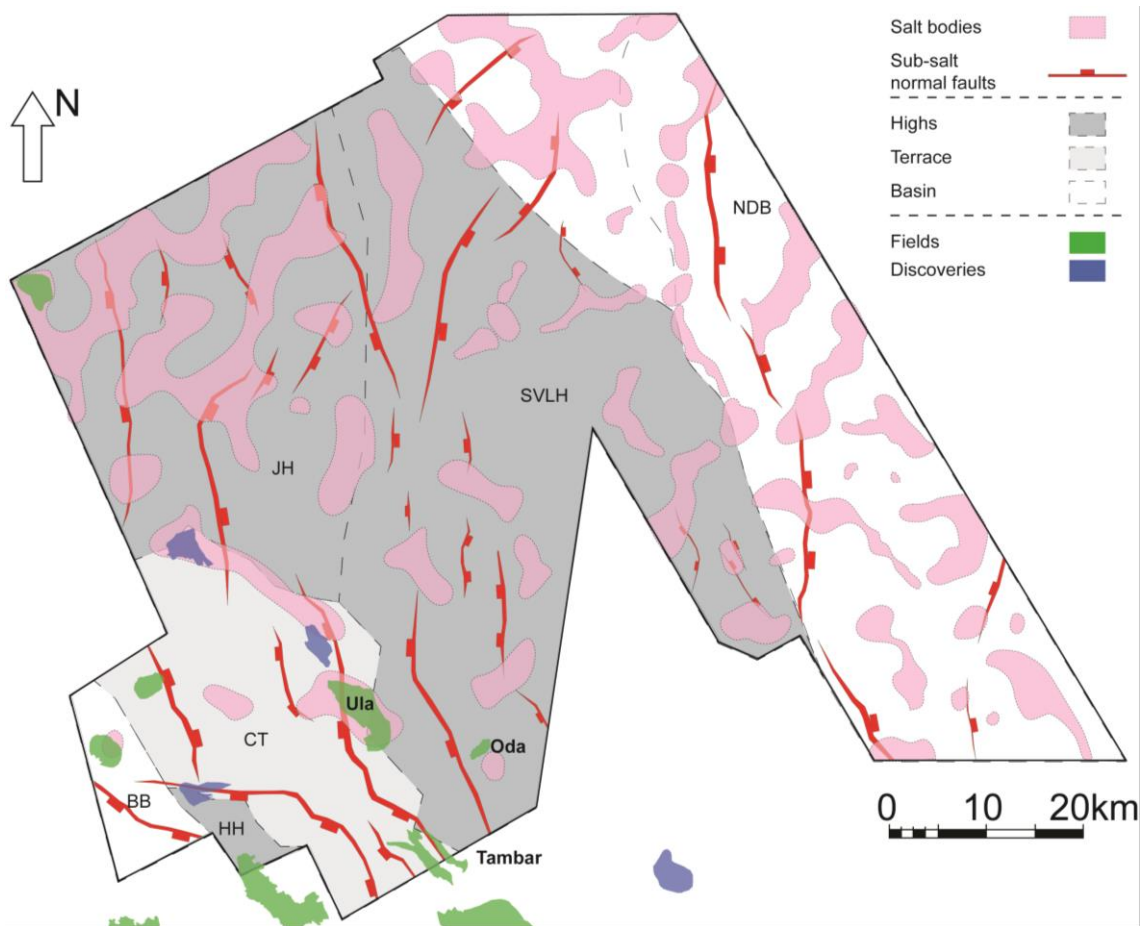


Figure 32. Sub-salt normal faults interpreted on top Rotliegend Group with overlying salt structures, field and discoveries. Structural elements include the (BB) = Breiflabb Basin; (CT) = Cod Terrace; (HH) = Hydra High; (JH) = Jæren High; (NDB) = Norwegian-Danish Basin; and (SVLH) = Sørvestlandet High).

4.1.2 Triassic and Jurassic

Structural styles and sediment distribution (145-251Ma)

The Jurassic interval is thin or absent throughout the study area and could therefore not be traced with great certainty, but it will be accounted for in greater detail during the local restorations. This also made interpreting the underlying Top Triassic boundary difficult as the seismic character will vary depending on the type of strata present. Thus, an intra-Triassic reflector was traced within the Triassic minibasins in a limited area constrained to the PGS16008 seismic survey. Above the crest of the salt structures where the Triassic is absent, the horizon was merged with the top Zechstein group (Fig. 33).

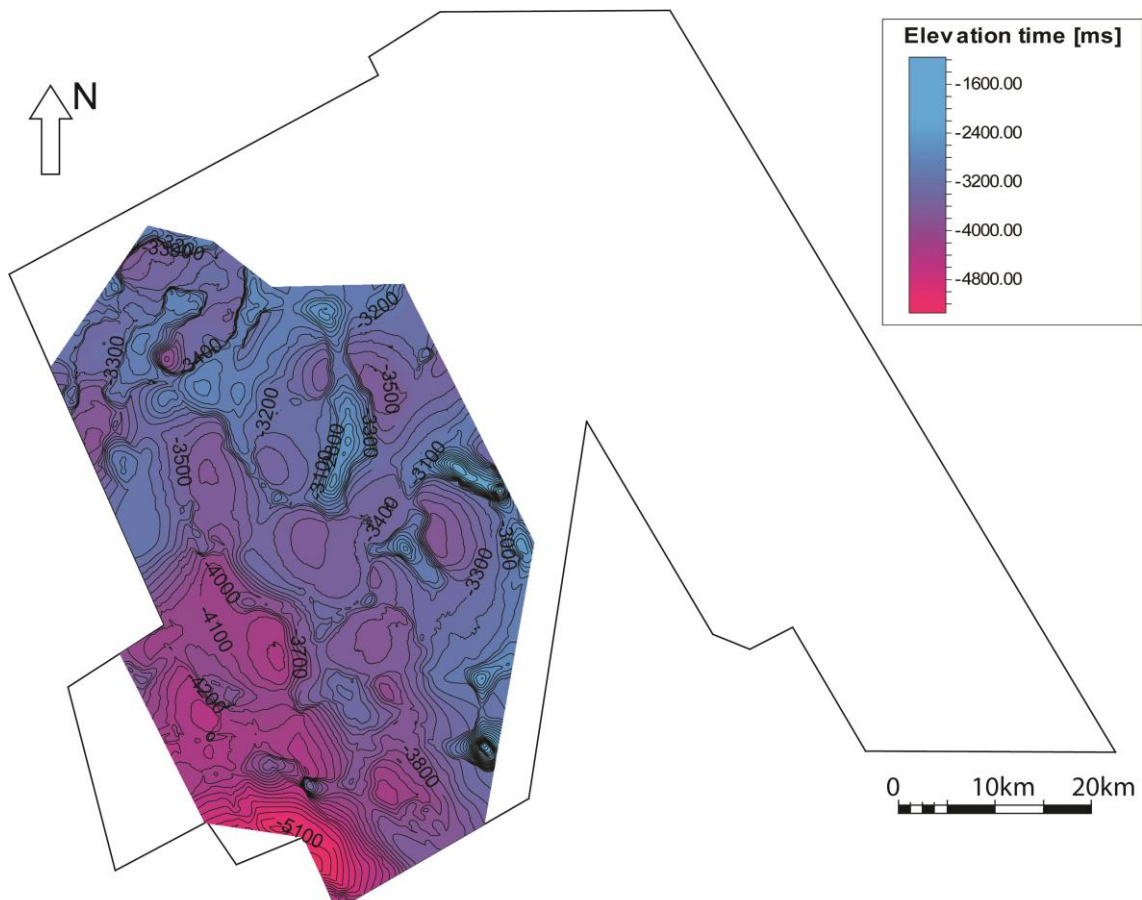


Figure 33. Top intra-Triassic interpretation. The surface is merged with the top Zechstein Group where $Z_{Triassic} \leq Z_{Zechstein}$. This means that the interpreted top intra-Triassic surface follows the interpreted top Zechstein Group surface where the elevation of the top intra-Triassic is lower than the top Zechstein Group.

The intra-Triassic package thickens towards the central part of the minibasins (Fig. 34A). However, above the intra-Triassic package, the location of maximum thickness changes during the Late Triassic and Jurassic (i.e. thickness change from south to north in a highlighted minibasin in Figure 34B).

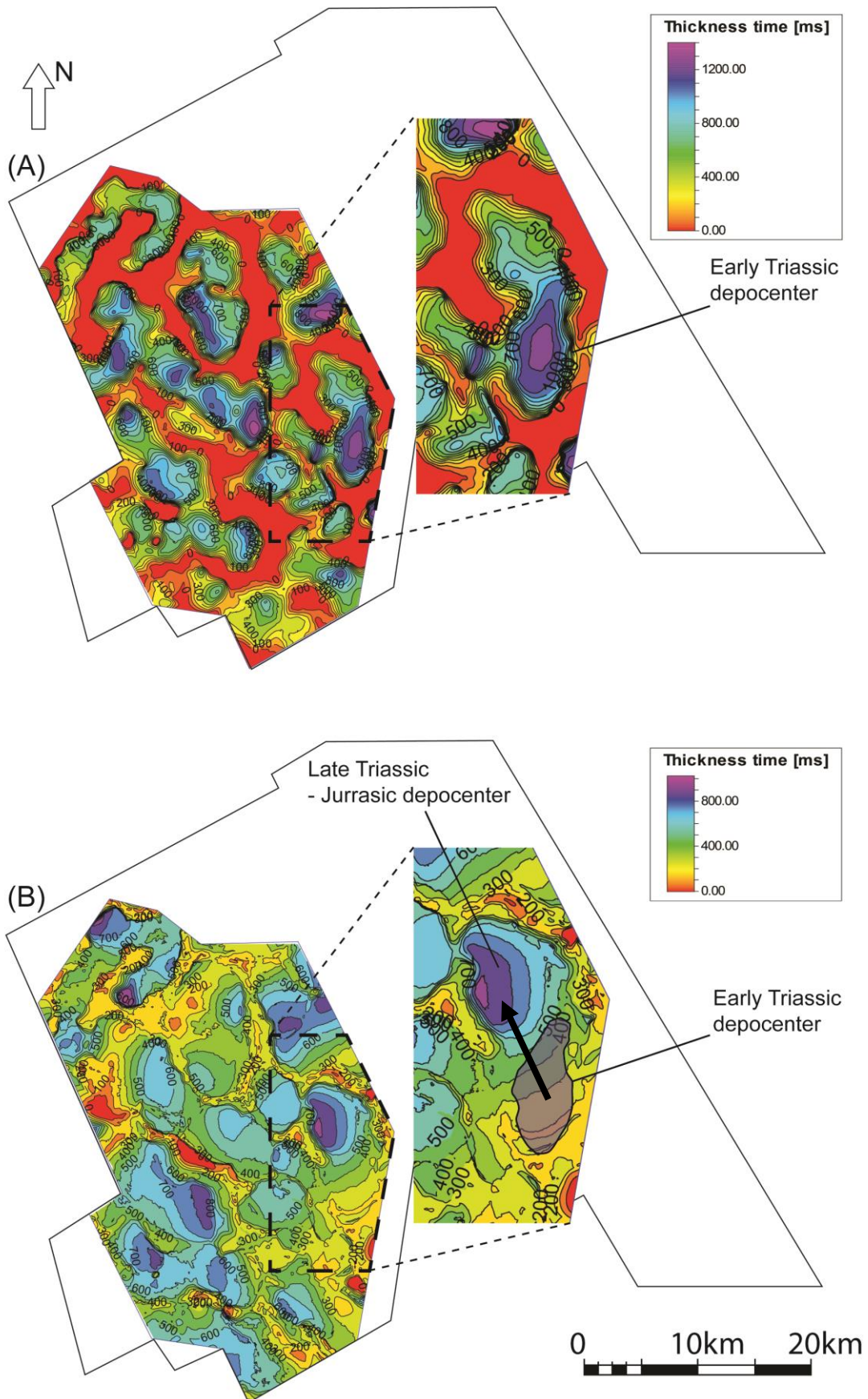


Figure 34. Time-thickness maps. (A) Top Zechstein Group - Intra-Triassic reflector; (B) Intra-Triassic reflector – BCU: Transparent polygon shows the position of a depocenter during Early Triassic (A) and the arrow illustrates how this depocenter shifted during Late Triassic - Jurassic.

4.1.3 Base Cretaceous Unconformity (BCU)

The first horizon showing a good seismic to well correlation is the Base Cretaceous Unconformity (BCU), which separates the Cretaceous and Jurassic, but also places Cretaceous sediments directly onto Triassic where the Jurassic succession is missing. However, the BCU could be traced with good confidence throughout the study area.

Structural style

The BCU variance map illustrates the Upper Jurassic and Lower Cretaceous deformation (Fig. 36A). Trends shown on this map represent the main supra-salt deformation. The crests of the salt structures are observed as highly deformed circular and elongated shapes and are present throughout the area. In the east, crestal deformation strikes NE-SW (Fig. 36A), the same trend as the underlying top salt structures (Fig. 30). The dominating fault orientation is parallel to the top salt geometries, but some fault sets strike perpendicular to the salt bodies (Fig. 36B). The overall dip-direction of the BCU, excluding the internal depressions, is SW (Fig. 36C).

Two styles of faults are observed offsetting the BCU (Figs. 35 and 36B). These faults have been divided into two fault families, F1 and F2. F1 consists of faults located above salt structures, including radial faults surrounding salt stocks and salt-induced normal faults above salt roller and salt wall geometries. F2 contains faults purely offsetting the Mesozoic, predominantly oriented NW-SE and located within Triassic pods where the underlying salt thickness is low.

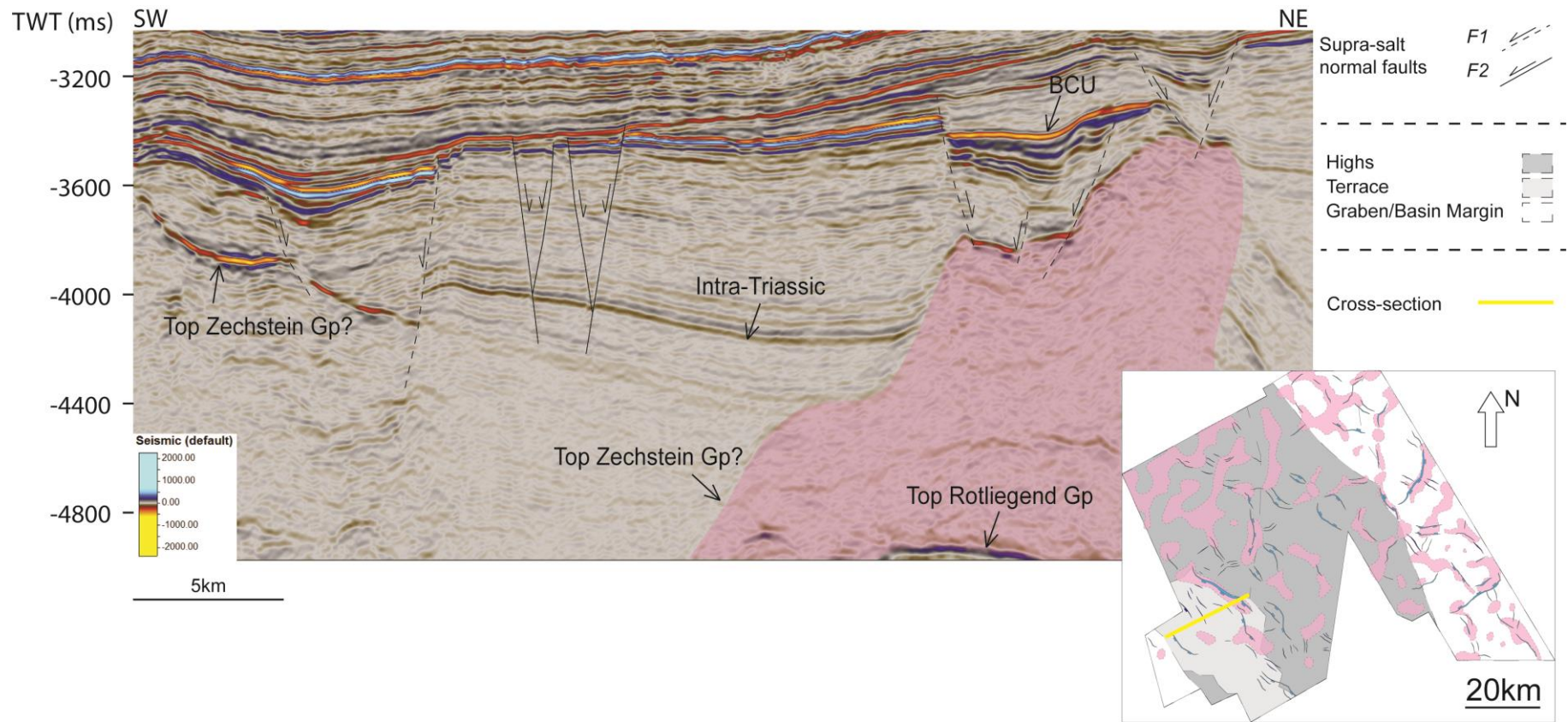


Figure 35. SW-NE cross-section within the PGS16008CGR cube (Inline 26658), including supra-salt fault families F1 and F2. Location of the section is shown on the map.

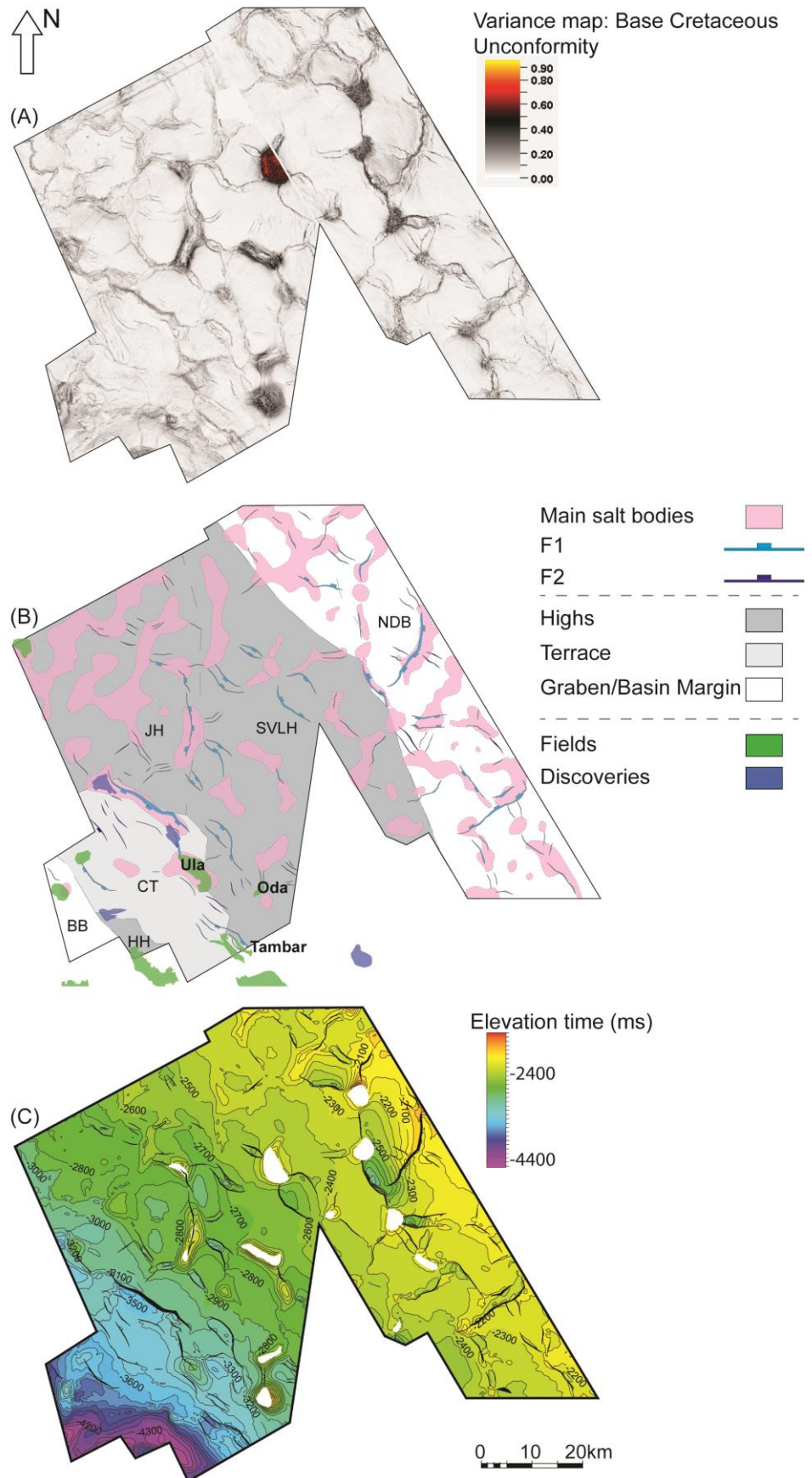


Figure 36. Base Cretaceous Unconformity configuration: (A) Variance map. Dark to red areas indicate structures; (B) Structural trends, including main salt bodies, supra-salt normal faults and fields and discoveries. (BB) = Breiflabb Basin; (CT) = Cod Terrace; (HH) = Hidra High; (JH) = Jæren High; (NDB) = Norwegian-Danish Basin; and (SVLH) = Sørvestlandet High); and (C) Structure map.

4.1.4 Cretaceous

Cromer Knoll Group (100-145Ma)

Structural style and sediment distribution

The top Cromer Knoll Group follows the same deformation trends as seen on the BCU attribute and structure maps (Fig. 36A and C), but they are less affected by faults and with lower topographic relief (Fig. 37A and B). Above the main salt structures, the horizon displays structural highs. The surface dips towards the SW, like the BCU (Fig. 37B).

The thickness of the Cromer Knoll Group is variable, ranging from 0 to 700 milliseconds (approximately 800m) (Fig. 37C). The areas which have thin sedimentary sequences are commonly located where the surface has high relief and are located above salt diapirs (Fig. 37C). On the other hand, above the diapirs on the CT and along the transition to the JH there are NW-SE thickening trends (Fig. 37C). Moving eastwards, to the NDB margin, a larger basin along the narrow salt structure connects the two tall salt diapirs. South of these diapirs, more localized depocenters are present. The localized basins are bound by radial faults propagating from the tall diapirs and major NW-SE and NE-SW oriented elongated salt bodies. Minor fault-bound depocenters are also observed on the SVLH. These are thinner and of less areal extent than those on the eastern margin. Southwest, beyond the CT, the Cromer Knoll Group thickens up to 700ms towards the limit of the map area (Fig. 37C).

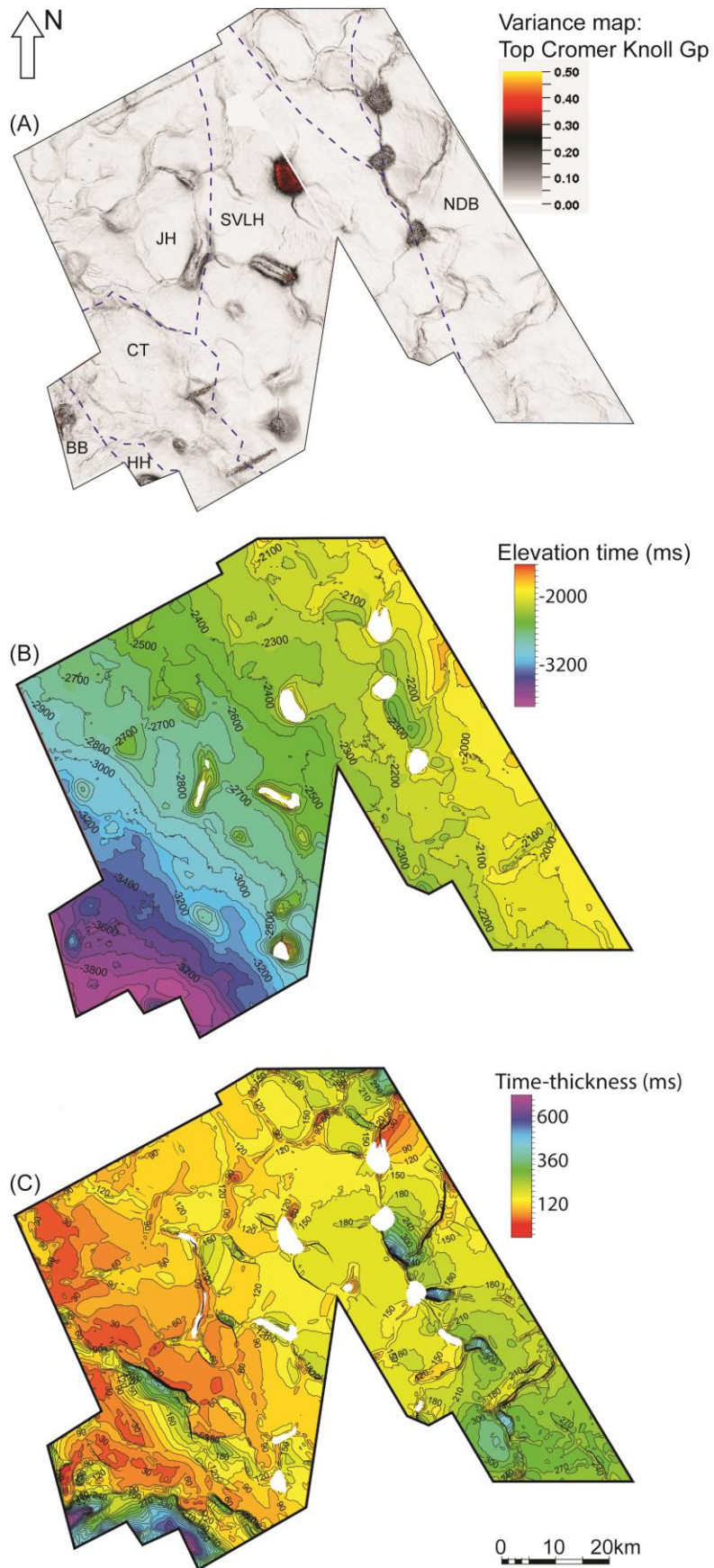


Figure 37. Cromer Knoll Group configuration: (A) Variance map. Dark to red areas indicate structures. Blue dashed lines represent approximate structural element boundaries: (BB) = Breiflabb Basin; (CT) = Cod Terrace; (HH) = Hydra High; (JH) = Jæren High; (NDB) = Norwegian-Danish Basin; and (SVLH) = Sørvestlandet High; (B) Structure map; and (C) Time-thickness map.

Shetland Group (66-100Ma)

Structural style and sediment distribution

During the Late Cretaceous, the depositional systems changed from siliciclastics to chalk of the Shetland Group (Chalk Group). In the southeast, the top Shetland Group was picked on a discontinuous and shifting reflector that is difficult to correlate. This uncertainty in the interpretation did not make a large difference for the time-thickness or surface maps, but structures are less pronounced on the variance attribute map in the southeastern part (Fig. 38A). The Shetland Group reflector is chaotic and less continuous above the main salt structures (Fig. 38A), compared to the top Lower Cretaceous, top Cromer Knoll Group (Fig. 37A). Observed on seismic, the Chalk Group is above most of the salt bodies but does not cover the tallest diapirs on the SVLH and basin margins (Fig. 38B, white outline).

There is a significant difference in the Shetland Group time-thickness map (Fig. 38C) relative to the Cromer Knoll Group time-thickness map (Fig. 37C). Here, the interval thins above the diapir crests, but the minor fault-bound depocenters in the Cromer Knoll Group are no longer evident. The Shetland Group is thinner on the SVLH and JH and thickens outwards to the eastern and western boundary of the study area, with thicknesses up to 500 ms (Fig. 38C).

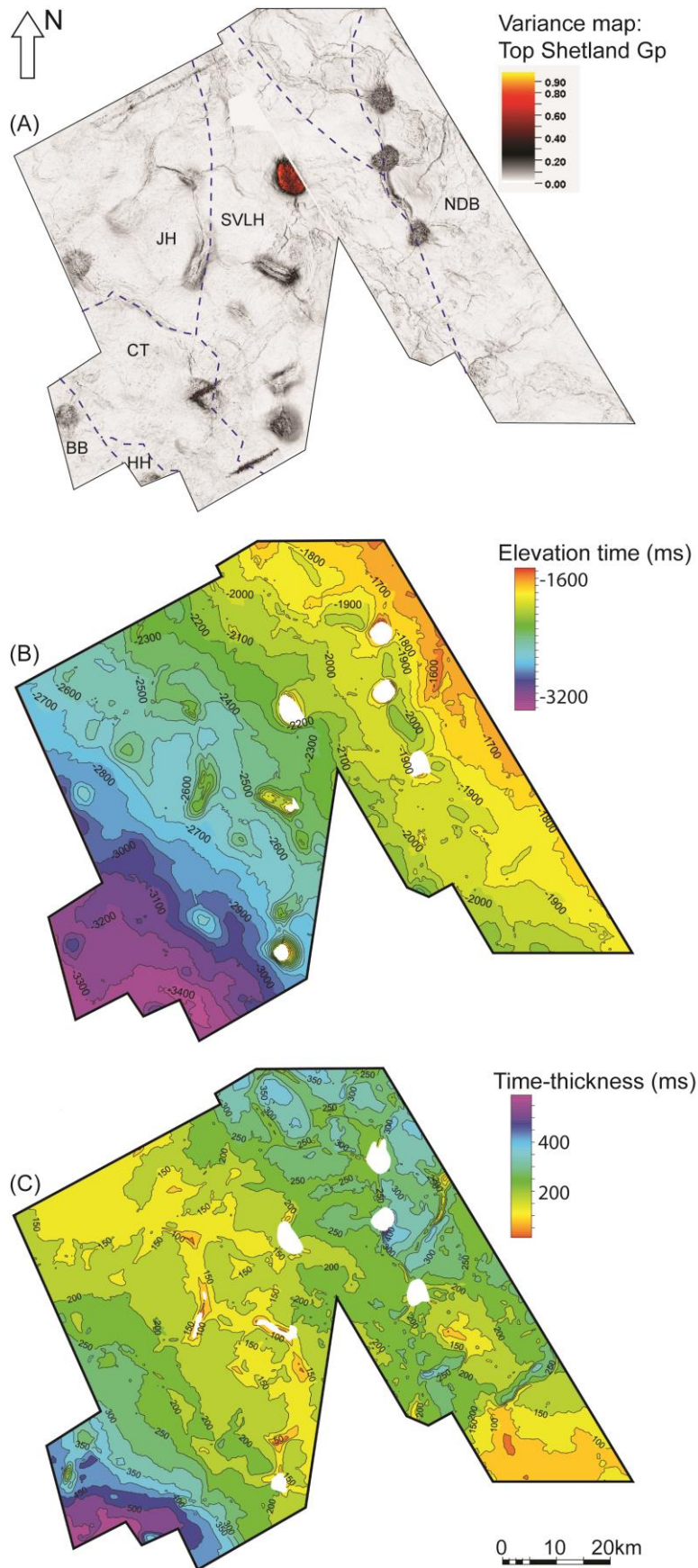


Figure 38. Shetland Group configuration: (A) Variance map. Dark to red areas indicate structures. Blue dashed lines represent approximate structural element boundaries: (BB) = Breiflabb Basin; (CT) = Cod Terrace; (HH) = Hydra High; (JH) = Jæren High; (NDB) = Norwegian-Danish Basin; and (SVLH) = Sørvestlandet High); (B) Structure map; and (C) Time-thickness map.

4.1.5 Cenozoic

Rogaland Group (56-66Ma)

Structural style and sediment distribution

The top Rogaland Group is influenced by polygonal faults (Fig. 39A). The main deformation trends still follow the underlying salt structures and thins above the diapir crests (Figs. 39B and C). Overall, the thickness of the Rogaland Group is quite low, 100-400ms. The thickest areas are placed on the JH and SVLH and continue towards the southeast, with greatest thicknesses near the tall diapirs, and thins towards the northeast and southwest (Fig. 39C).

Hordaland Group (14-56Ma)

Structural style and sediment distribution

In Figure 40A and B, the top Hordaland Group surface does not provide significant information. Still, Figure 40B contains gaps where the reflector is absent, illustrating the height and longevity of the tall diapirs. This can also be seen on the variance map, where circular areas of deformation remain prominent in the south and northeast (Fig. 40A). The structure map shows higher relief up-dip on the tall diapirs and above the major diapirs on the SVLH and JH (Fig. 40B). The Hordaland Group thickness reveals thinning above diapir crests and wide depocenters near the major structures on the SVLH and JH. From east to west, the Hordaland Group increases in thickness (Fig. 40C).

The Hordaland Group was divided in two stratigraphic intervals by adding an internal Hordaland Group surface, the intra-Hordaland. This improves the information regarding the basin evolution during deposition of this unit. Unfortunately, it is not possible to map with accuracy the intra-Hordaland reflector in the eastern half of the study area.

The Intra-Hordaland surface does not provide much information, but the time-thickness maps from the top Rogaland Group – Intra-Hordaland (T1) and Intra-Hordaland – Hordaland Group (T2) are quite useful (Figs. 41, T1 and T2). T1 has large thickness variations, especially near the salt structures, with thin sediments above the diapir crests and thick sediments in areas surrounding the salt structures. Locally, the areas close to the Ula structure, Oda structure and northern diapirs have less intra-Hordaland thickness compared to the north and south (Fig. 41, T1). T2 on the other hand, gradually increases in thickness towards the SW. The Ula structure, Oda structure and northern diapirs are areas of slight thickness decrease, although not as clear as in T1 (Fig. 41, T2).

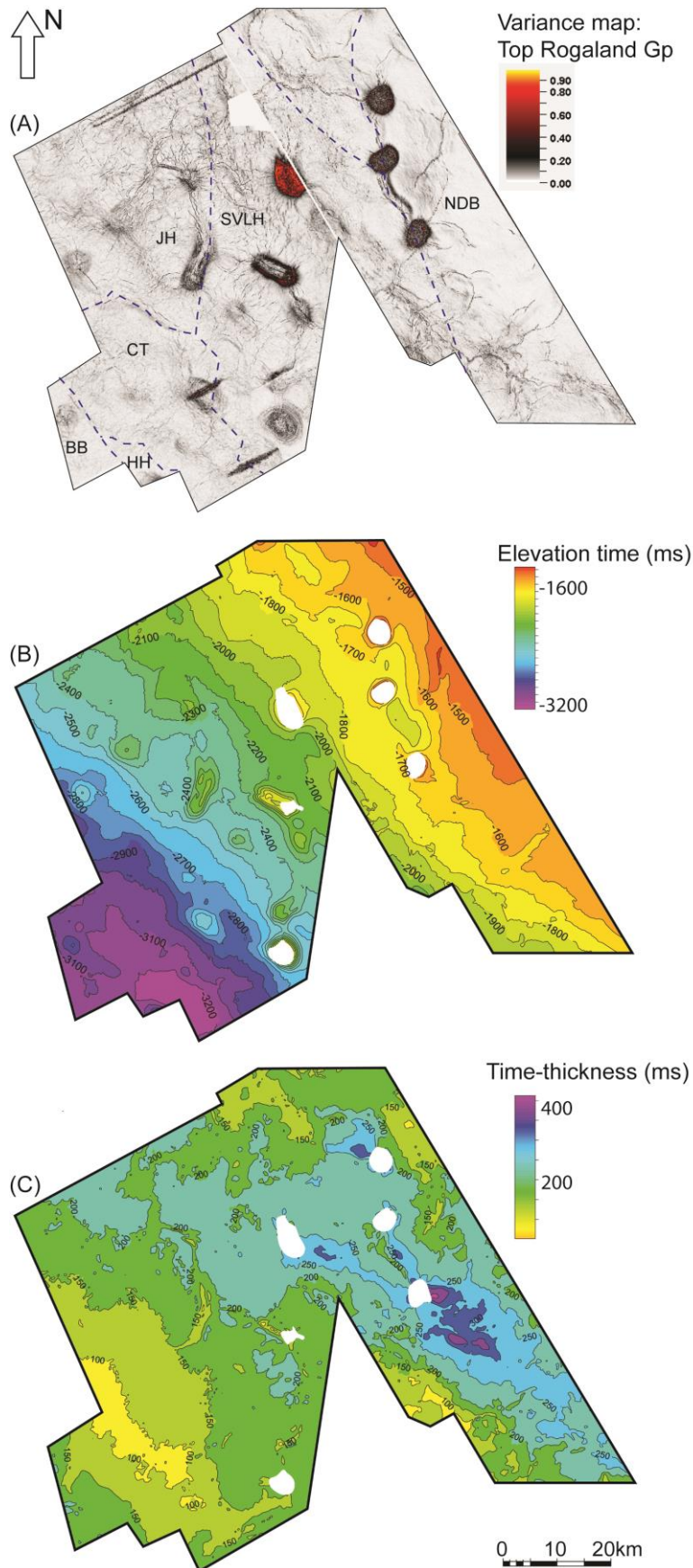


Figure 39. Rogaland Group configuration: (A) Variance map. Dark to red areas indicate structures. Blue dashed lines represent approximate structural element boundaries: (BB) = Breiflabb Basin; (CT) = Cod Terrace; (HH) = Hydra High; (JH) = Jæren High; (NDB) = Norwegian-Danish Basin; and (SVLH) = Sørvestlandet High; (B) Structure map; and (C) Time-thickness map.

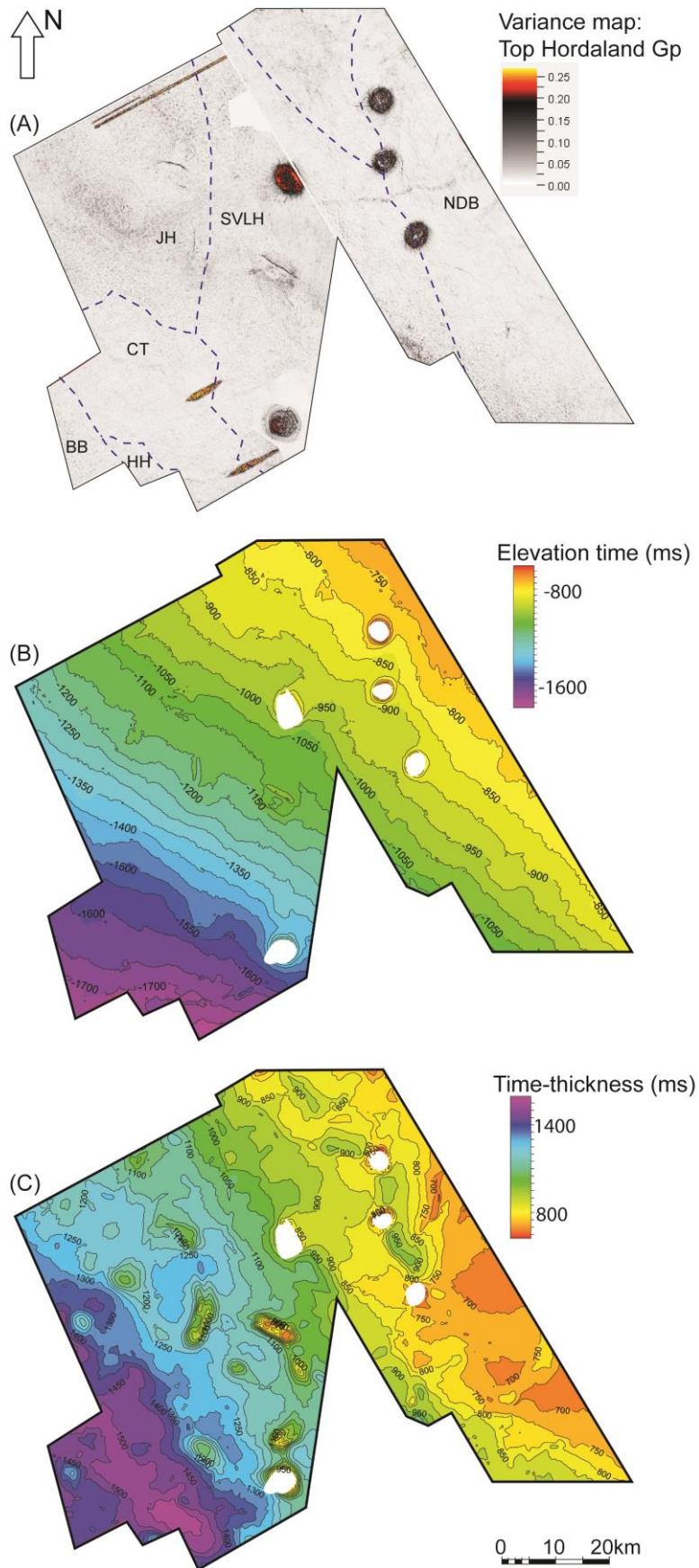


Figure 40. Hordaland Group configuration: (A) Variance map. Dark to red areas indicate structures. Blue dashed lines represent approximate structural element boundaries: (BB) = Breiflabb Basin; (CT) = Cod Terrace; (HH) = Hydra High; (JH) = Jæren High; (NDB) = Norwegian-Danish Basin; and (SVLH) = Sørvestlandet High; (B) Structure map; and (C) Time-thickness map.

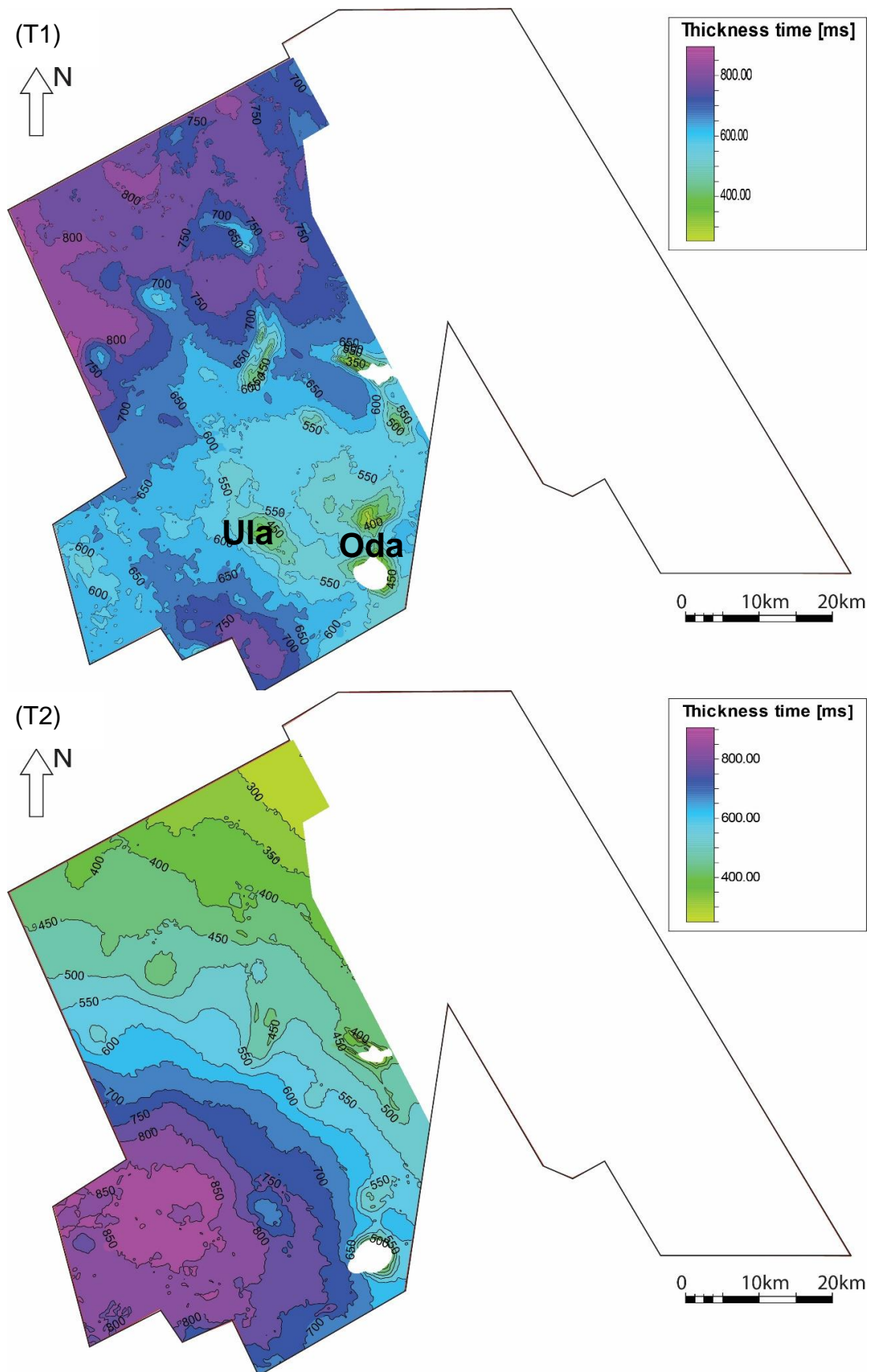


Figure 41. Time-thickness maps. (T1) Top Rogaland Group - Intra-Hordaland Group reflector; (T2) Intra-Hordaland Group reflector - Top Hordaland Group. The intra-Hordaland Group reflector is identified on the cross-section in Figure 23.

Nordland Group (0-14Ma)

Sediment distribution

The Nordland Group is the youngest interpreted reflector, providing information on the most recent development of the basin. As observed in the Hordaland Group, there is gradual thickening towards the SW in this unit (Fig. 42). Above the elongated salt bodies on the JH and central parts of the SVLH, the Nordland Group has little to no thickness changes. However, the interval thins above the tallest diapirs and above the Oda structure.

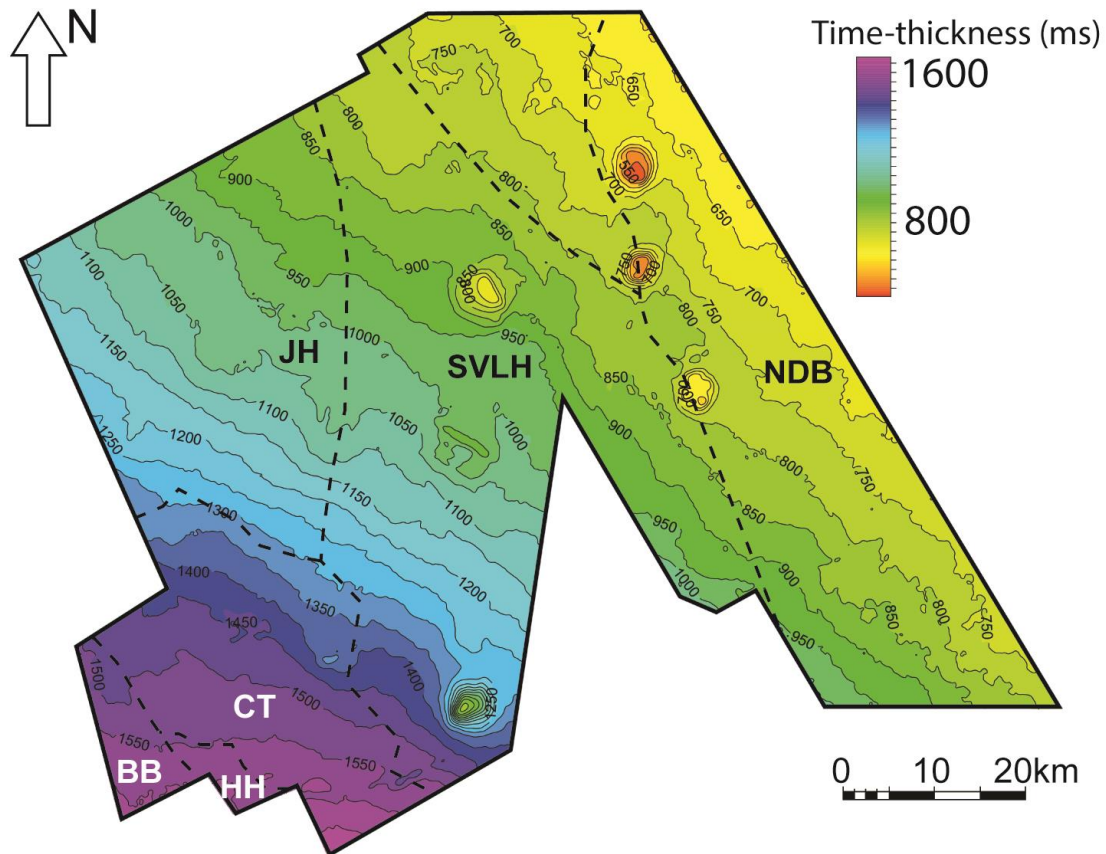


Figure 42. Nordland Group time-thickness map. Black dashed lines represent approximate structural element boundaries: (BB) = Breiflabb Basin; (CT) = Cod Terrace; (HH) = Hydra High; (JH) = Jæren High; (NDB) = Norwegian-Danish Basin; and (SVLH) = Sørvestlandet High).

4.2 Local analysis

Local structural evaluation focuses on the following structures and their adjacent minibasins: (1) Ula structure (B-B`); (2) Oda structure (C-C`); (3) NE-SW trending salt diapir (D-D`); and (4) NW-SE trending salt diapir (E-E`) on the Cod Terrace and Sørvestlandet High (Fig. 43). These structures are restricted to two diapir subgroups which I classify later. At first sight, the four structures have distinct characteristics, in terms of geometry and orientation, but later in the discussion it will be clear that there are other important similarities and differences related to their structural evolution. Each structure is evaluated individually through seismic analysis and sequential restorations.

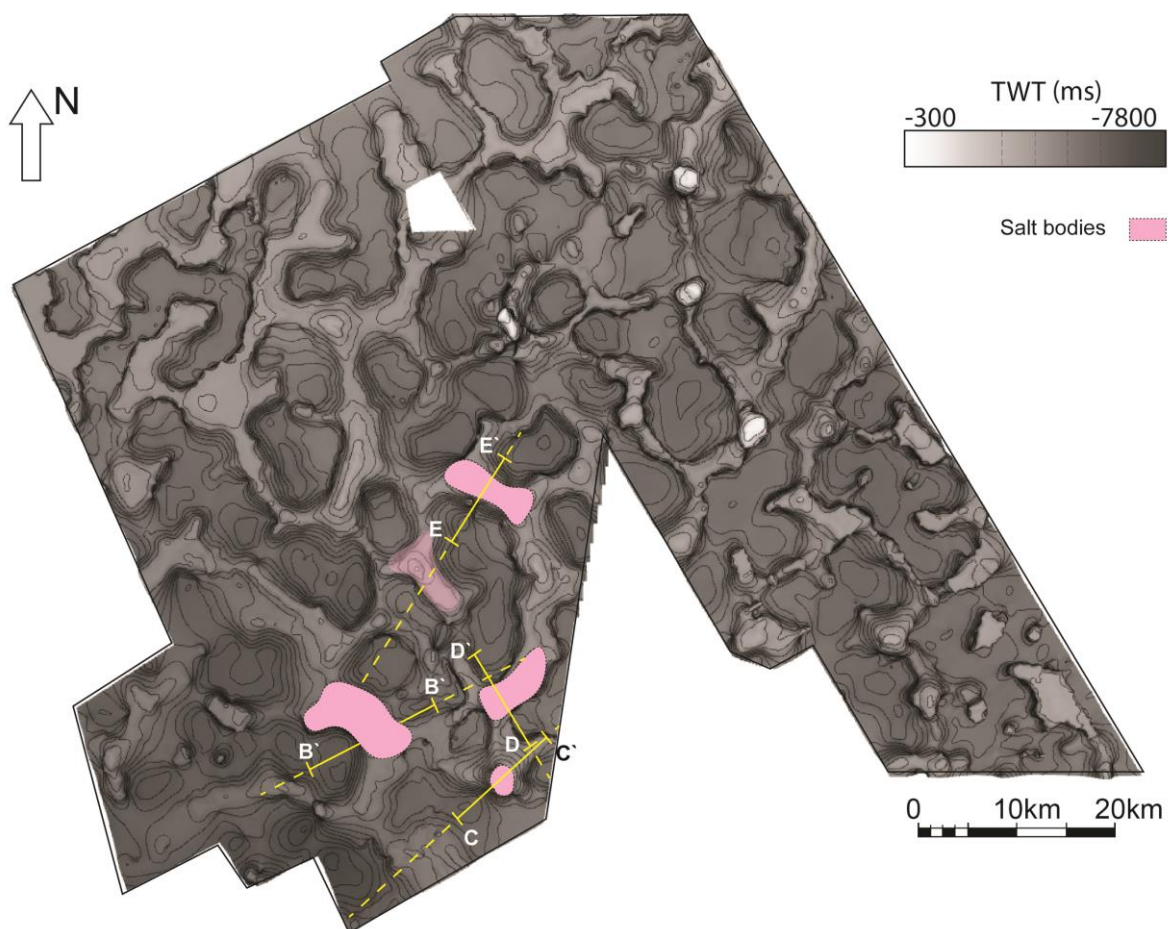


Figure 43. Top Zechstein Group interpretation highlighting a set of diapirs. The restored cross-sections are shown by the yellow lines: B-B` = Ula structure C-C` = Oda structure; D-D` = NE-SW salt diapir and E-E` = NW-SE trending salt diapir.

4.2.1 Ula Structure

Seismic stratigraphy

The Ula structure lies on the footwall of a N-S trending sub-salt normal fault, with minibasins on each side. The Mesozoic and Cenozoic sediments overlying the salt structure are of variable thickness and form an anticline (Fig. 44).

The Triassic interval is thickest within the minibasins flanking the salt structure and thinnest over the crest. Internally, the Triassic minibasins show clear thickness variation within the intervals and the sequences are truncated by the near top Triassic unconformity (Fig. 44). All the internal reflectors have a westerly dip. The Jurassic situated on top of the Triassic display thickening over the salt structure, whereas the Cretaceous package thickens on the flanks of the diapir. The same can be observed in the post Cretaceous package (Fig. 44). The Rogaland Group and Hordaland Group have broadly constant thicknesses, but they thin above the diapir crest. The uppermost Nordland Group is tabular.

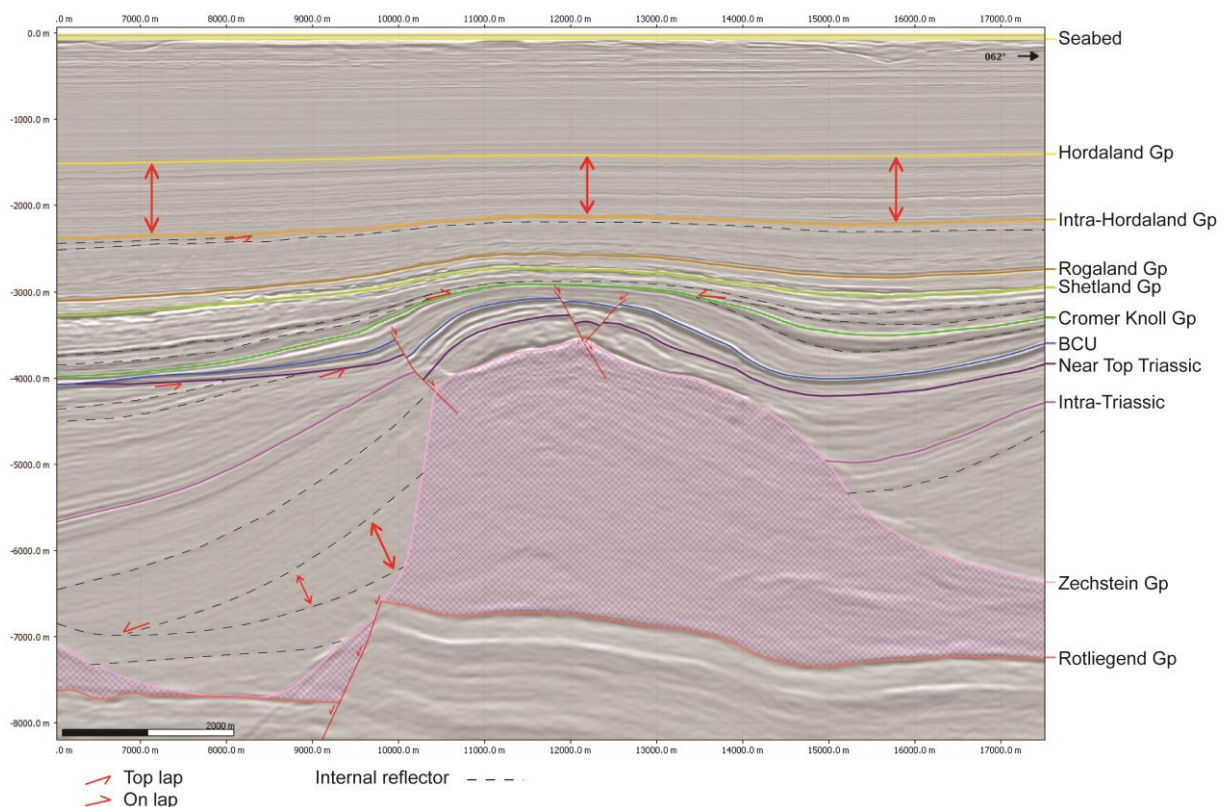


Figure 44. WSW-ENE cross-section across the PGS16008CGR cube, including bedding relationships near the studied salt diapir or Ula Structure. The location of the section is shown in Figure 43 (B-B').

2D Restorations

The restoration for the Ula section is carried out through ten steps. The first nine steps are made using the *Move modules* (decompaction, unfolding and move on fault), while the final step, top Zechstein Group, is presented for illustrational purposes. This is done for all the restorations (see Appendix II for further descriptions). At present day, the Triassic minibasins are welded to the sub-salt Rotliegendes (Fig. 45A). On this section, a hard-linked normal fault that cross cuts from the Permian and into the Cretaceous needs to be accounted for during the restoration.

The restoration indicates regional subsidence between present-day and the top intra-Hordaland Group (Figs. 45A, B and C). In the intra-Hordaland Group and the Rogaland Group, the package thins towards the diapir crest (Figs. 45C and D).

For the Late Cretaceous Shetland Group, the succession thickens westwards and shows substantial thinning and onlaps above the diapir (Fig. 45E), which is in agreement with the observations in Figure 38C. The Lower Cretaceous, Cromer Knoll Group, thins above the diapir crest and has two defined supra-salt minibasins on each diapir flank. The group is partially absent on the western Triassic minibasin (Fig. 45F). The Jurassic interval has a similar configuration as the described Cromer Knoll Group, but deposition is localized to the crest of the diapir (Figs. 45F and G).

On the unfolded near top Triassic, the same local units observed in the Jurassic are present above the diapir (Fig. 45H). This Late Triassic interval also has thick deposits both in the eastern and western minibasins. Finally, to restore the intra-Triassic, restoration of the hard-linked sub-salt normal fault was done (Fig. 45I). In this last supra-salt restoration step, the salt remains welded above the eastern fault block.

The Jurassic and Lower Cretaceous sediments which accumulated during diapir collapse are discussed in Chapter 5.2.3 and 5.2.4.

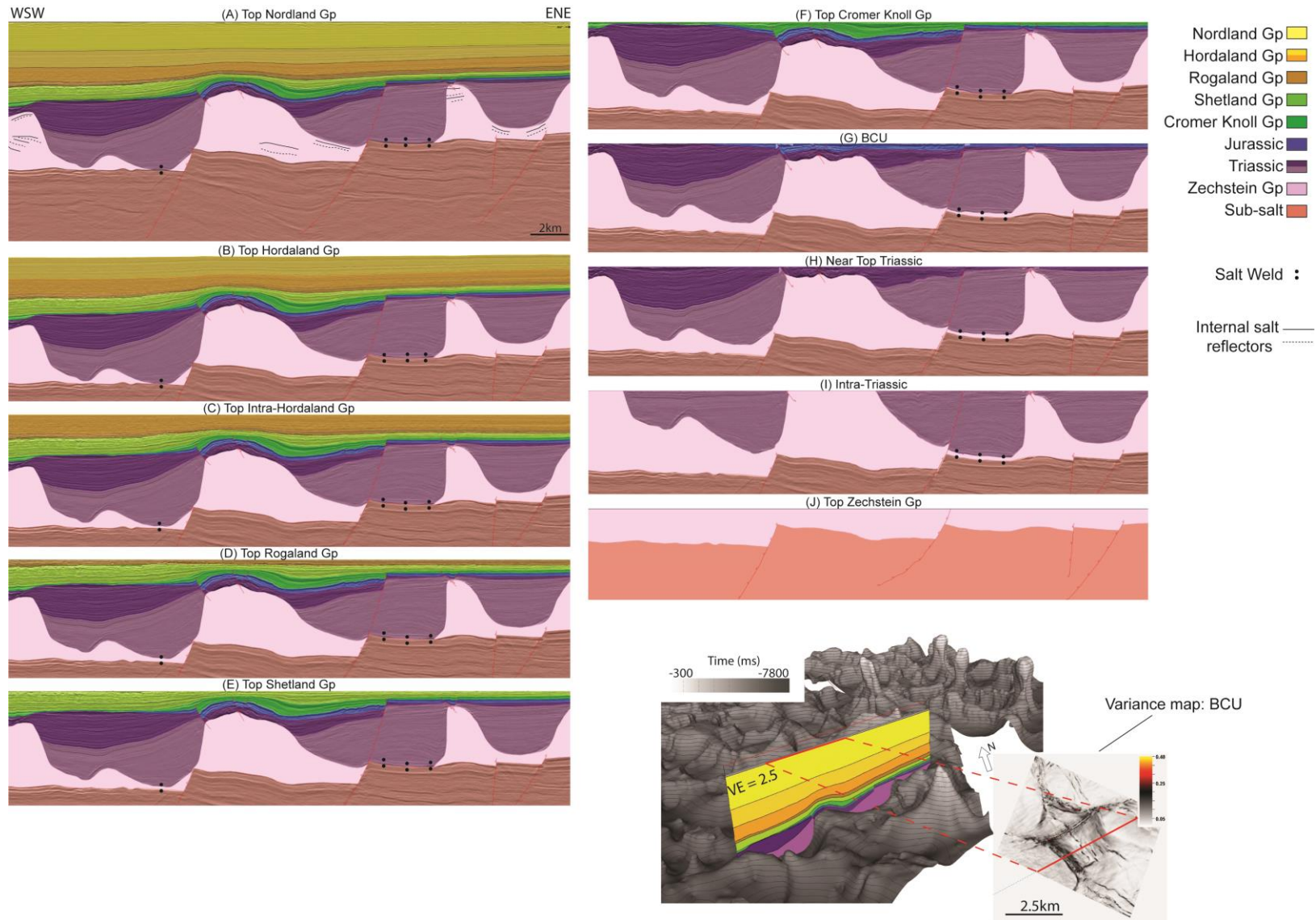


Figure 45. Restored and unfolded sections of the Ula structure, collapsed diapir, from the present to the top Zechstein Group. The location of the section is shown on the three-dimensional surface, displayed with a VE = 2.5. Additionally, a variance map covering the structure is included. (See Appendix II)

4.2.2 Oda Structure

Seismic stratigraphy

Seismic analysis of the Oda structure includes interpretations from two seismic cubes, PGS16008CGR and CE1202R15, where the second survey contains poor resolution above the diapir and pull-up effects beneath the salt. This led to modifications to the sub-salt geometry before restoring the section, which was done by flattening the base salt reflector (Fig. 46). Despite the simplification, a lot of information can be found from the section.

In the Jurassic and Triassic, the near top Triassic reflector could not be mapped with confidence, resulting in a polygon that includes both the Upper Triassic and Jurassic. In addition, the reflectors within the Triassic succession were not continuous, but reflectors dipping to the west, as observed in the Ula section, are present (Fig. 46).

For the Cretaceous, Cromer Knoll and Shetland Groups, the intervals are thickening westwards and they are partially absent or very thin above the diapir (Fig. 46). Moving upwards, the Rogaland Group is evenly distributed until it intersects the normal fault. In the Hordaland Group, internal onlaps on the western flank and toplaps (truncation) on the diapir flanks are observed. In both the Hordaland Group and Nordland Group, there are thinning towards the diapir crest, until offset by the two normal faults above the diapir. These faults propagate further upward than what is interpreted on the section.

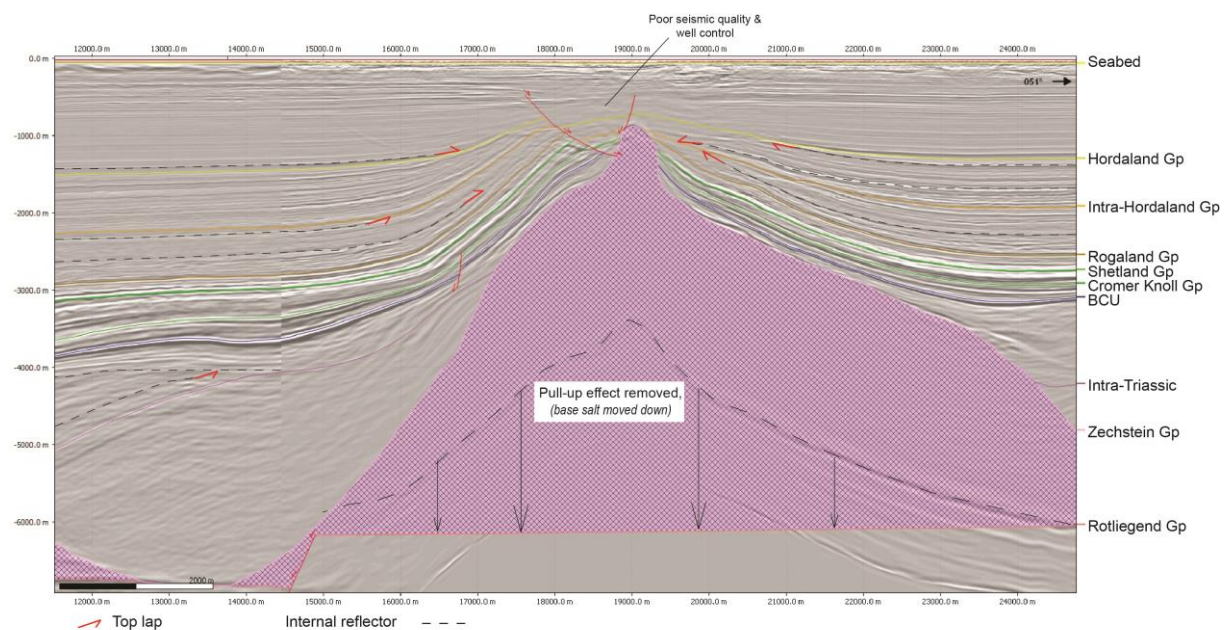


Figure 46. SW-NE cross-section in the PGS16008CGR and CE1202R15 cubes, including bedding relationships near the addressed salt diapir, Oda Structure. Location of the section is shown in Figure 43 (C-C').

2D Restoration

The restoration of the Oda structure contains nine steps, one less than the previous restoration, because the Upper Triassic and Jurassic are treated as one unit. West of the section, there is a second salt structure, which underlies the northern part of the Tambar field. This structure has several normal faults detaching from the top Zechstein Group, as well as a 2.5 km throw fault at Rotliegendes level (Fig. 47A).

The present-day top Nordland Group is almost evenly distributed with a gentle increase in thickness towards the west, but also display faulting and thinning over the diapir (Fig. 47A). For the restorations between top Nordland Group and intra-Hordaland Group, regional subsidence and salt movement influence the basin (Figs. 47A, B and C). Here, the intervals are thick above the Triassic minibasins and thin towards the diapir crest. The Zechstein group is emergent after removing the upper part of the Hordaland Group (Fig. 47C).

The Shetland Group thickens towards the west and thins above the emergent diapir (Fig. 47E). In the Cromer Knoll Group there are more localized depocenters, controlled by the salt movement and fault displacement, and an extensive growth package onlapping the Jurassic in the west (Fig. 47F). To account for the thickness variations in the Cretaceous intervals, salt continues to fill the available space above the top Rotliegend Group (Fig. 47G).

During the Jurassic – Late Triassic, there is a thin layer above the main diapir and a thicker unit with well defined internal geometries above the western diapir (Fig. 47G). Lastly, the intra-Triassic step displays wide passive diapirs as salt is emergent, with local supra-salt minibasins above the diapirs and Triassic minibasins separating the diapirs (Fig. 47H).

The Shetland Group thins above the diapir and marks a clear transition from extension to shortening between Early and Late Cretaceous, this will be discussed in Chapter 5.2.4.

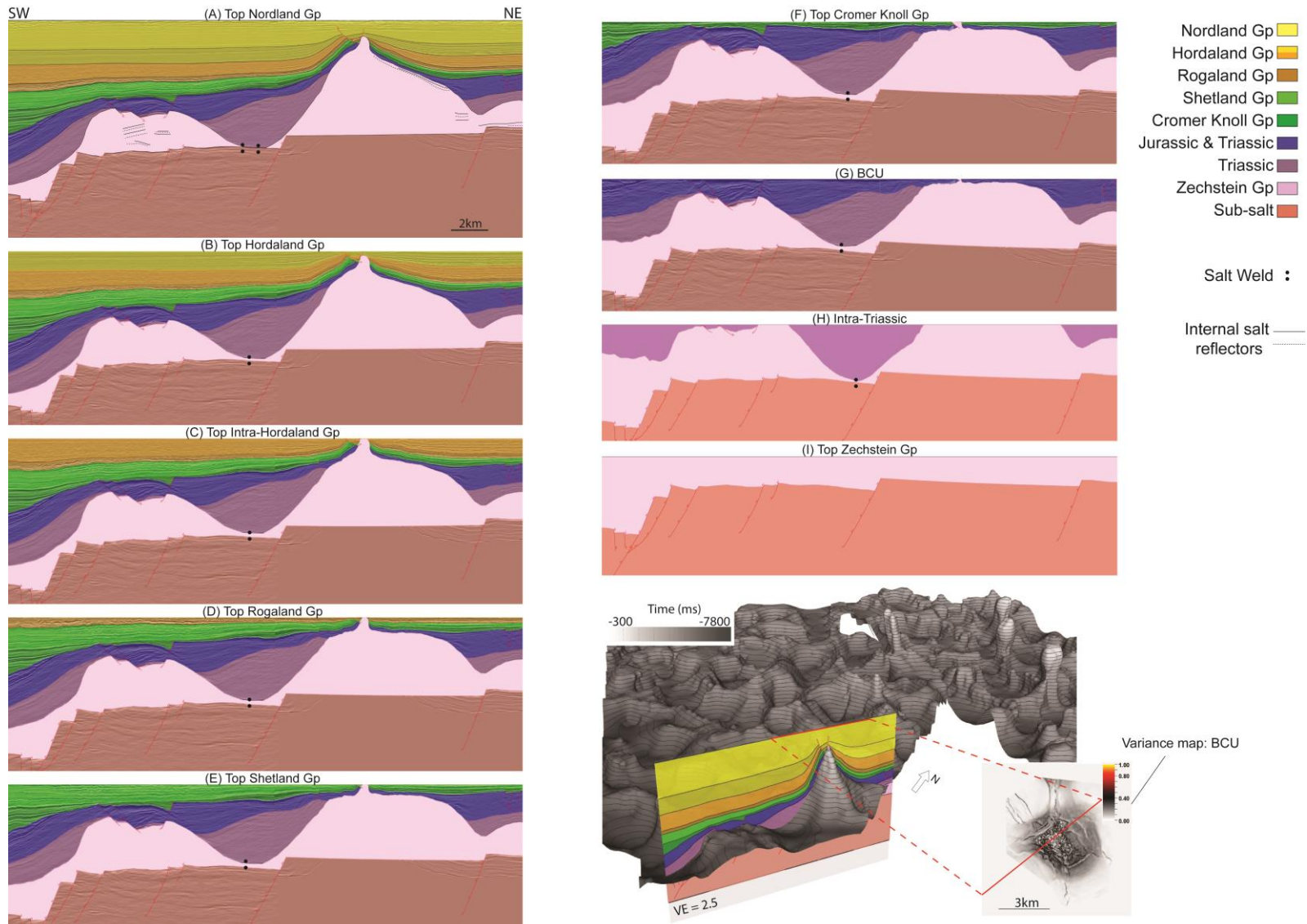


Figure 47. Restored and unfolded sections of the Oda structure, a reactivated diapir, from the present to the top Zechstein Group. The location of the section is shown on the three-dimensional surface, displayed with a VE = 2.5. Additionally, a variance map covering the structure is included. (See Appendix II)

4.2.3 NE-SW trending diapir

Seismic stratigraphy

The NE-SW trending diapir varies from the previously described structures, as it is not overlying or is directly adjacent to a sub-salt normal fault (Fig.48). The salt body includes a possible diapir overhang on the eastern side. In this area, the seismic quality of the CE1202R15 cube has limited resolution within the Triassic succession and along the diapir flanks. Therefore, internal Triassic geometries are poorly constrained in the eastern half (Fig. 48). There are however a few continuous reflectors marked on the section (Fig. 48, dashed lines), which provide some information on the evolution of the Triassic minibasins. From these observed reflectors and nearby wells, a near top Triassic horizon was interpreted.

Above the near top Triassic horizon, toplaps, onlaps, low-angle normal faults and thickness variations are observed (Fig. 48). The toplaps terminate below the BCU, while the onlaps are present within the Shetland Group and the intra-Hordaland Group. The onlaps are observed in intervals that are thin towards and above the diapir. The successions above the Rogaland Group show a slight thickening above the diapir crest related to the northerly dipping fault, which is detaching from the Zechstein Group with growth strata in the hanging wall (Fig. 48)

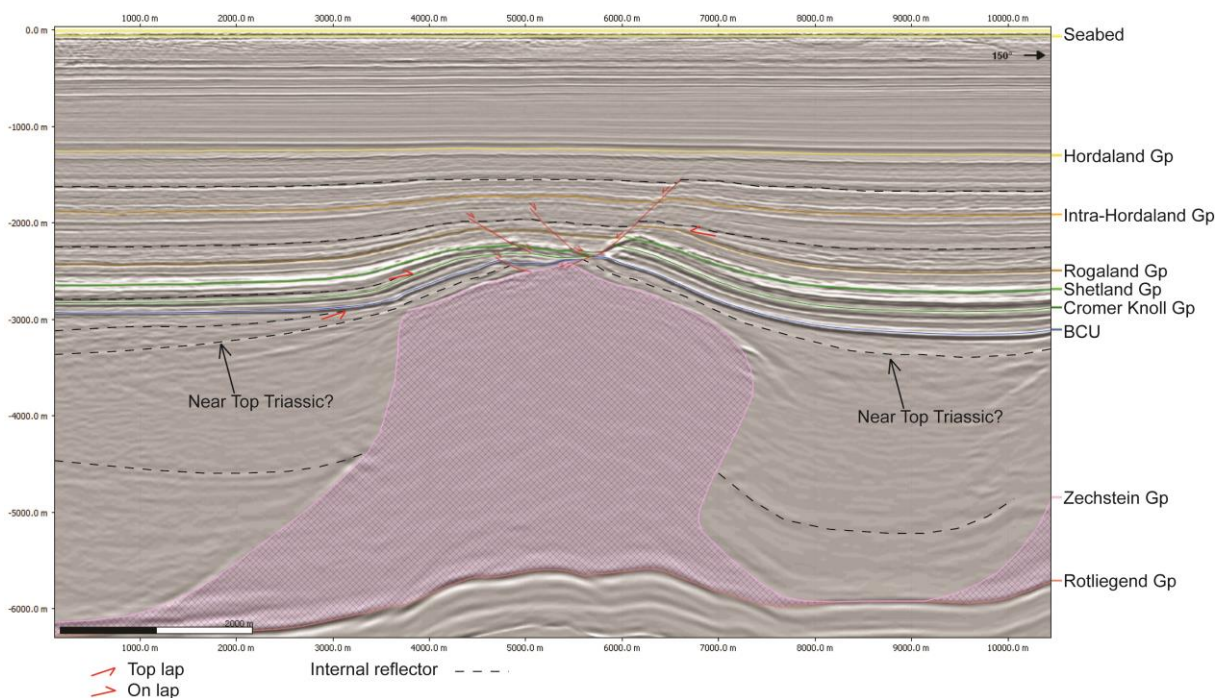


Figure 48. NNW-SSE cross-section in the CE1202R15 cube, including bedding relationships near the NE-SW trending diapir. Location of the section is shown in Figure 43 (D-D').

2D Restorations

The restoration of the NE-SW trending diapir does not contain a separate Jurassic interval. Therefore, it consists of nine steps where Upper Triassic and Jurassic are confined to the same interval, similarly to the Oda restoration. The present-day section includes internal salt geometries within the eastern diapir (Fig. 49A). Here, the reflectors are faulted and overlain by less continuous (chaotic) seismic reflections.

In the second step, the Hordaland Group thickens slightly in the hanging wall (Fig. 49B). Hanging wall thickening is also observed in the two next steps, top intra-Hordaland Group and top Rogaland Group (Figs. 49C and D). These two intervals are both influenced by the main salt structure and its overlying fault, whereas the sediments above the eastern structure are less effected. Artifacts related to the diapir overhang are clear above the southern diapir flank (Fig. 49D). These artifacts, resembling spikes, can be ignored throughout the restorations. In the Shetland Group and the Cromer Knoll Group, there is a change to thinner intervals above the diapir crest (Figs. 49E and F).

After removing the Cromer Knoll Group, the Zechstein evaporites are possibly emergent with thin Upper Triassic and Jurassic sediments on each diapir flank (Fig. 49G). Comparable stratigraphic and structural relationships are observed in the intra-Triassic step (Fig. 49H). At this time, the western Triassic minibasin is rotated as salt flows into the section. Between the two final steps, it is likely that the entire salt body was at the surface and grew as a passive diapir, like in the previous restorations (Figs. 49H and I). This is not observed in the restored section because the Triassic and Jurassic are part of the same polygon.

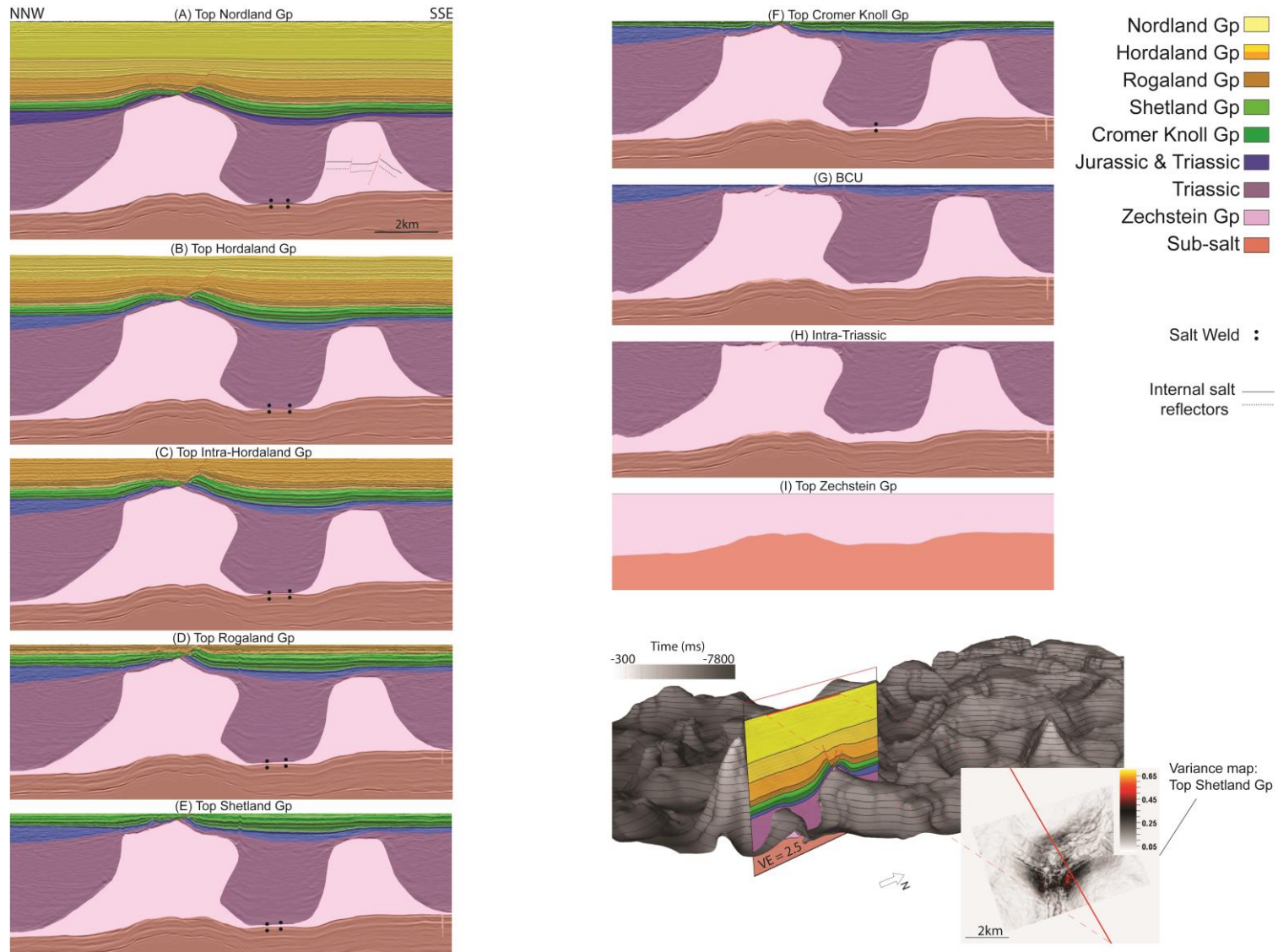


Figure 49. Restored and unfolded sections of a NE-SW trending reactivated diapir from the present to top the Zechstein Group. The location of the section is shown on the three-dimensional surface, displayed with a VE = 2.5. Additionally, a variance map covering the structure is included. (See Appendix II)

4.2.4 NW-SE trending diapir

Seismic stratigraphy

The final structure that was assessed is a NW-SE trending diapir. Its structural orientation is orthogonal to the previously described diapir (Fig. 43). Geometry-wise, the structure also differs from the NE-SW trending structure as it does not include any overhangs, has a more distinct narrowing upward shape and is overlain by two large faults propagating from its crest (Fig. 50). In the Triassic, internal reflections become weak next to the steeply dipping diapir flanks. In contrast to the poor reflections along the flanks, the seismic image above the diapir crest captures a lot of detail. This enables a likely top Triassic reflector to be interpreted in this area (Fig. 50, near top Triassic).

On the eastern diapir flank, there are three minor faults offsetting the BCU, Cromer Knoll Group, Shetland Group and Rogaland Group. These faults do not propagate through the entire Rogaland Group, and show thickening in the hanging walls. Adjacent to the faults, onlaps within the Shetland Group and intra-Hordaland Group are observed. The intervals above the salt structure thin towards the diapir flanks, but in the hanging wall stratigraphy near the diapir crest, the intra-Hordaland Group, Hordaland Group and Nordland group thicken.

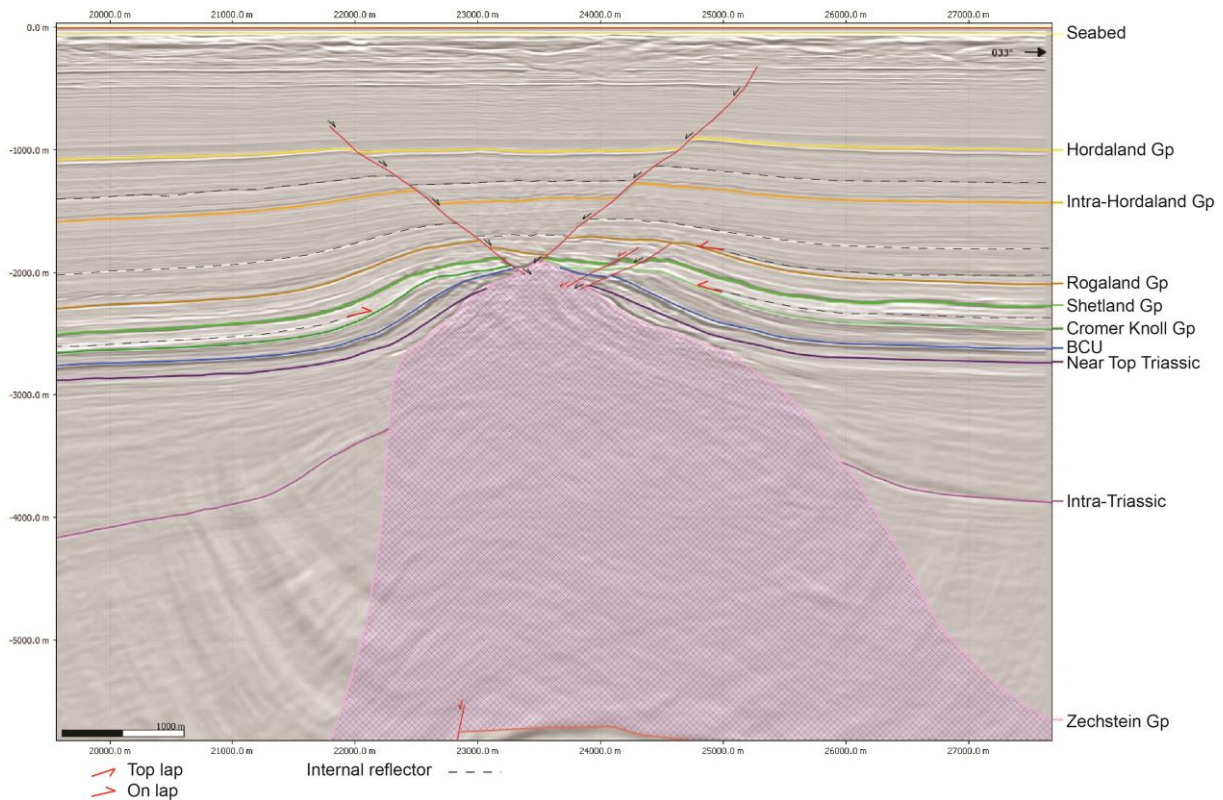


Figure 50. SSW-NNE cross-section in the PGS16008CGR cube, including bedding relationships near the addressed salt diapir, north of Oda. Location of the section is shown in Figure 43 (E-E’).

2D Restorations

The major sub-salt normal faults follow the same trends as in the former sections, dipping to the west. In the section, there are several salt welds between the major and minor salt diapirs. Internal salt reflectors are only observed in the eastern flank of the central diapir (Fig. 51A).

The Nordland Group thickens to the west, with associated deformation from the major supra-salt faults (Fig. 51A). In the following step, the Hordaland Group thickens westwards, while close to the main diapir, this group thins towards the diapir flanks and thickens within the graben above the diapir crest (Fig. 51B). Similar geometries above the diapir are observed in the intra-Hordaland Group, although this unit is thickest between the two largest diapirs (Fig. 51C). For the restored top Rogaland Group, there is some thickening of the Rogaland Group in the hanging wall of the normal faults, but otherwise thinning above the major diapir as it narrows upwards (Fig. 51D).

In the Cretaceous intervals, the Upper Cretaceous Shetland Group thickens westwards and thins above the major diapir (Fig. 51E). At this stage, the diapir reaches the surface and there is a local depocenter on its western flank. During the Lower Cretaceous, Cromer Knoll Group, the Zechstein Group is still at the surface and with local depocenters on each diapir flank (Fig. 51F). In the western part, there is thickening above both diapirs, especially within the fault-bound minibasin. The same observations can be made for the Jurassic succession (Fig. 51G).

In the three final sections including the BCU to intra-Triassic (Figs. 51H, I and J), the stratigraphic configuration changes. Minibasins on the diapir flanks and emergent, wide, salt structures are observed (Fig. 51H). During the intra-Triassic, salt begins to flow into the section and the previously well-defined salt welds are no longer present (Fig. 51I).

The local depocenters on the diapir flanks during the Lower Cretaceous, Cromer Knoll Group, with associated uplift of the Jurassic sediments, are discussed in Chapter 5.2.3 and 5.2.4.

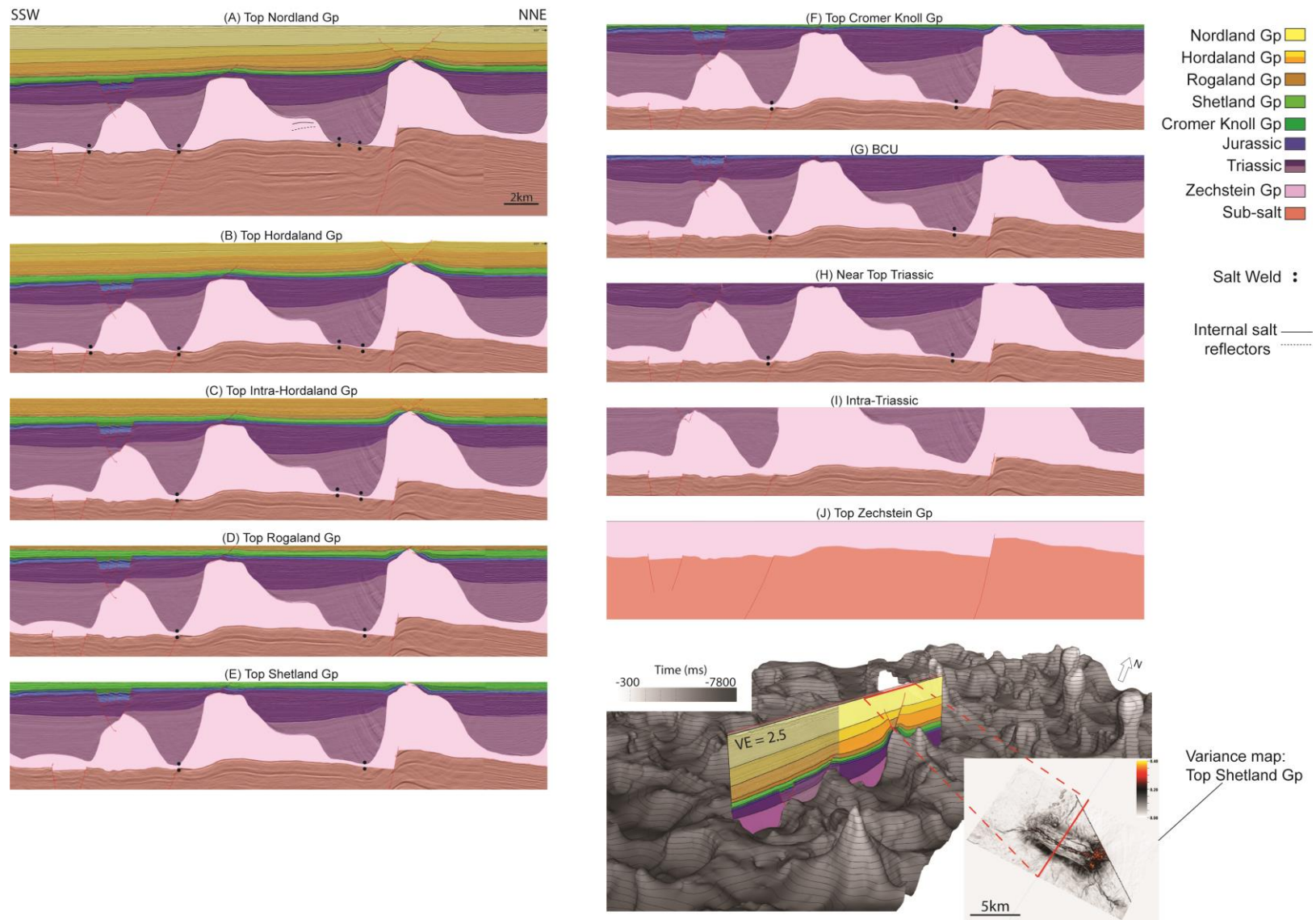


Figure 51. Restored and unfolded sections of a NW-SE trending reactivated diapir from the present to the top Zechstein Group. The location of the section is shown on the three-dimensional surface, displayed with a VE = 2.5. Additionally, a variance map covering the structure is included. (See Appendix II)

5 Discussion

The observations from the cross-sections, structure maps, attribute maps, thickness maps and restored sections are used to: (1) define the structural styles in the area; (2) determine the diapir evolution, in terms of timing and controlling factors on salt mobilization; and (3) derive implications for the petroleum system.

5.1 Structural Styles

5.1.1 Diapir classification

The Zechstein evaporites are unevenly distributed throughout the study area. The geometry of the salt bodies can be described in terms of Jackson and Talbot (1986)'s classification (Fig. 52), with tall diapirs on the eastern half resembling salt stocks and laterally connected elongated structures resembling salt walls and salt rollers. However, this classification does not provide any constrain to the structure evolution, in terms of timing of salt movement. Therefore, by combining the restorations with the structural framework, insight into the structural development can be added. This enables a more detailed classification of the salt structures. In the study area, salt structures can be described by five criteria: **buried diapirs, collapsed diapirs, reactivated diapirs, salt rollers and walls, and salt stocks** (Fig. 53). These are not purely based on diapir geometries, but also on their overlying and adjacent Mesozoic and Cenozoic sediment growth.

Buried diapir

The intra-Triassic thickness map show the development of depocenters surrounding the salt structures, indicating a close link between salt withdrawal and sedimentation during Triassic (Figs. 34A). Both buried and collapsed diapirs appeared as salt walls at this stage, but their growth patterns are different. For the buried diapirs, there is little to no renewed growth or collapse after their initial Triassic structuring, resulting in a tabular overburden with little influence by salt tectonics. In the northwest, the buried diapirs have a fairly flat top with abrupt vertical flanks and tabular overlying stratigraphy. This has been used as a reference for their physical appearance when classifying them (Fig. 53).

Collapsed diapirs

The collapsed diapirs are not following the same growth patterns or present-day geometry definitions as the buried diapirs. These structures have undergone periods of diapir collapse. The collapse is indicated during the Jurassic, as seen in the Ula restoration (Fig. 45), and

similarly to Mannie et al. (2014)'s description of diapir collapse during Late Jurassic. Here, sediments are confined to supra-salt minibasins. The Cromer Knoll group thickens above the Ula structure (Figs. 37C and 45F). This indicates a later collapse, however, now it is the outermost parts of diapir flanks that are collapsing and being filled. The diapir collapse is followed by structural rejuvenation. This is captured in the Ula restoration and identified on structure and thickness maps, where the Shetland Group is thinning and has positive structural relief above the Ula structure (Figs. 45E, 38B and C). Additionally, there are some slight thickness and structural changes above the northern collapsed diapir (Figs. 38B and C). Geometry-wise, the diapir flanks are gently dipping, more dome shaped and without horizontal roofs compared to the buried diapirs.

Reactivated diapirs

The reactivated diapirs are classified based on their extensive post-Jurassic structural reactivation, growing as active or passive diapirs. Renewed salt growth is inferred from the narrowing-upward diapir shape and sediment thickness variation, combined with the faulting and folding of overlying sediments (e.g. restored reactivated diapirs, Oda structure, Fig. 47; NE-SW trending diapir, Fig. 49; and NW-SE trending diapir, Fig. 51). Additionally, from the restorations of the reactivated diapirs, salt has been emergent or near the surface for a longer period than the collapsed diapir. The elongated reactivated diapirs north of the Oda structure resemble salt walls in their overall geometry, while the Oda structure is more cone-shaped (Fig. 53).

Salt rollers and walls

The salt rollers and walls on the NDB margin and SVLH are gathered in the same sub-group, although, geometry-wise, there are large dissimilarities between these structures (Fig. 53). In addition, a few of the salt walls are in a transition between reactivated diapirs and buried diapirs. To simplify, they are placed together in this group since a detailed analysis on each structure could not be made, nor could they be linked to buried or reactivated diapirs with great certainty.

Salt stocks

Finally, the four tallest salt structures in the area were classified as salt stocks (Fig. 53). These are narrow localized structures, which almost pierce the seafloor and are surrounded by heavily deformed and uplifted beds. The salt stocks are likely to have grown as passive diapirs through most of the Mesozoic and Cenozoic, until they were covered during high sedimentation rates in the Upper Cenozoic.

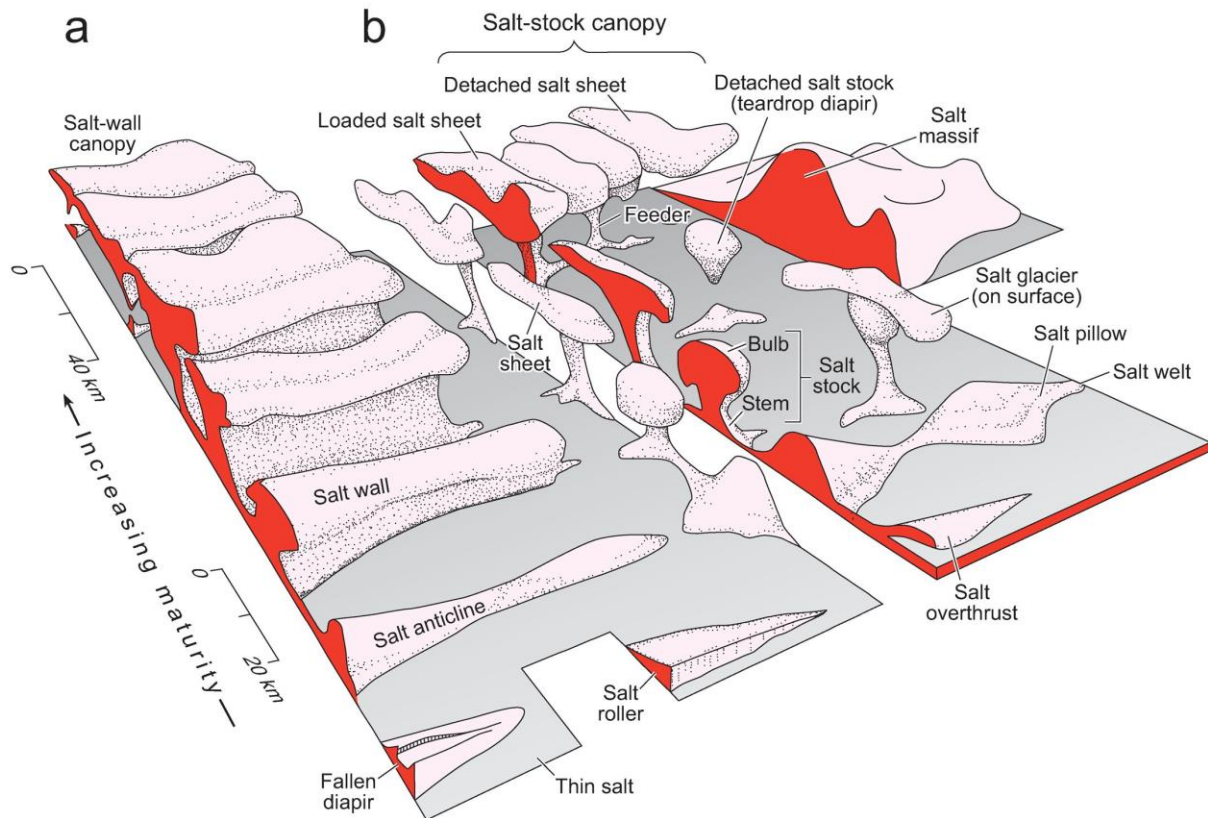


Figure 52. Diapir classification by Hudec and Jackson (2017), made after Jackson and Talbot (1986).

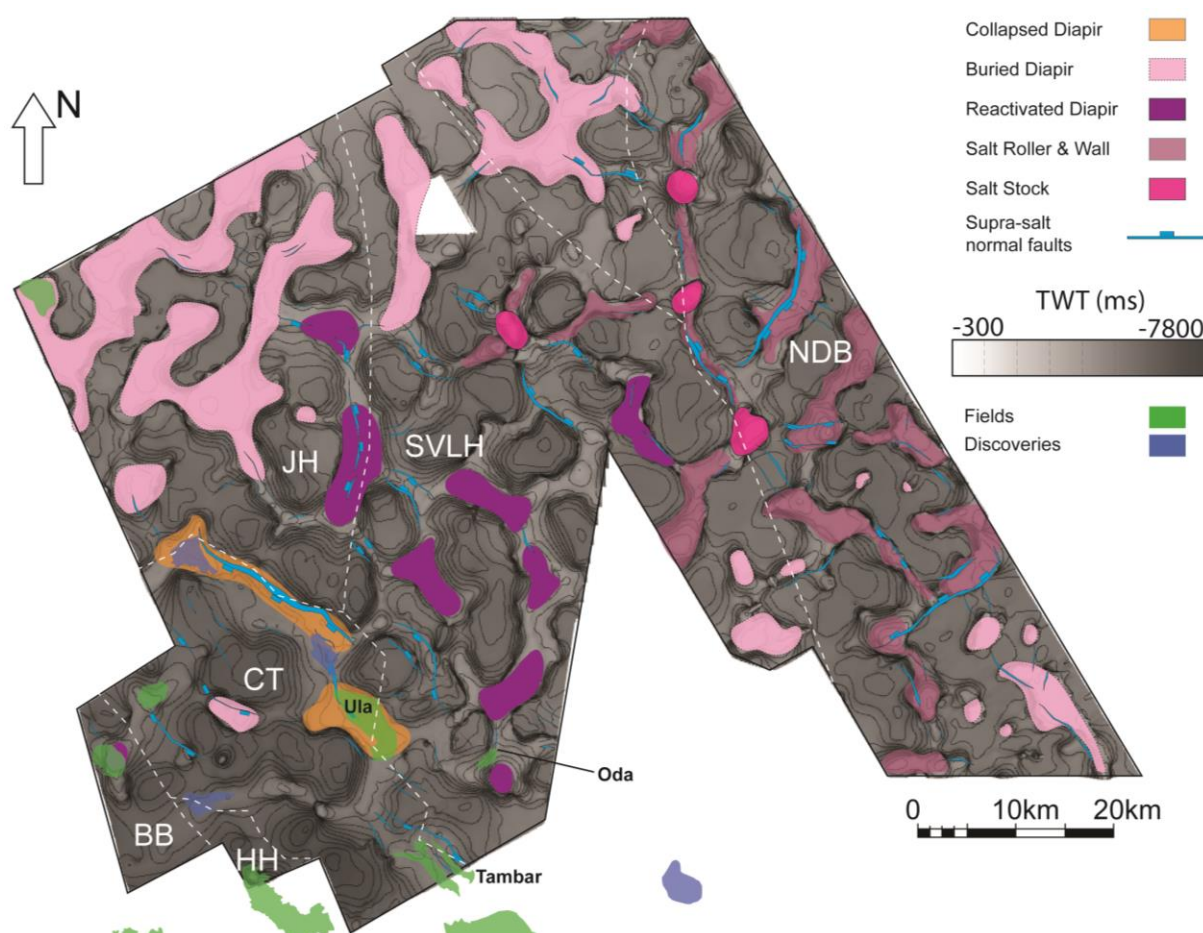


Figure 53. Interpretation of the different diapir types in the top Zechstein Group map. Structural elements included are the (BB)=Breiflabb Basin; (CT)=Cod Terrace; (HH)=Hidra High; (JH) = Jæren High; (NDB)=Norwegian-Danish Basin and (SVLH)=Sørvestlandet High.

5.1.2 Structural distribution

The classified structures are not strictly confined to a specific location. However, there are spatial relationships between the structure types: collapsed diapirs are positioned on the Cod Terrace (CT) and along the Jæren High (JH) margin; reactivated diapirs are mostly restricted to the JH and Sørvestlandet High (SVLH); buried diapirs can be found north of the reactivated diapirs and dispersed throughout the area; while salt stocks, walls and rollers are located in the eastern boundary towards the Norwegian-Danish Basin (NDB) (Fig. 54).

Relative to the normal faults offsetting the top Rotliegend Group, the major N-S aligned salt stocks and rollers follow the fault trends (Fig. 55). It is unclear, with the exception of these salt stocks and rollers, what impact the sub-salt normal faults have on the salt distribution in the study area. The salt walls and rollers, oriented NE-SW, propagating from the NDB do not follow the N-S sub-salt fault trends, suggesting that other mechanisms are influencing their geometries. This could be explained by the direction of the Triassic depositional systems, with

SW sediment-oriented transport directions, which could result in the development of NE-SW trending minibasins and associated salt withdrawal. This will result in linear salt walls developed parallel with the Triassic minibasins as observed to-day (similar systems and salt structuring have been described by Banham and Mountney, 2013).

Moving eastward to the SVLH and the reactivated diapirs, most of the structures are placed above the footwall or directly above the sub-salt faults (Fig. 55). However, laterally, the salt structures do not follow the underlying deformation.

On the CT, the collapsed diapir defining the Ula structure is located along an underlying normal fault, while, moving north, the elongated collapsed diapir does not follow any of the underlying structures. The northern collapsed diapir seems to be largely related to the supra-salt deformation, which together with the salt movement, accommodates the deformation of the sub-salt faults beneath the diapir (Fig. 53). This suggests a diapir that is influenced by deformation tied directly to Upper Jurassic – Early Cretaceous rifting, rather than pure diapir collapse as seen on the Ula structure. From the descriptions above, it is evident that there is a diversity in structural styles within the area, even between structures classified on the same basis.

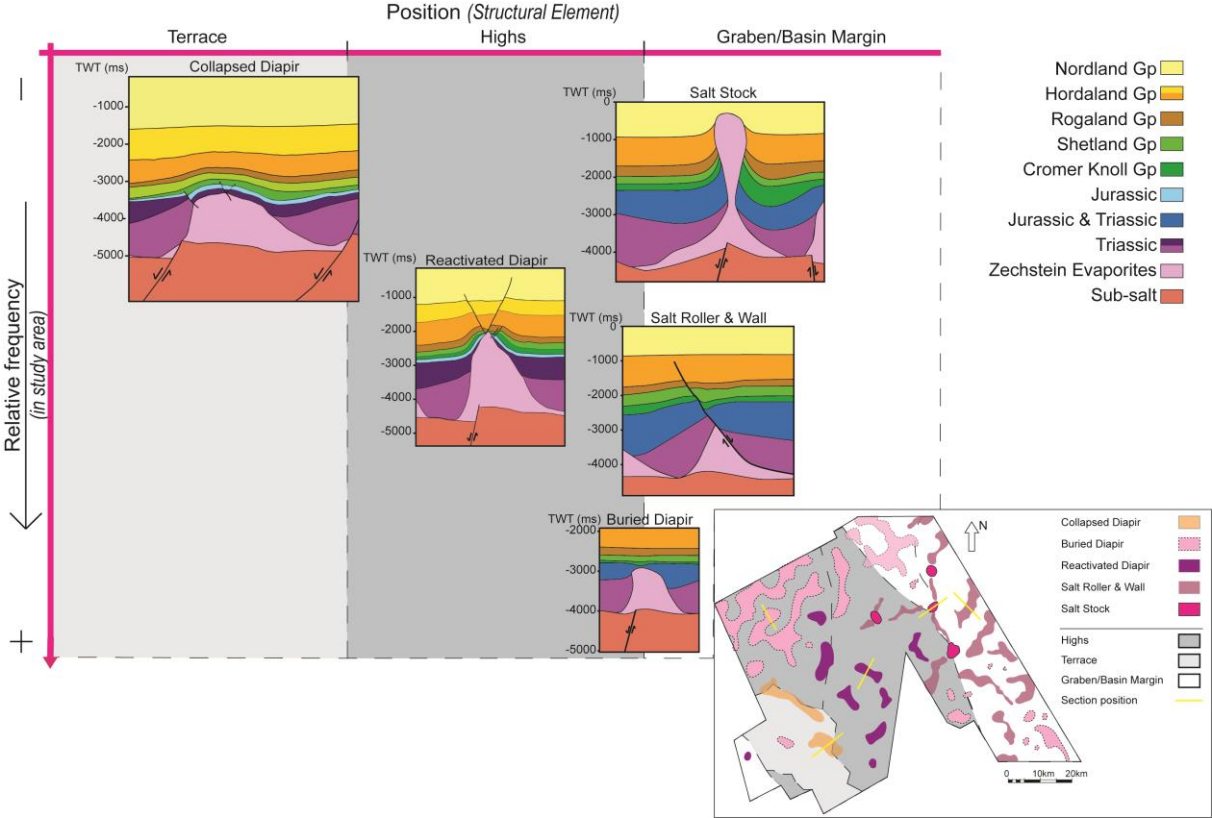


Figure 54. Salt classification plot. X-axis provides position in terms of structural element. Y-axis is the relative abundance of the selected structure within the study area. Vertical exaggeration = 3

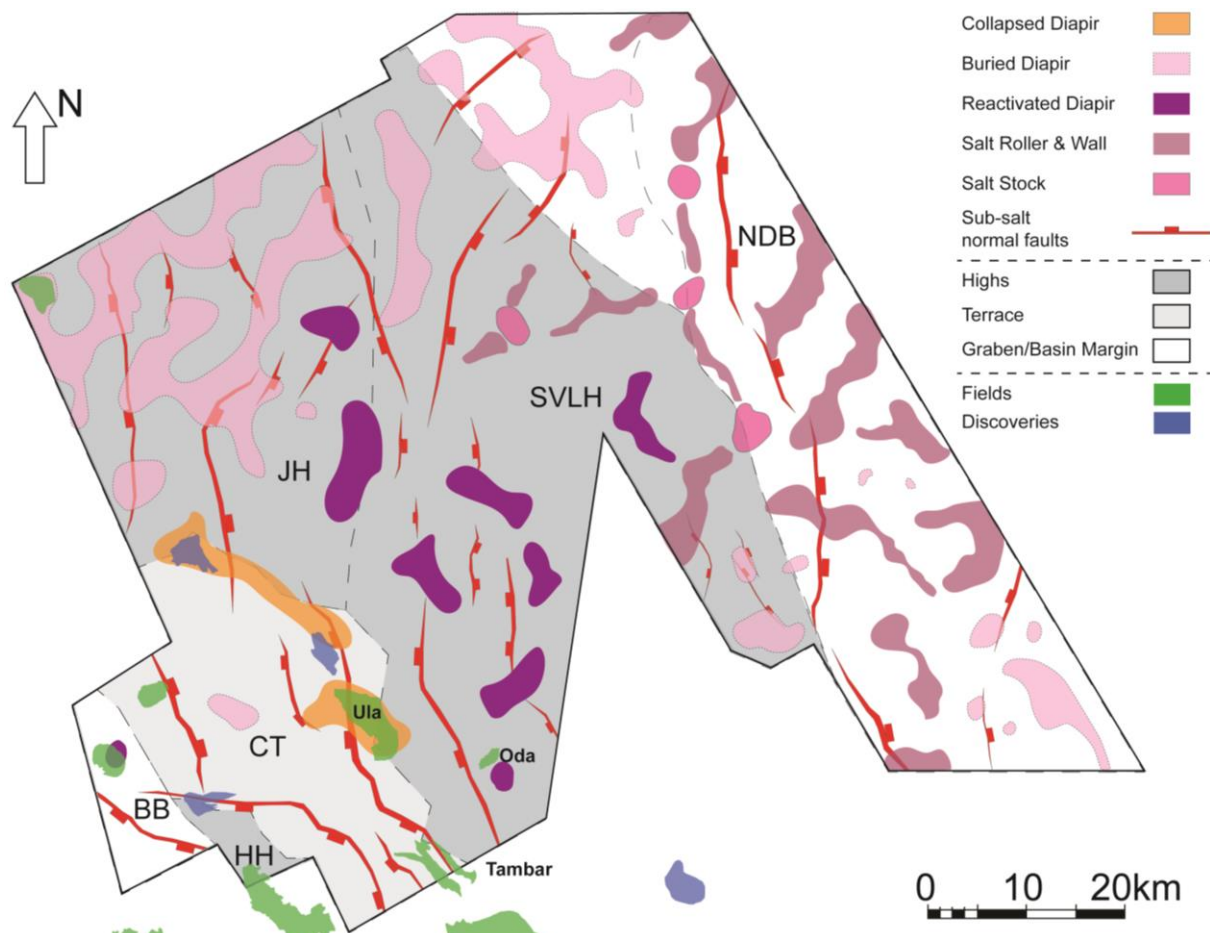


Figure 55. Sub-salt normal faults interpreted on the top Rotliegend Group with overlying salt structures, field and discoveries. Structural elements included are the (BB)=Breiflabb Basin; (CT)=Cod Terrace; (HH)=Hydra High; (JH) = Jæren High; (NDB)=Norwegian-Danish Basin and (SVLH)=Sørvestlandet High.

5.1.3 Salt composition

As discussed in the introduction, internal salt sedimentary packages influence salt mobility (Ch. 1.3.2, Salt characteristics). This affects the magnitude of salt movement, which plays a role in the development of minibasin, structural styles and tectonostratigraphic evolution. Duffy et al. (2017) investigate the lateral mobility of minibasins during shortening in the Precaspian Basin. This region is highly salt influenced, leading to the generation of supra-salt minibasins, which later have undergone contraction. Therefore, implications to Late Cretaceous – Early Paleogene compression in the North Sea can be made.

In the Precaspian Basin, a relationship between the position of minibasins, salt geometries, adjacent deformation and intra-salt sedimentary packages was established (Duffy et al., 2017). Here, areas without intra-salt sedimentary bodies experienced a large degree of diapir squeezing and deformation at minibasin margins, while, locations with abundant intra-salt sediments surrounding the minibasins were less effected by shortening (Duffy et al., 2017). This

observation led to the conclusions that intra-salt sedimentary packages kept the minibasins more stable and reduced squeezing and narrowing of the salt structures, and they remained as wide structures. There was still arching and squeezing of these structures, but not to the same extent as in areas containing purely mobile salt. Hence, the internal Zechstein Group composition can be a factor in why we see the variations in structural styles within the study area.

In the Central North Sea, Figure 56 illustrates similar observations on the Cod Terrace (CT), Jæren High (JH) and Sørvestlandet High (SVLH), where a continuous internal salt horizon was identified together with several intervals containing strong local reflectors, some of these local reflectors are covered by salt which resembles a salt canopy (i.e. northwest in Figure 56). Here, the continuous reflectors may represent intra-salt siliciclastic or carbonate packages, which are less mobile compared to the halite dominated Zechstein Group (Jackson et al., 2019). The overlying salt structures in this section are broad (i.e. collapsed diapirs). Similar observations cannot be made towards the NDB margin. This either indicates that the Zechstein Group becomes more halite-prone (Jackson et al., 2019) (Fig. 57), or that the seismic imaging is too poor to capture internal salt geometries in the eastern seismic cube, MC3D-Q8-2008. On the other hand, structural styles on the basin margins include a higher frequency of nearly pinched salt stocks and salt rollers (Fig. 54), where minibasins are almost colliding and they have undergone severe deformation (Fig.23).

The less mobile areas, which include internal salt packages within wider salt structures, are observed on the CT and SVLH. A transition towards mobile salt, defined by no internal salt reflectors and narrower structures is identified on the NDB margin (Fig. 57). Despite the possible link between internal salt packages and structural styles from east to west, the extent of intra-salt geometries within salt structures and minibasins need to be assessed further before arriving to any conclusions.

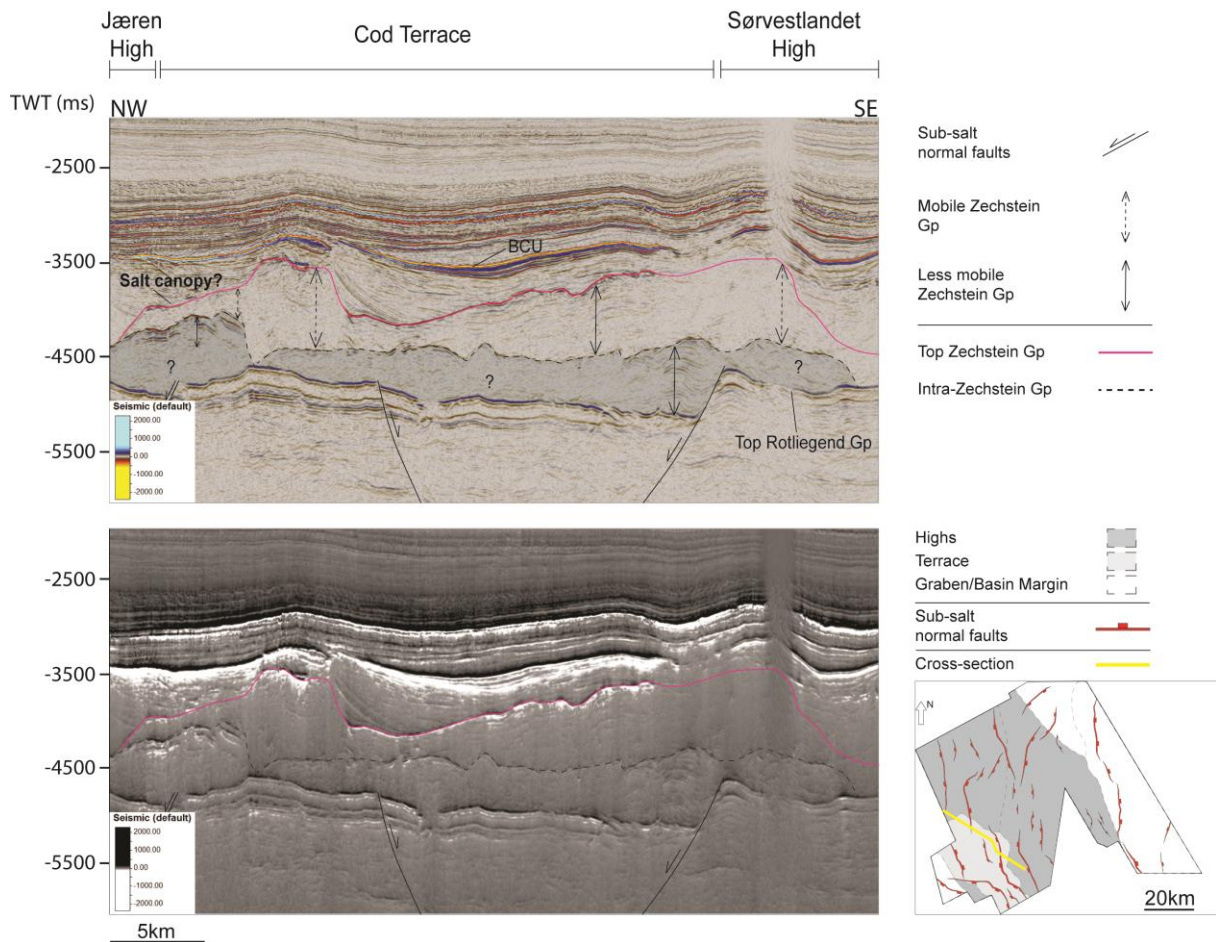


Figure 56. NW-SE cross-sections: upper section from original PGS seismic; lower section generated by using the "outcrop attribute".

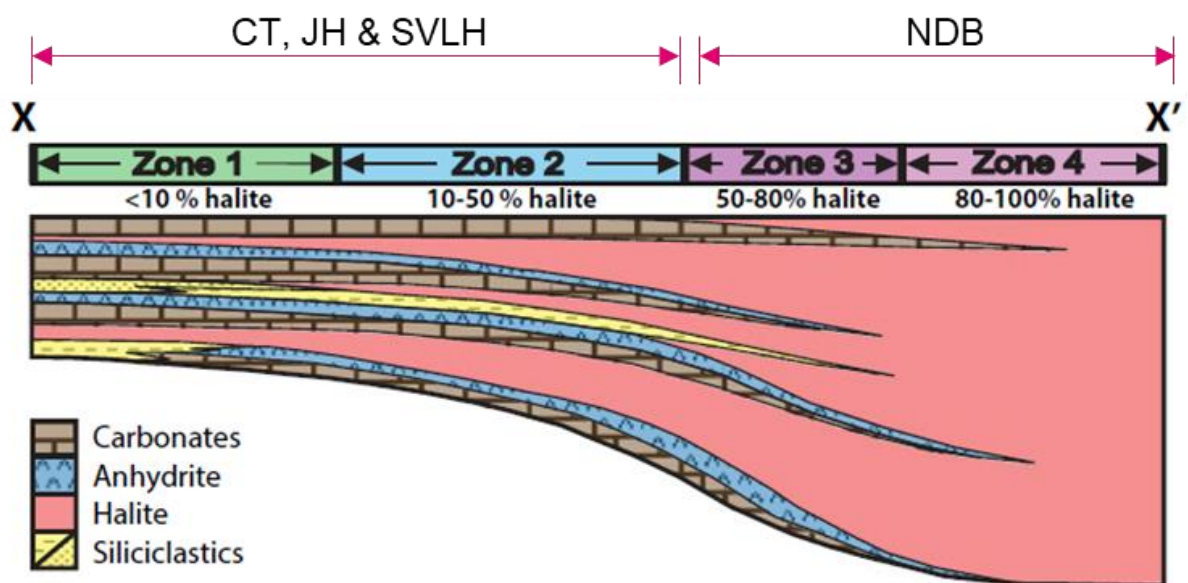


Figure 57. Salt composition from the basin-centre towards the basin margins, defined by four zones (from Jackson et al., 2019). Proposed ranges within study area are displayed; CT = Cod Terrace, JH = Jæren High, SVLH = Sørvestlandet High and NDB = Norwegian-Danish Basin.

5.2 Structural evolution

The next discussion point is the structural evolution of the area, with comparisons between collapsed and reactivated diapirs. Timing of salt movement and related triggers are evaluated.

5.2.1 Permian

Pre-existing faults and sub-salt basin configuration

Observations in chapter 4 show that the sub-salt sediments are offset by normal faults with throws up to 2.5 km on the CT (e.g. Oda restoration, Fig. 47). An E-W section north of Oda through the SVLH and CT, show several normal faults offsetting the Rotliegend Group (Fig. 58). From west to east, the Rotliegendes interval is gradually thickening. This indicates that the basin was tilted eastwards during the Permian with the largest accommodation space on the SVLH, suggesting that this area was not a structural high at this time. Additionally, an important relationship regarding timing of the sub-salt fault movement can be made. The Rotliegendes interval reveals no drastic thickness variations, and certainly no growth strata related to faulting. This constrains the main deformation to the post Rotliegendes deposition.

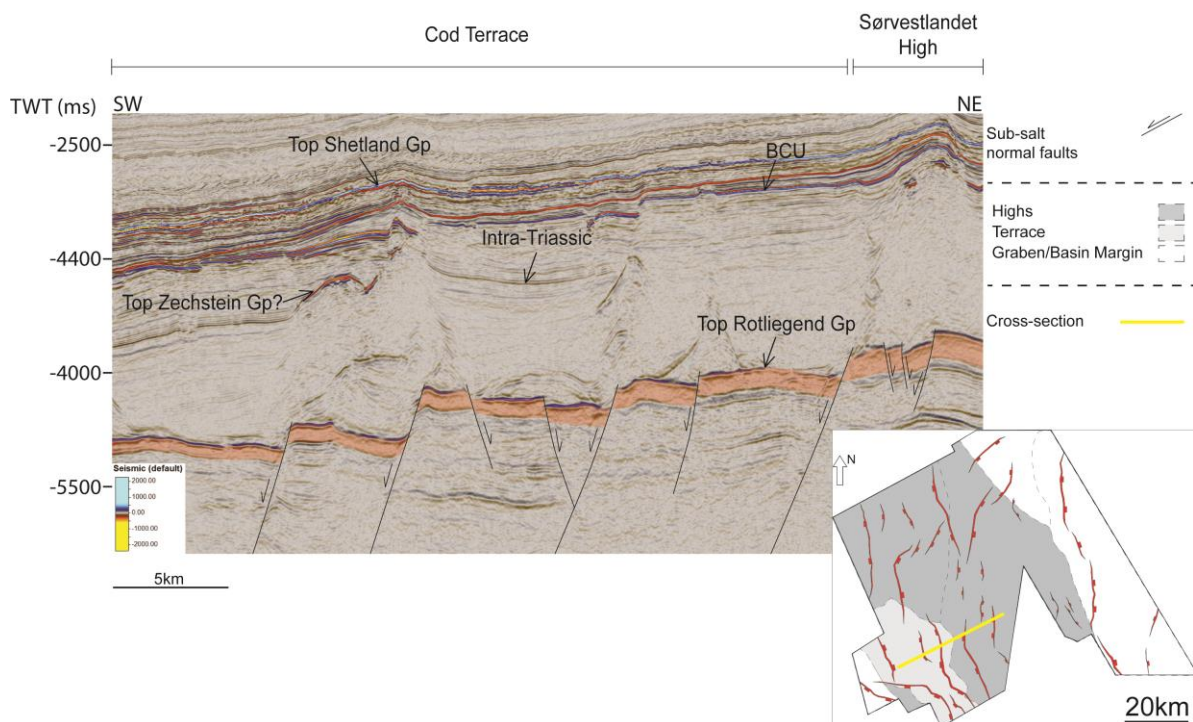


Figure 58. E-W cross-section across the PGS16008CGR cube, including a sub-salt interval and faults.

5.2.2 Triassic

Initial Triassic sedimentation is typically indicated by tabular reflectors at the base of minibasins (Figs. 59 and 60), suggesting relatively stable deposition. The presence of growth strata that onlap onto the lowermost tabular packages (Fig. 59B) suggest that soon after initial deposition the basins began to differentially subside. At Ula and other salt structures on the CT and SVLH this may have been directly linked to the reactivation of sub-salt normal faults (Fig. 59C). Localisation of sediment deposition over sub-salt faults was accommodated by salt evacuation to adjacent diapirs.

During the early Triassic the minibasins began to ground against the sub-salt Rotliegendes. This is best illustrated by a small turtle structure situated on the footwall of a sub-salt fault east of Ula (Fig 60). A change in maximum package thickness from the centre to the flanks of the minibasin indicate that the base of the minibasin had grounded and the flanks began to collapse (Figs. 60 B and C). Subsequently, the grounded basins became buried by tabular packages. Elsewhere, minibasin growth continued in the non-grounded areas resulting in thick late Triassic packages and the rotation of partly grounded minibasins. Rotation may have resulted in local erosion or non-deposition above the grounded areas (Fig. 59 B and C).

By the end of the Triassic the salt diapirs had become increasingly isolated by minibasins. This restricted the salt supply and, in some locations, resulted in the crests being buried by late Jurassic sediments (59A).

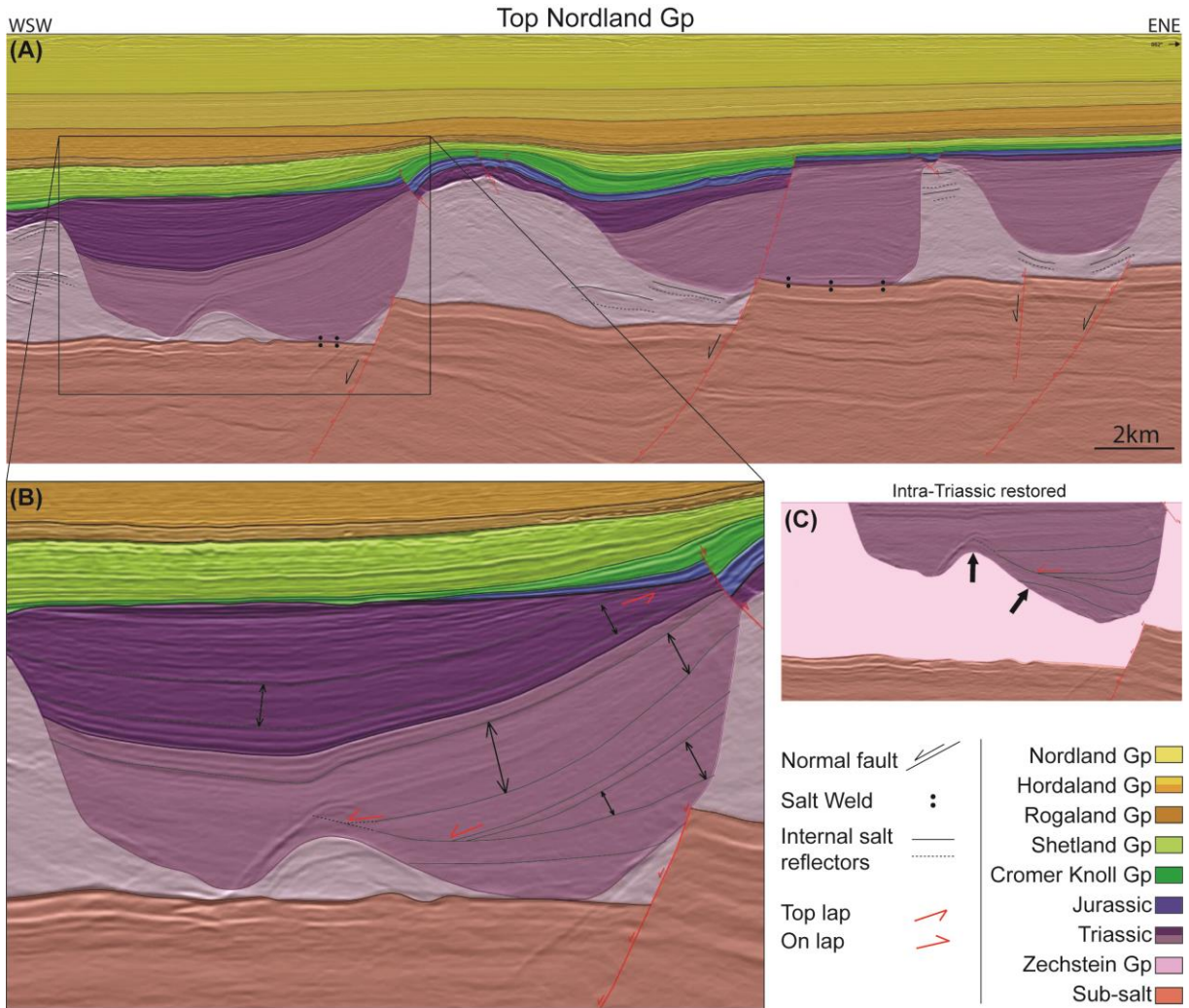


Figure 59. W-E cross section illustrating intra-Triassic reflector geometries covering the collapsed diapir, Ula Structure: (A) present-day section of the collapsed Ula structure; (B) present-day strata-terminations; and (C) Intra-Triassic restored section with strata-terminations. VE = 1

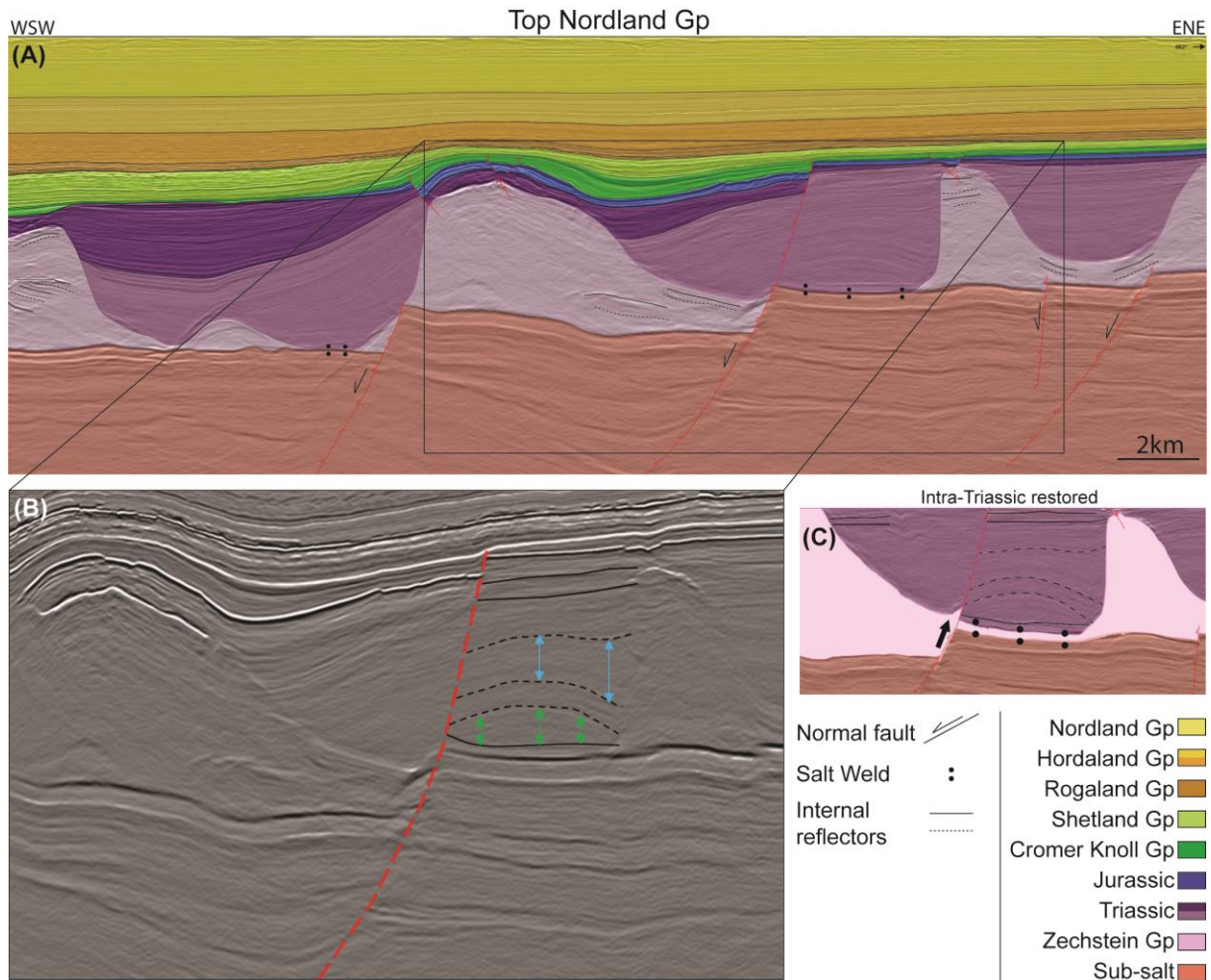


Figure 60. W-E cross section illustrating intra-Triassic reflector geometries covering the collapsed diapir, Ula Structure: (A) present-day section; (B) a present-day turtle structure observed east of the Ula Structure, where green arrows represent the first growth package, and the blue arrows mark a shift in the depocenter towards the east; and (C) Intra-Triassic restored section with the turtle structure still present. VE = 1

5.2.3 Jurassic

In the Jurassic, the studied collapsed and reactivated diapirs show different magnitudes of salt movement and diapirism. For the collapsed diapirs, Mannie et al. (2014) suggests that the accommodation space generated during salt collapse was triggered by regional Jurassic extension. Their observations fit with the restoration of the Ula structure (Fig. 61A). Here, two supra-salt minibasins above the diapir crest subsided during deposition of the Jurassic sediments.

Approximately 20 kilometers NE of the Ula structure, the NW-SE trending reactivated diapir was restored (Fig. 61B). This structure shows two different characteristics during the Jurassic compared to the collapsed diapir. First, the reactivated diapir is slightly higher and narrower than the collapsed diapir (Figs. 61A and B). Second, the salt is emergent, indicating a phase of passive diapirism, and shows minor collapse above the diapir flanks (Figs. 61A and B). This leads to less available space and thinner intervals above the diapir crest. Despite this, supra-salt minibasins on the flanks of the reactivated diapir could host comparable Upper Jurassic units as seen above the collapsed diapirs (Fig. 61B).

For the other reactivated diapirs, the Oda structure and the NE-SW trending diapir, the Jurassic stratigraphy is included in the “Jurassic & Triassic” sequence (Figs. 47G and 49G). Whilst the Jurassic layer is thinner and difficult to resolve on seismic data, it is expected to have a similar geometry to the NW-SE trending diapir (Fig. 61B) (Midland Valley internal report).

The differences between the collapsed and reactivated diapirs suggests different lateral salt mobility in each area, either caused by salt composition or structural configuration. Salt flows from the collapsed diapirs and feed the reactivated diapirs. However, as mentioned above, the reactivated diapirs also experience minor salt withdrawal (Fig. 61B) which implies that lateral mobility between structures is complex.

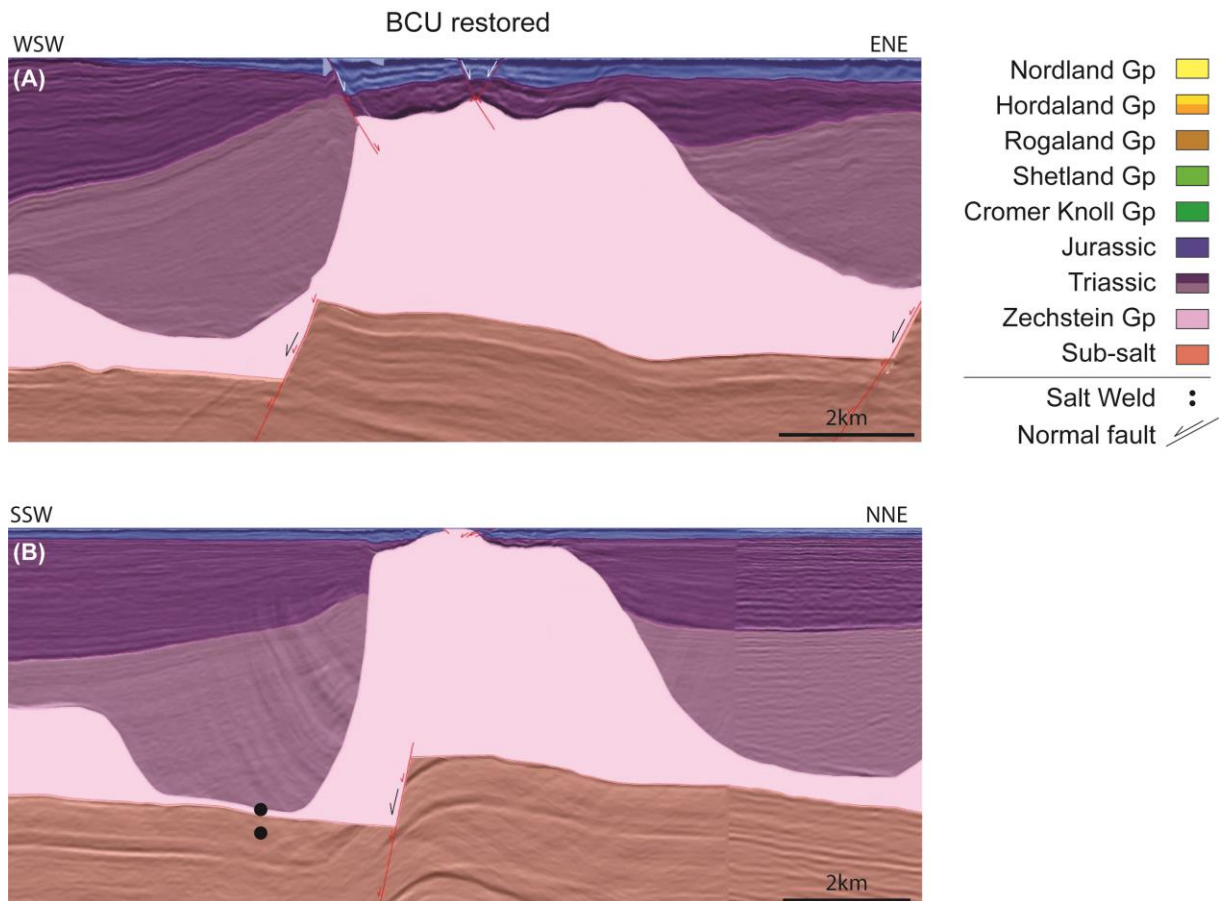


Figure 61. W-E restored BCU cross section for (A): Collapsed diapir, Ula structure; and (B): NW-SE trending reactivated diapir. VE = 1

5.2.4 Cretaceous

Lower Cretaceous

In the Lower Cretaceous salt withdrawal continued, based on the large thickness variations that are observed on the Cromer Knoll Group time-thickness map (Fig. 37C). Here, the group is thin above most salt structures, implying that these structures were local structural highs at the time.

Development of flank faults above the collapsed diapirs and formation of rollovers generated more accommodation space at the flanks (e.g. Fig. 62A). Also, for the collapsed Ula diapir and NW-SE trending reactivated diapir there is evidence of salt withdrawal towards the diapir flanks from the Cromer Knoll Group flank thickening (Figs. 62A and B). Both structures were likely undergoing minor diapirism, triggered by extension and the sediment load inferred to the diapir flanks. Despite this similarity, the collapsed diapir was covered completely by sediments, while the reactivated diapir was still emergent (Figs. 62A and B). The deformation therefore varies; the collapsed diapir was deforming its overburden and generating positive structural relief

directly above the diapir crest, while the NW-SE reactivated diapir was folding the underlying layers upward.

The two other reactivated diapirs show little to no evidence of diapir collapse during this period. They were likely near or at surface at the time, growing as passive or active diapirs (Figs. 47F and 49F).

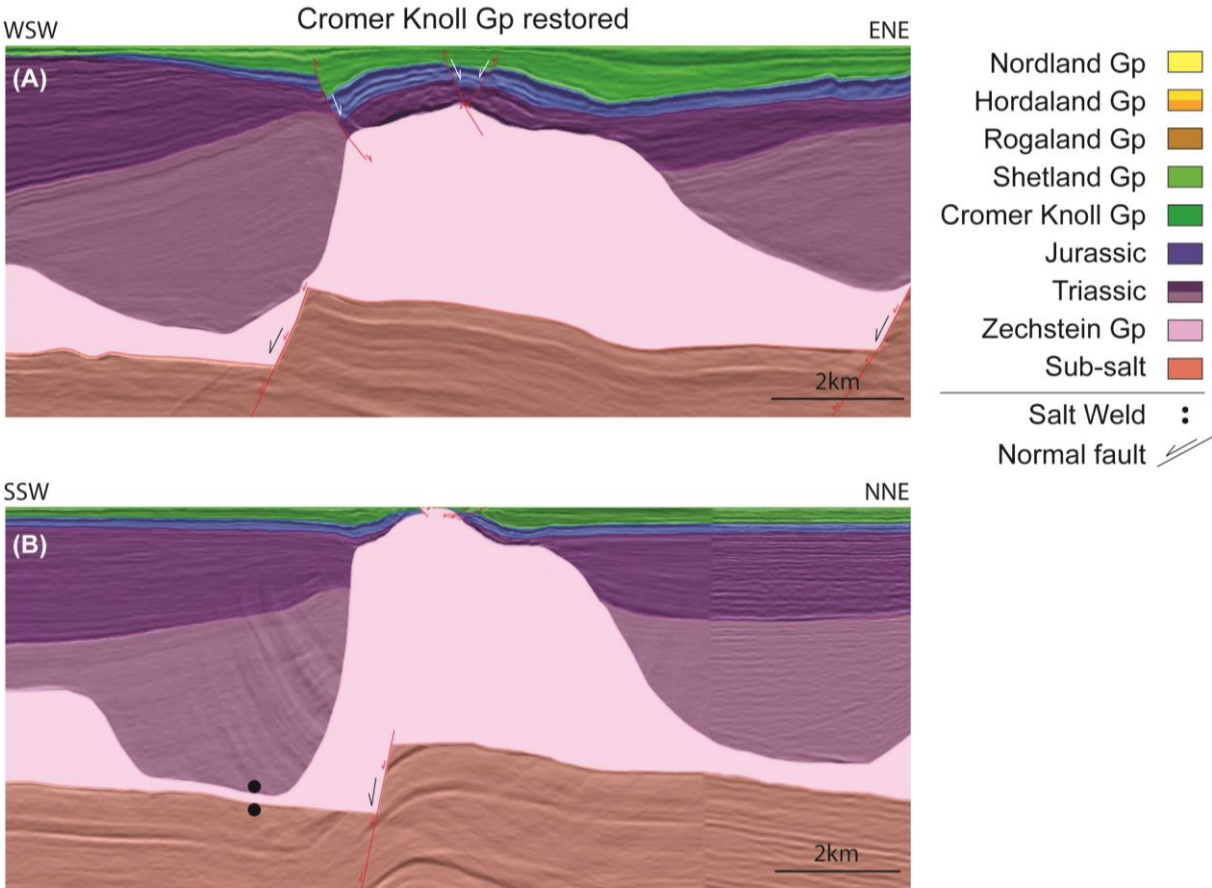


Figure 62. W-E restored Cromer Knoll Group cross-section for (A): Collapsed diapir, Ula structure; and (B): NW-SE trending reactivated diapir. VE = 1

Upper Cretaceous

In the time-thickness map of the Shetland Group, the group thins above diapir crests (Fig. 38C), indicating that the diapirs still were structural highs during the Late Cretaceous. Additionally, the structural development from the restored Cromer Knoll Group to the restored Shetland Group reveals uplift of the top Cromer Knoll Group horizon beyond its regional level (Figs. 63B and C). Similar observations are made in all of the restored sections, demonstrating that the structural rejuvenation is related to a regional event affecting the terrace and the highs (Figs. 45E, 47E, 49E and 51E). Also, layers within the lower part of the Shetland Group are lapping onto the Cromer Knoll Group for both collapsed and reactivated diapirs, which emphasises that the diapirs were in fact areas of positive structural relief during the early stages of chalk deposition. Therefore, the salt remobilization must have initiated early in Upper Cretaceous, likely triggered by regional shortening (Kley and Voigt, 2008). This transition into the Upper Cretaceous marks a change from periods dominated by regional extension and subsidence to a period of compression acting on the basin. Shortening caused salt to remobilize, overprinting earlier events.

Above collapsed and reactivated diapirs, the upper part of the Shetland Group thins without visible onlaps and is overlain by a near top Ekofisk Formation reflector. This reflector becomes chaotic and discontinuous away from the diapir crest (e.g. Fig. 44, western flank of the Ula structure), suggesting that the chalk group was uplifted once more and redeposited towards the basins surrounding the diapirs (Hodgson et al., 1992).

Overall, the diapirs were influenced by at least two pulses of shortening separated by periods of tectonic quiescence and gradual deposition. This led to folding of the Jurassic and Lower Cretaceous successions immediately after the extension phase and redeposition of the Chalk Group during the transition to the Paleogene.

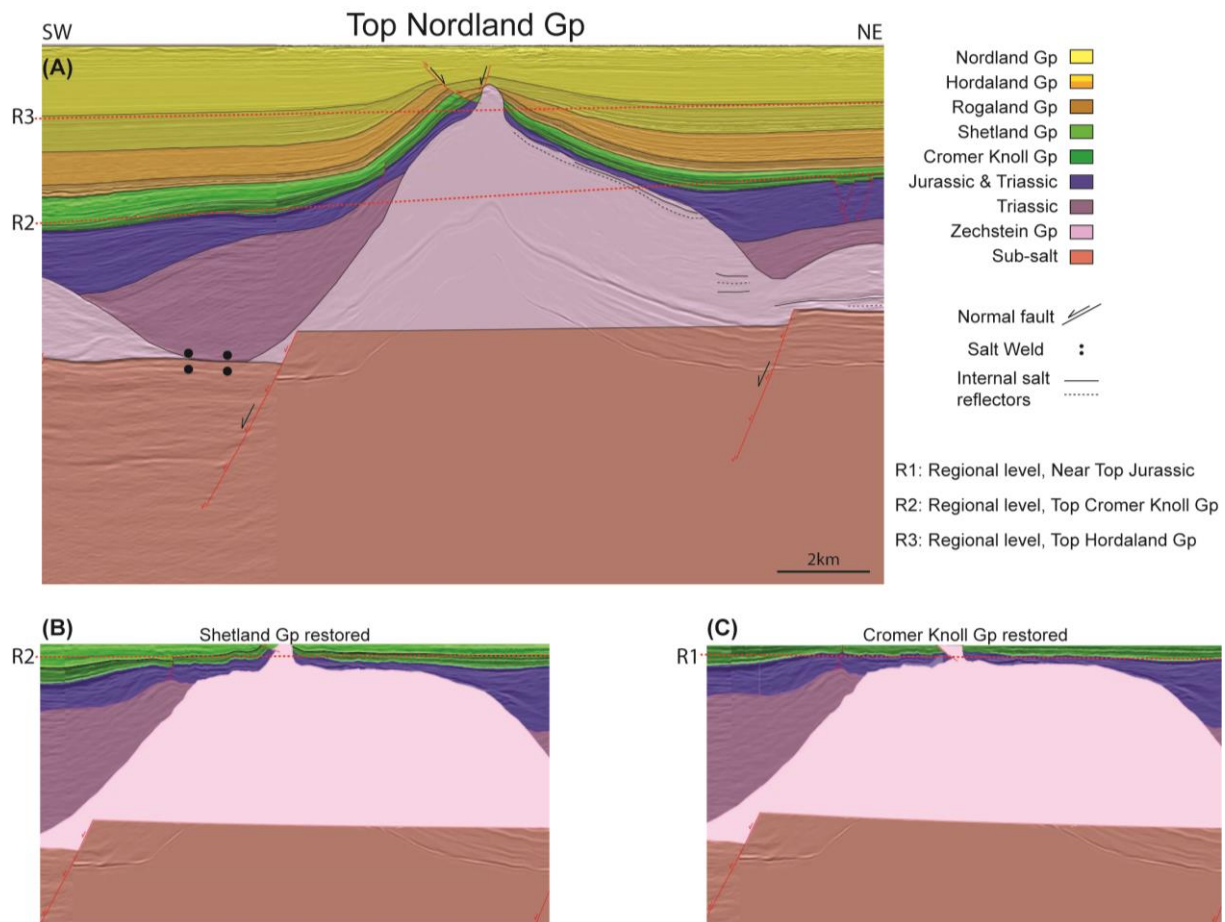


Figure 63. W-E cross-section capturing the Oda structure. (A): Present-day geometries. R2 and R3 are regional levels for top Cromer Knoll Group and top Hordaland Group, respectively; (B): Restored Shetland Group. R2 is the regional level for the top Cromer Knoll Group; and (C): Restored Cromer Knoll Group. R1 is the regional level for the near top Jurassic (BCU). VE = 1

5.2.5 Cenozoic

Paleogene and Neogene

In the Early Paleogene, shortening continued, associated to the Alpine orogeny and NE-Atlantic ridge-push. These events likely lead to renewed salt movement, based on the following discussion.

Focussing on the Paleogene and Neogene salt development, the collapsed diapirs and the reactivated diapirs experience various degrees of structural rejuvenation. Throughout these periods, the Oda structure was emergent or near surface (Fig. 63A), whereas the NW-SE and NE-SW trending reactivated diapirs and the Ula structure were buried by sediments (Figs. 45 B, C and D; 47 B, C and D; 49 B, C and D; and 51 B, C and D).

During the onset of the Rogaland Group deposition, the collapsed diapir was covered by more than 1 km of sediments (Fig. 45D). It is expected that areas with large amounts of mobile salt

and weak overburdens will undergo more deformation than deeply buried salt structures and areas without mobile salt. This applies to the structural evolution of the structures on the CT and SVLH, where the magnitude of salt growth is reduced with increasing amounts of sediments covering the diapirs and likely influenced by the salt composition (e.g. Figs. 56 and 57). Moreover, the diapirs with less sediment cover are prone to salt remobilization.

Timing of reactivation can be derived from the Oda structure (Fig. 63A), where evidence supporting diapir growth by shortening is shown in the restored Cenozoic sections (Fig. 64). The Shetland Group, Rogaland Group and intra-Hordaland Group were folded upwards and lifted above their regional levels (Fig. 64A, B and C), suggesting that the salt structure remobilized during each time step. The uplift above the regional is largest in the restored intra-Hordaland Group, implying that the amount of shortening during deposition of the intra-Hordaland group was the greatest. This is in agreement with the observed thickness variation on the time-thickness maps (Figs. 39C, 41T1 and 41T2), where the largest thickness differences above the diapirs are within the intra-Hordaland Group.

In the upper part of the Hordaland Group, there is little evidence supporting growth of the collapsed diapirs, as identified from the Oda section (Fig. 64A). The thickness variations related to salt structures within the upper Hordaland Group are mainly constrained to the intervals overlying the reactivated diapirs (Fig. 41T2). However, this unit thins above some of the collapsed and buried diapirs, which is likely attributed to differential compaction. The restored top Hordaland Group from the collapsed diapir confirms this; the intra-Hordaland reflector is not lifted far above its regional level, suggesting that there was little to no salt remobilization (Fig. 65).

Quaternary

The final stage is captured by the Nordland Group, which displays a clear SW thickening trend, only affected by the major salt stocks and reactivated diapirs (Fig. 42). Sedimentation rates were high, which stack thick units above the collapsed and buried diapirs making them difficult to remobilize. At the same time, shortening could have acted as a trigger to further mobilize the reactivated diapirs and salt stocks, based on the uplift of the top Hordaland Group above its regional level (Fig. 63A).

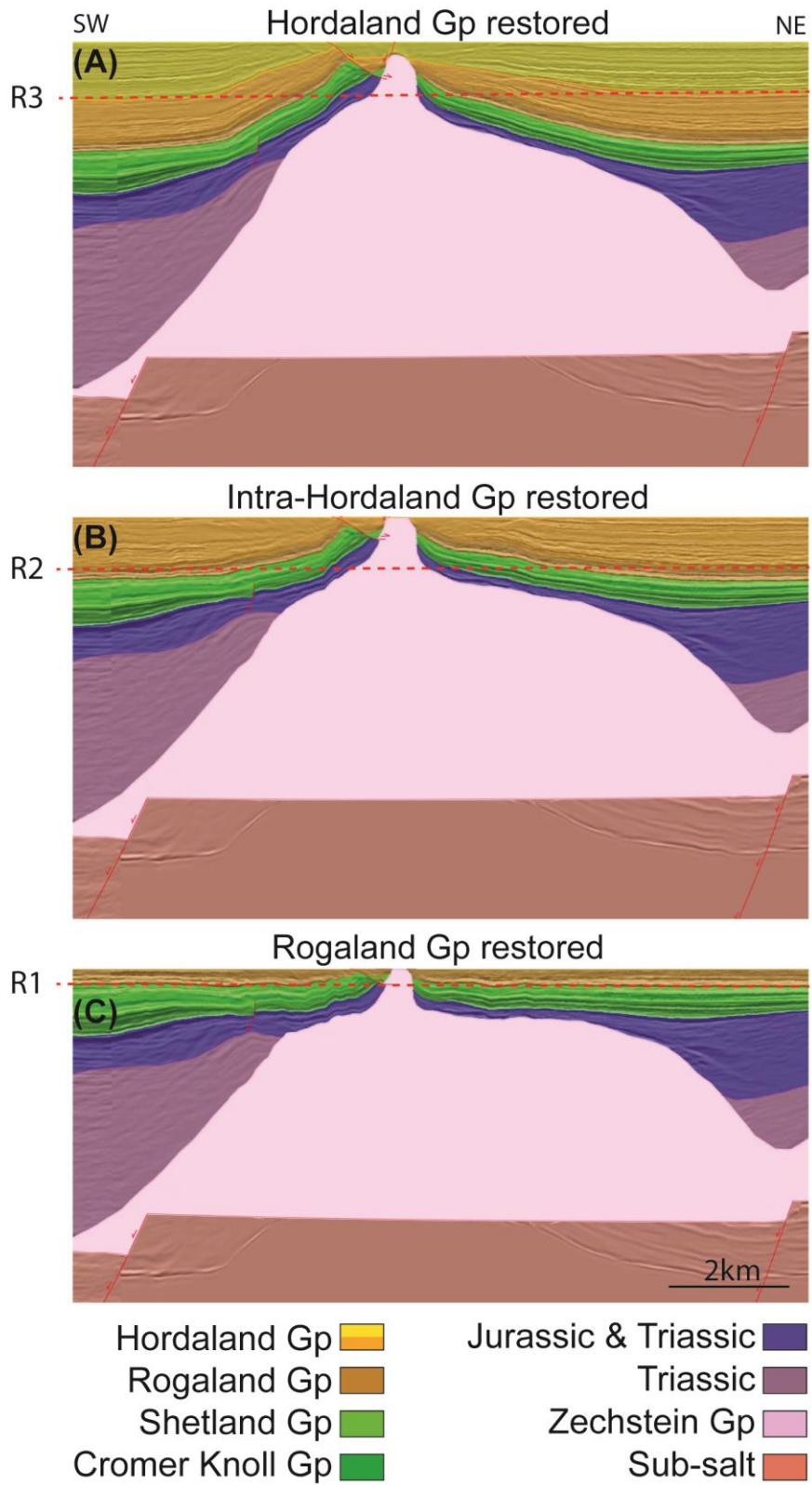


Figure 64. W-E cross-section capturing the Oda structure. (A): Restored top Hordaland Group. R3 is the regional level for the top intra-Hordaland Group; (B): Restored intra-Hordaland Group. R2 is the regional level for the top Rogaland Group; and (C): Restored Rogaland Group. R1 is the regional level for the top Shetland Group. VE = 1

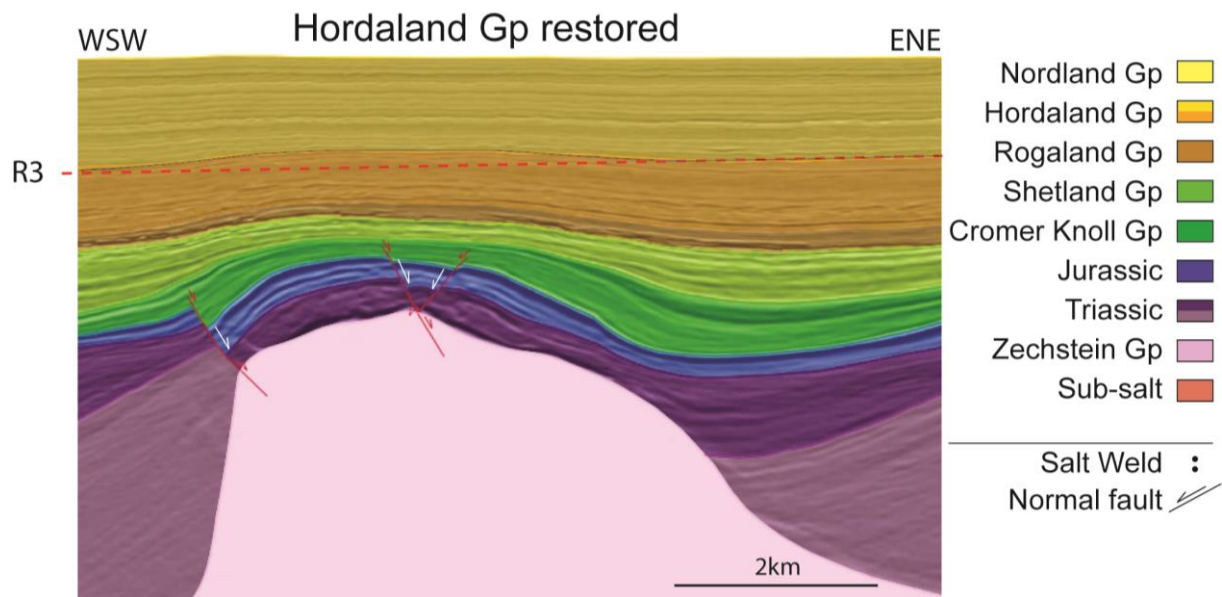


Figure 65. W-E restored top Hordaland Group cross-section capturing the Ula structure. R3 is the regional level for the top intra-Hordaland Group. VE = 1

5.3 Implications for the petroleum system

Similar to chapter 5.2, *Structural evolution*, the focus will be the collapsed and reactivated diapirs on the Cod Terrace (CT) and Sørvestlandet High (SVLH).

5.3.1 Reservoir

Jurassic reservoir potential is proven throughout the Cod Terrace (e.g. Ula, Tambar and Gyda fields) and in specific locations on the Sørvestlandet High (i.e. Oda field). From the restorations, detailed Jurassic reservoir distributions cannot be made. However, in terms of reservoir presence, the collapsed diapir created accommodation space above the diapir crest for a thick Jurassic interval. Additionally, the NW-SE reactivated diapir looks promising for accumulation of a Jurassic interval near the diapir crest (Ch. 5.2.3), although generally the reactivated diapirs grew and preserved less supra-salt Jurassic sediment.

5.3.2 Trap types and timing

The broad range of salt geometries and correspondent deformation in the study area generates different hydrocarbon traps near collapsed and reactivated diapirs. The timing of trap formation for the two diapir types (i.e. collapsed and reactivated diapirs) is not consistent.

Collapsed diapir

From Mannie et al. (2014) the main trap forming period is the Late Cretaceous – Early Paleogene compression, which arguably is the most defined event remobilizing salt and

structuring the supra-salt successions throughout the CT and SVLH (Ch. 5.2.4 and 5.2.5). Nevertheless, for specific structures such as the collapsed Ula diapir, this is not the case.

In the Ula diapir, structuring of the Jurassic interval occurred shortly after its deposition during flank-collapse in the Early Cretaceous (Ch. 5.2.4). The flank-collapse folds the overburden, resulting in an anticline traps above the salt structure (Fig. 45F). This structure was then enhanced by Late Cretaceous – Early Paleogene shortening (Figs. 45D and E). In the Cenozoic, there is little evidence of salt movement in the collapsed diapirs (Figs. 45A, B and C). This results in only minor deformation, leaving the trap intact.

Reactivated diapirs

A clear distinction between collapsed and reactivated diapirs is the frequency of salt remobilization, where the reactivated diapirs have undergone significant salt movement (e.g. Oda structure, NW-SE trending diapir and NE-SW trending diapir). The successions above and adjacent to the reactivated diapirs are therefore heavily deformed by folding and faulting. Thus, the related traps are commonly fault dependent traps or salt flank traps (Fig. 10). Based on the restored sections, these traps initiate during the Late Cretaceous – Early Paleogene shortening (Fig. 63B). However, for the NE-SW and NW-SE trending reactivated diapirs, the Jurassic sediments deforms during Early Cretaceous deposition (Figs. 49F and 51F), similar to the collapsed diapirs but influenced by less flank collapse (Fig. 62B).

The reactivated diapirs continue to grow during Cenozoic, triggering new faults and reactivation of existing supra-salt faults (e.g. Figs. 64A, B and C). Salt remobilization and associated deformation increase the likelihood of trap failure for this structure type.

6 Conclusions

Four seismic datasets covering parts of the Cod Terrace (CT), Sørvestlandet High (SVLH), Jæren High (JH) and Norwegian-Danish Basin (NDB) were the basis for this study. Through various interpretation and modelling techniques (i.e. conventional 3D interpretation, multi-directional salt interpretation, attribute maps and 2D sequential structural restoration), an evaluation of the salt geometries and their structural evolution leads to the following conclusions:

Based on their geometries and associated sediment growth patterns, the salt structures are divided into five groups, (1) buried diapirs; (2) collapsed diapirs; (3) reactivated diapirs; (4) salt walls and rollers; and (5) salt stocks. The salt structures formed during the Early Triassic sedimentation and were partially separated by grounded minibasins in the Late Triassic. After the Triassic salt structuring, the diapirs showed different magnitudes of salt movement:

- 1) the buried diapirs accommodated minor post-Triassic salt movements and are buried by thick post-Triassic tabular successions;
- 2) the collapsed diapirs experience salt withdrawal and supra-salt deposition during Jurassic – Early Cretaceous, followed by Late Cretaceous – Paleogene structural rejuvenation and Cenozoic burial;
- 3) the reactivated diapirs underwent minor Jurassic – Early Cretaceous collapse and major Cenozoic structural rejuvenation with associated deformation;
- 4) the salt walls and rollers were not evaluated in great detail, and appear to represent a transition between buried and reactivated diapirs; and
- 5) the salt stocks grew through the Mesozoic and Cenozoic with associated deformation and were covered by the uppermost Cenozoic sediments.

The structural evolution of the collapsed and reactivated diapirs on the Cod Terrace and Sørvestlandet High can be described as follows:

- Rapid Early Triassic deposition occurred during differential loading and salt withdrawal, likely accompanied by reactivation of sub-salt normal faults. At the end of the Triassic, salt supply was restricted as the minibasins grounded and salt structures became increasingly isolated.
- Late Jurassic – Early Cretaceous extension triggered diapir collapse and supra-salt sedimentation, with largest impact on the Cod Terrace. The Cromer Knoll Group deposition was focussed on the diapir flanks, as a response to flank collapse. This

resulted in deformation of the Jurassic interval, where an anticline formed above the collapsed diapir, Ula structure, and layers were folded near the reactivated diapirs (i.e. NW-SE and NE-SW trending reactivated diapirs).

- The Late Cretaceous – Early Paleogene marks a change in the tectonic regime from extension to shortening. The shortening is best captured from the restoration of the Oda structure, but is also identified on the other restorations. The shortening resulted in inversion of the minor Jurassic minibasins near the reactivated diapirs and enhanced the anticline above the collapsed diapir, Ula structure.
- During the Paleogene and Neogene, shortening continued with different impact on the Cod Terrace and Sørvestlandet High. The intra-Hordaland Group indicates structural rejuvenation for both the collapsed and reactivated diapirs, while the upper part of the Hordaland Group indicates salt remobilization of only the reactivated diapirs, restricted to the Sørvestlandet High. The collapsed diapirs suggest growth during the Hordaland Group deposition, but this could also be caused by differential compaction.
- High sedimentation rates during the Quaternary resulted in thick Quaternary successions covering the salt structures. The major reactivated diapirs (e.g. Oda structure) on the Sørvestlandet High are still undergoing salt remobilization, likely triggered by shortening.

Based on the structural evolution of the salt diapirs on the Cod Terrace and Sørvestlandet High, the associated risk related to reservoir presence and trap potential increase for the reactivated diapirs (i.e. on the Sørvestlandet High).

7 Recommendations for further work

The provided high-quality 3D seismic dataset (in courtesy of PGS), made it possible to identify the intra-Zechstein Group geometries. I propose that these geometries observed on the Cod Terrace and Sørvestlandet High should be investigated further, by mapping out the intra-salt sedimentary packages and, if possible, tie them to specific rock types. This will increase the understanding of the Zechstein Group deposition, structural development and structural styles in the area.

Additionally, similar to what this study has provided on a local scale, the regional interplay between the Zechstein Group distribution and the supra-salt configuration should be assessed. This would improve the understanding of regional salt and minibasin development.

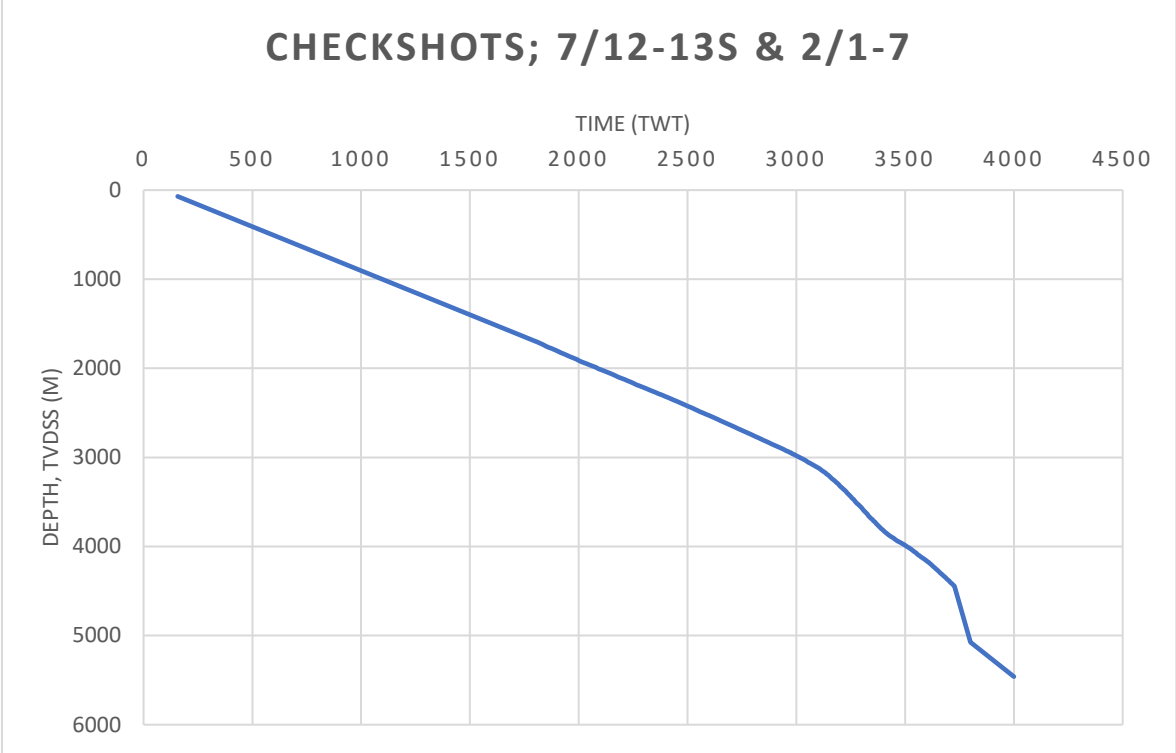
8 References

- BANHAM, S. G. & MOUNTNEY, N. P. 2013. Evolution of fluvial systems in salt-walled mini-basins: A review and new insights. *Sedimentary Geology* 296, 142-166.
- BARTON, D. C. 1933. Mechanics of formation of salt domes with special references to Gulf Coast salt domes of Texas and Louisiana. *American association of Petroleum Geologists Bulletin*.
- BOWIE, W. 1927. The part played by isostasy in geophysics and geology. *Journal of the Washington Academy of Sciences*, 17, 101-117.
- COWARD, M. P., DEWEY, J. F., HEMPTON, M. & HOLROYD, J. 2003. Tectonic evolution. In: EVANS, E. D., GRAHAM, C., ARMOUR, A. & BATHURST, P. (eds.) *The Millennium Atlas: Petroleum Geology of the Central and Northern North Sea*. Geological Society, London.
- DUFFY, O. B., FERNANDEZ, N., HUDEC, M. R., JACKSON, M. P. A., BURG, G., DOOLEY, T. P. & JACKSON, C. A.-L. 2017. Lateral mobility of minibasins during shortening: Insights from the SE Precaspian Basin, Kazakhstan. *Journal of Structural Geology* 97 257-276.
- ERIKSEN, S. H., ANDERSEN, J. H., STOKER, M. & BRZOZOWSKA, J. 2003. Oil and gas resources. In: EVANS, D., GRAHAM, C., ARMOUR, A. & BATHURST, P. (eds.) *The millennium atlas: Petroleum Geology of the Central and Northern North Sea*. London: Geological Society of London.
- ERRATT, D., THOMAS, G. M. & WALL, G. R. T. 1999. The evolution of the Central North Sea Rift. *Petroleum Geology of Northwest Europe: Proceeding of the 5th Conference* London.
- FOSSEN, H. 2010. Salt tectonics. *Structural Geology*. Cambridge: Cambridge University Press.
- GE, Z., GAWTHORPE, R. L., ROTEVATN, A. & THOMAS, M. B. 2017. Impact of normal faulting and pre-rift salt tectonics on the structural style of salt-influenced rifts: the Late Jurassic Norwegian Central Graben, North Sea. *Basin Research*. International Association of Sedimentologists and European Association of Geoscientists and Engineers and John Wiley & Sons Ltd.
- GRADSTEIN, F. & BÄSTRÖM, S. 1996. Cainozoic biostratigraphy and palaeobathymetry, northern North Sea and Haltenbanken. *Norsk Geologisk Tidsskrift*, 76, 3-32.
- GROWERS, M. B., HOLTAR, E. & SWENSSON, E. 1993. The structure of the Norwegian Central Trough (Central Graben area). *Petroleum Geology of Northwest Europe*. The Geological Society of London.
- HARDING, R. & HUUSE, M. 2015. Salt on the move: Multi stage evolution of salt diapirs in the Netherlands North Sea. *Marine and Petroleum Geology* 61 39-55.
- HODGSON, N. A., FARNSWORTH, J. & FRASER, A. J. 1992. Salt-related tectonics, sedimentation and hydrocarbon plays in the Central Graben, North Sea, UKCS. *Geological Society Special Publication No. 67*, 31-63.

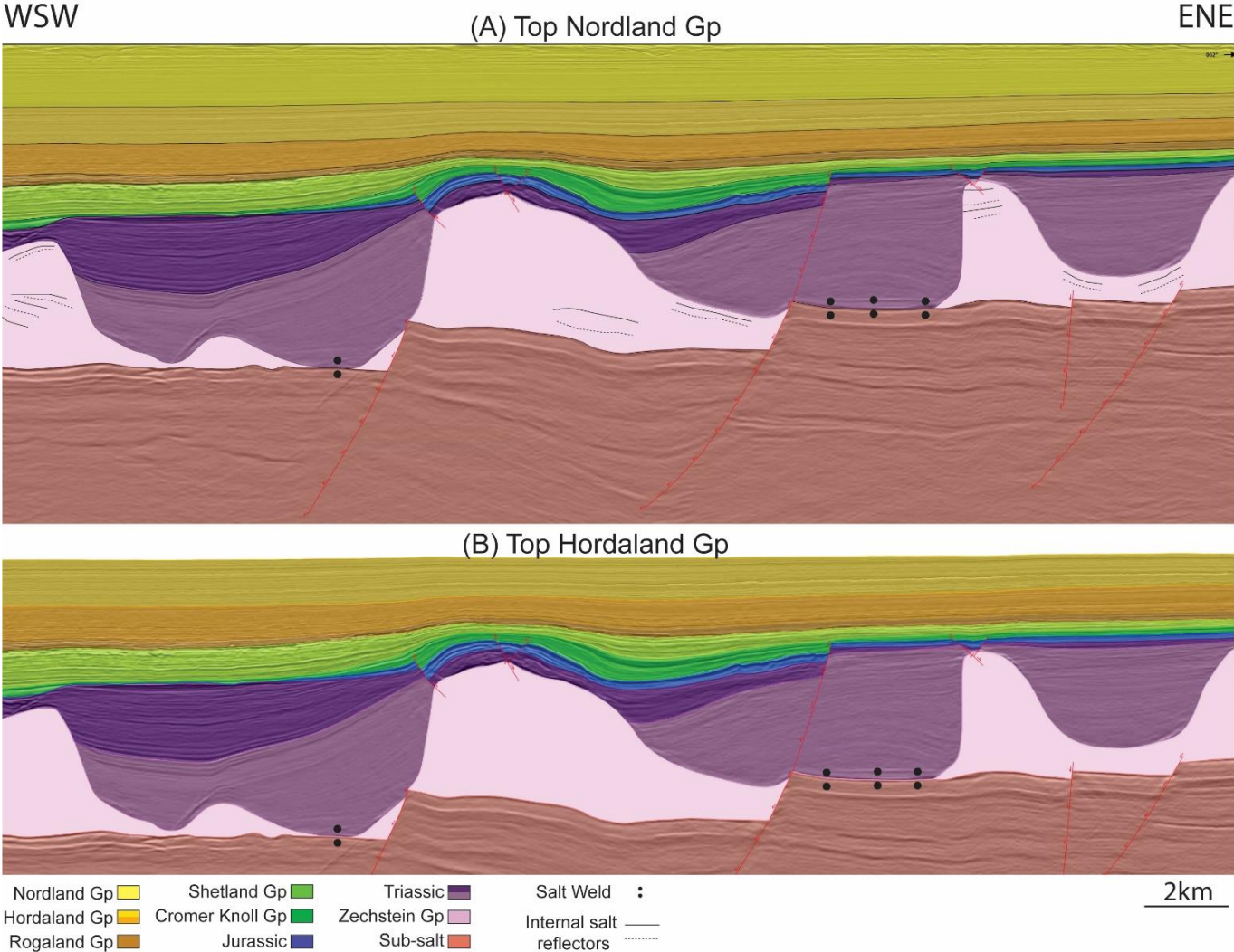
- JACKSON, C. A.-L. & LARSEN, E. 2009. Temporal and spatial development of a gravity-driven normal fault array: Middle-Upper Jurassic, South Viking Graben, northern North Sea. *Journal of Structural Geology*, 31, 388–402.
- JACKSON, C. A.-L. & LEWIS, M. M. 2016. Structural style and evolution of a salt-influenced rift basin margin: The impact of variations in salt composition and the role of polyphase extension. *Basin Research*, 28, 81–102.
- JACKSON, C. A. L., ELLIOTT, G. M., ROYCE-ROGERS, E., GAWTHORPE, R. L. & AAS, T. E. 2019. Salt thickness and composition influence rift structural style, northern North Sea, offshore Norway. *Basin Research*, 1-25.
- JACKSON, M. P. & TALBOT, C. J. 1986. External shapes, strain rates, and dynamics of salt structures. *Geological Society of America Bulletin*, 97, 305-323.
- JACKSON, M. P. A. & HUDEC, M. R. 2017. Salt Tectonics: Principles and Practice. Cambridge: Cambridge University Press.
- JACKSON, M. P. A., VENDEVILLE, B. C. & SCHULTZ-ELA, D. D. 1994. Structural Dynamics of Salt Systems. *Annual Review of Earth and Planetary Sciences* 22, 93-117.
- KARLO, J. F., BUCHEM, F. S. P. V., MOEN, J. & MILROY, K. 2014. Triassic-age salt tectonics of the Central North Sea. *Interpretation*, Vol. 2, No. 4, SM19–SM28.
- KLEY, J. & VOIGT, T. 2008. Late Cretaceous intraplate thrusting in central Europe: Effect of Africa-Iberia-Europe convergence, not Alpine collision. *Geology*, 36, 839-842.
- KNOX, R. W. O. B., BOSCH, J. H. A., RASMUSSEN, E. S., HEILMANN-CLAUSEN, C., HISS, M., DE LUGT, I. R., KASINKSI, J., KING, C., KOTHE, A., SŁODKOWSKA, B., STANDKE, G. & VANDENBERGHE, N. 2010. Cenozoic. In: DOORNENBAL, J. C. & STEVENSON, A. G. (eds.) *Petroleum Geological Atlas of the Southern Permian Basin Area*. EAGE Publications.
- LEWIS, M. M., JACKSON, C. A.-L. & GAWTHORPE, R. L. 2013. Salt-influenced normal fault growth and forced folding: The Stavanger Fault System, North Sea. *Journal of Structural Geology* 54 156-173.
- MANNIE, A. S., JACKSON, C. A.-L. & HAMPSON, G. J. 2014. Shallow-marine reservoir development in extensional diapir-collapse minibasins: An integrated subsurface case study from the Upper Jurassic of the Cod terrace, Norwegian North Sea. *AAPG Bulletin*, v. 98, no. 10 2019–2055.
- MARCUSSEN, Ø., FALEIDE, J. I., JAHREN, J. & BJØRLYKKE, K. 2010. Mudstone compaction curves in basinmodelling: a study of Mesozoic and Cenozoic Sediments in the northern North Sea. *Basin Research*, 22, 324-340.
- MCKIE, T. 2014. Climatic and tectonic controls on Triassic dryland terminal fluvial system architecture, central North Sea. In: MARTINIUS, A. W., RAVNÅS, R., HOWELL, J. A., STEEL, R. J. & WONHAM, J. P. (eds.) *From Depositional Systems to Sedimentary Successions on the Norwegian Continental Margin*. First Edition ed.

- MIDLANDVALLEYEXPLORATION 2016. Geometric restoration and structural analysis in the proximity of the Butch Discovery, Norwegian North Sea Q9035.
- PENGE, J., TAYLOR, B., HUCKERBY, J. A. & MUNNS, J. W. 1993. Extension and salt tectonics in the East Central Graben. *Petroleum Geology of Northwest Europe: Proceedings of the 4th Conference*, 1197-1209.
- PETROLEUMEXPERTS 2018. Move Knowledge Base. Edinburgh.
- ROBERTS, A. M., KUSZNIR, N. J., YIELDING, G. & BEELEY, H. 2019. Mapping the bathymetric evolution of the Northern North Sea: from Jurassic synrift archipelago through Cretaceous–Tertiary post-rift subsidence. *Petroleum Geoscience*
- ROWAN, M. G. 1993. A systematic technique for the sequential restoration of salt structures. *Tectonophysics*. Amsterdam: Elsevier Science Publishers.
- SEARS, R. A., HARBURY, A. R., PROTOY, A. J. G. & STEWART, D. J. 1993. Structural styles from the Central Graben in the UK and Norway. *Petroleum Geology Conference series* 1231-1243.
- STEWART, S. A. 2007. Salt tectonics in the North Sea Basin: a structural style template for seismic interpreters. *Geological Society, London, Special Publications*, 361-396.
- STEWART, S. A. & COWARD, M. P. 1995. Synthesis of salt tectonics in the southern North Sea, UK. *Marine and Petroleum Geology, Vol. 12, No. 5*, 457-475.
- TRUSHEIM, F. 1960. Mechanism of salt migration in North Germany. *AAPG Bulletin* 44 1519-1540.
- TVEDT, A. B. M., ROTEVATN, A., JACKSON, C. A.-L., FOSSEN, H. & GAWTHORPE, R. L. 2013. Growth of normal faults in multilayer sequences: A 3D seismic case study from the Egersund Basin, Norwegian North Sea. *Journal of Structural Geology* 55 1-20.
- VENDEVILLE, B. C. & JACKSON, M. P. A. 1992. The rise of diapirs during thin-skinned extension. *Marine and Petroleum Geology*
- WILLIAMS-STROUD, S. C. & PAUL, J. 1977. Initiation and growth of gypsum piercement structures in the Zechstein Basin. *Journal of Structural Geology* 19, 897-907.
- ZANELLA, E. & COWARD, M. P. 2003. Structural framework. In: EVANS, D., GRAHAM, C., ARMOUR, A. & BATHURST, P. (eds.) *The Millennium Atlas: petroleum geology of the central and northern North Sea*. The Geological Society of London
- ZIEGLER, P. A. 1990. *Geological atlas of western and central Europe*, Shell Internationale Petroleum Maatschappij B.V.

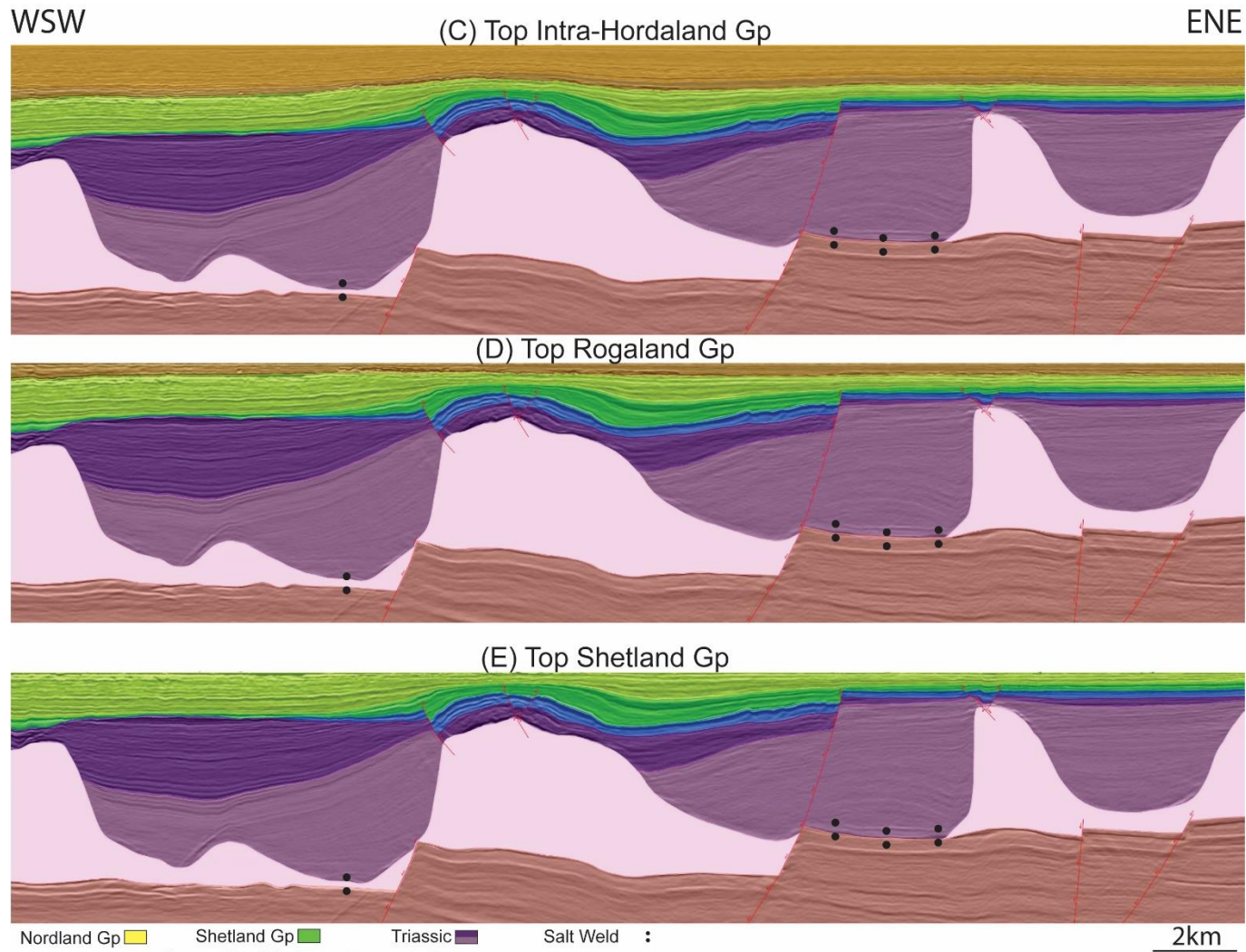
9 Appendix I



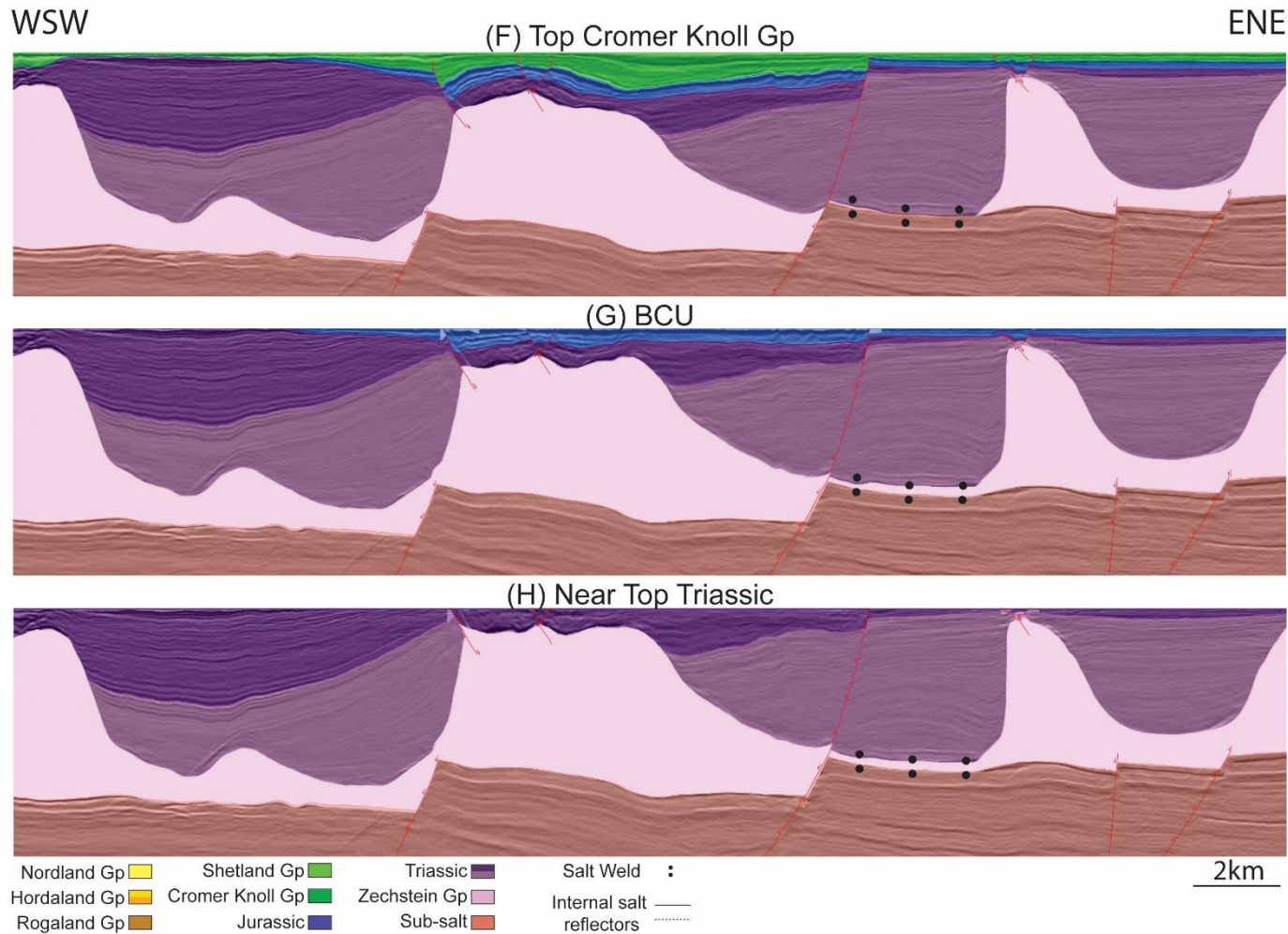
10 Appendix II



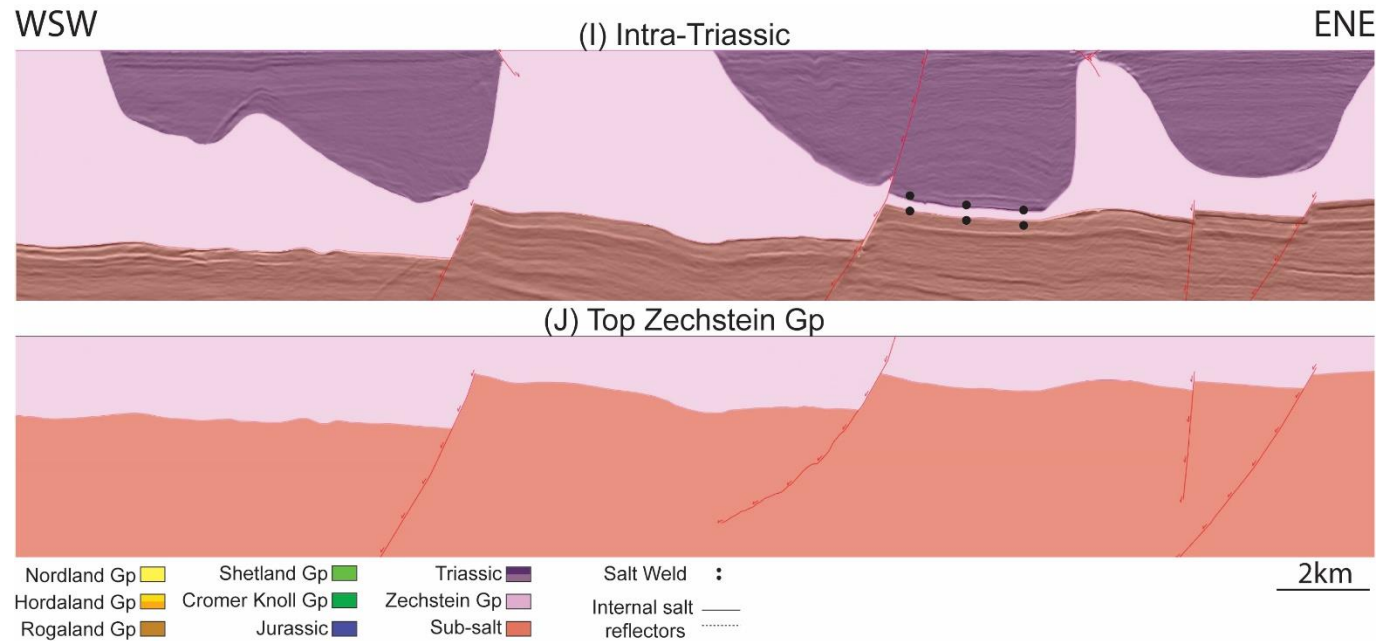
Restored Ula structure: (A) Present day geometries; and (B) Nordland group removed, underlying units are decompacted down to top Zechstein Group and flexural isostasy is accounted for.



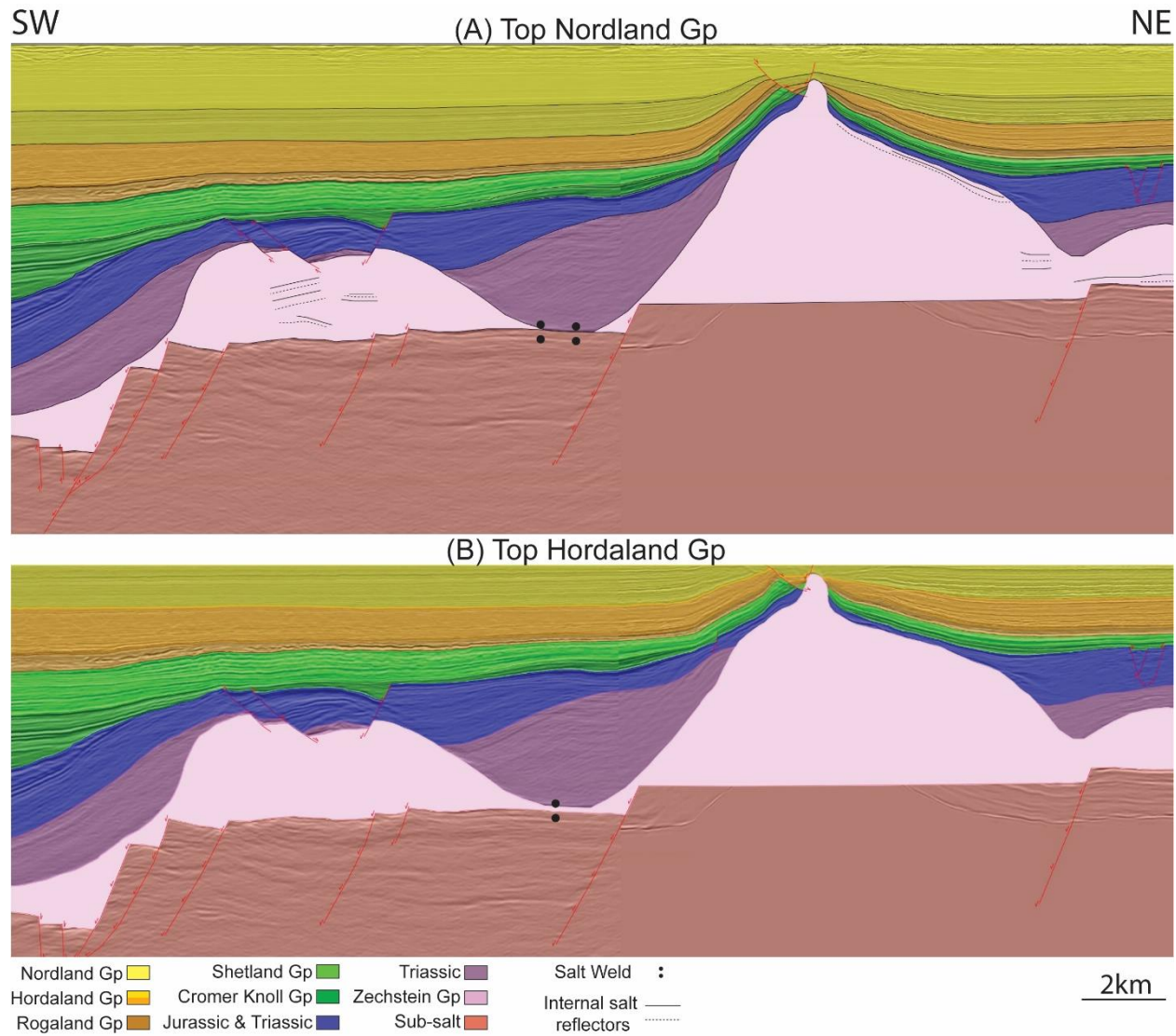
Restored Ula structure: (C) upper Hordaland Group removed, underlying units are decompacted down to top Zechstein Group, flexural isostasy is accounted for and beds are unfolded; (D) intra-Hordaland Group removed, underlying units are decompacted down to top Zechstein Group, flexural isostasy is accounted for and beds are unfolded; and (E) Rogaland Group removed, underlying units are decompacted down to top Zechstein Group, flexural isostasy is accounted for and beds are unfolded.



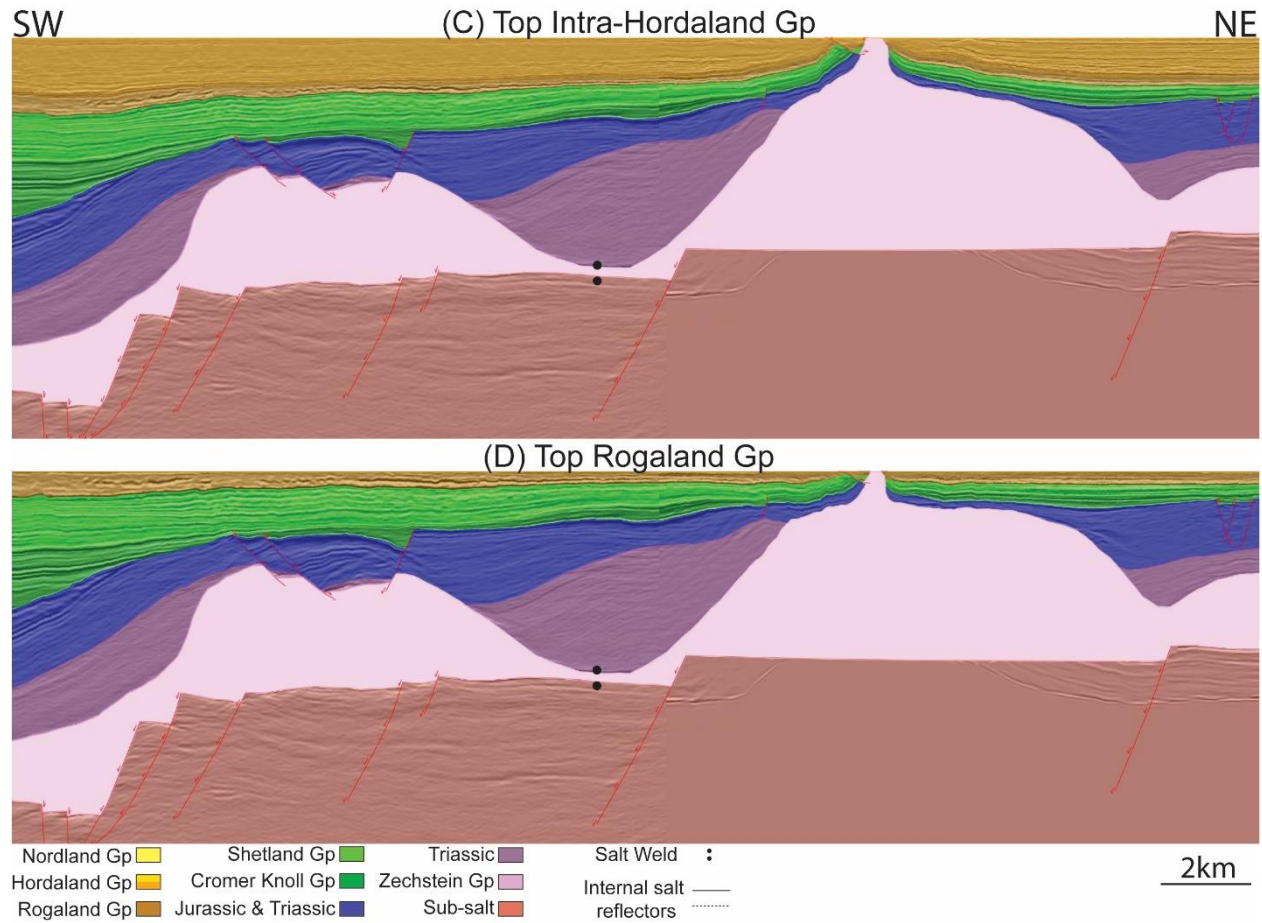
*Restored Ula structure. The hard-linked fault is restored using **simple shear** with a 60-degree angle, while supra-salt faults are restored using **elliptical fault flow**. (F) Shetland Group removed, underlying units are decompacted down to top Zechstein Group, flexural isostasy is accounted for and beds are unfolded; (G) Cromer Knoll Group removed, underlying units are decompacted down to top Zechstein Group, flexural isostasy is accounted for and beds are unfolded; and (H) Jurassic unit is removed, underlying units are decompacted down to top Zechstein Group, flexural isostasy is accounted for and beds are unfolded.*



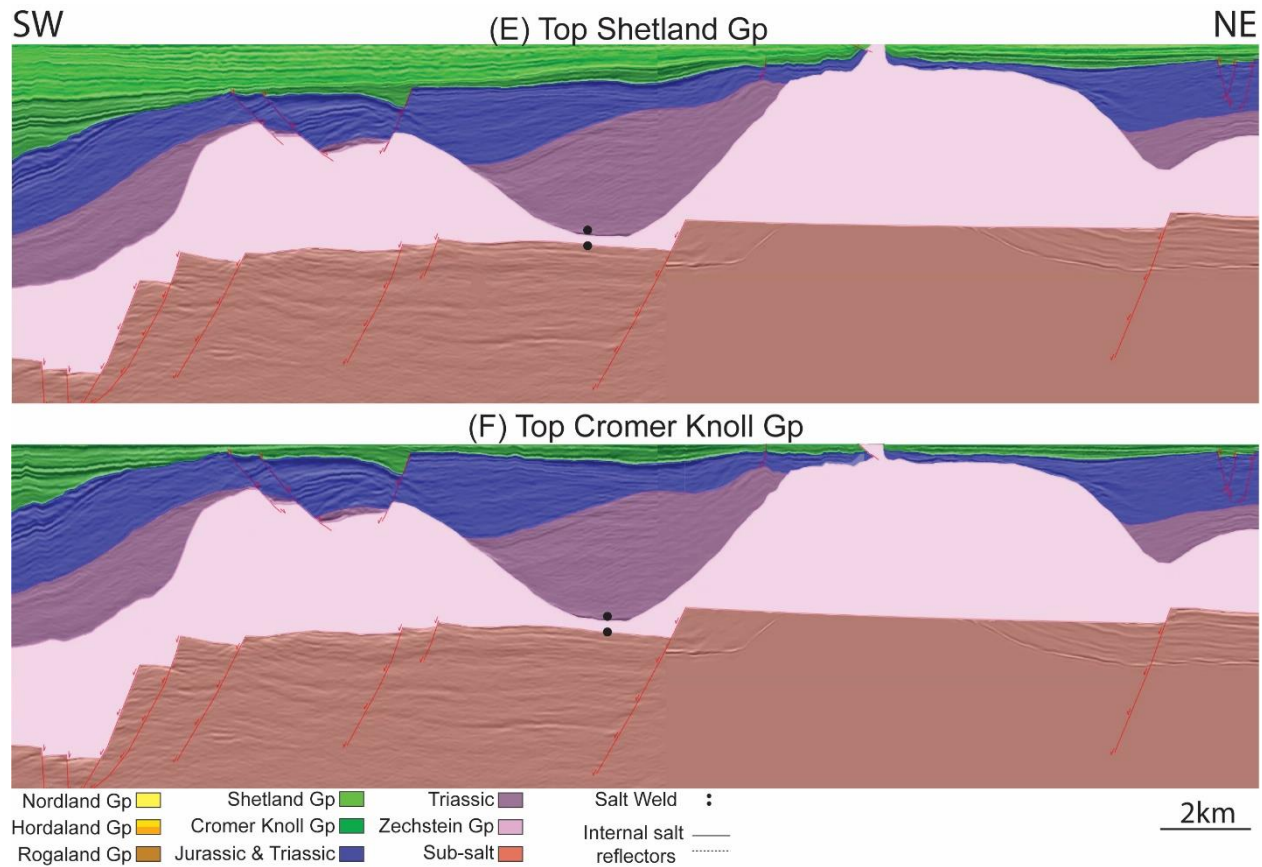
*Restored Ula structure. The hard-linked fault is restored using **simple shear** with a 60-degree angle, while supra-salt faults are restored using **elliptical fault flow**. (I) Upper Triassic is removed, underlying units are decompacted down to top Zechstein Group, flexural isostasy is accounted for and beds are unfolded; (J) Lower Triassic is removed. The final section has been made for illustrational purposes, where the underlying faults are kept fixed and the top Zechstein Group is flattened to a regional level which represents a conceptual Zechstein Group thickness (i.e. less than 2 km).*



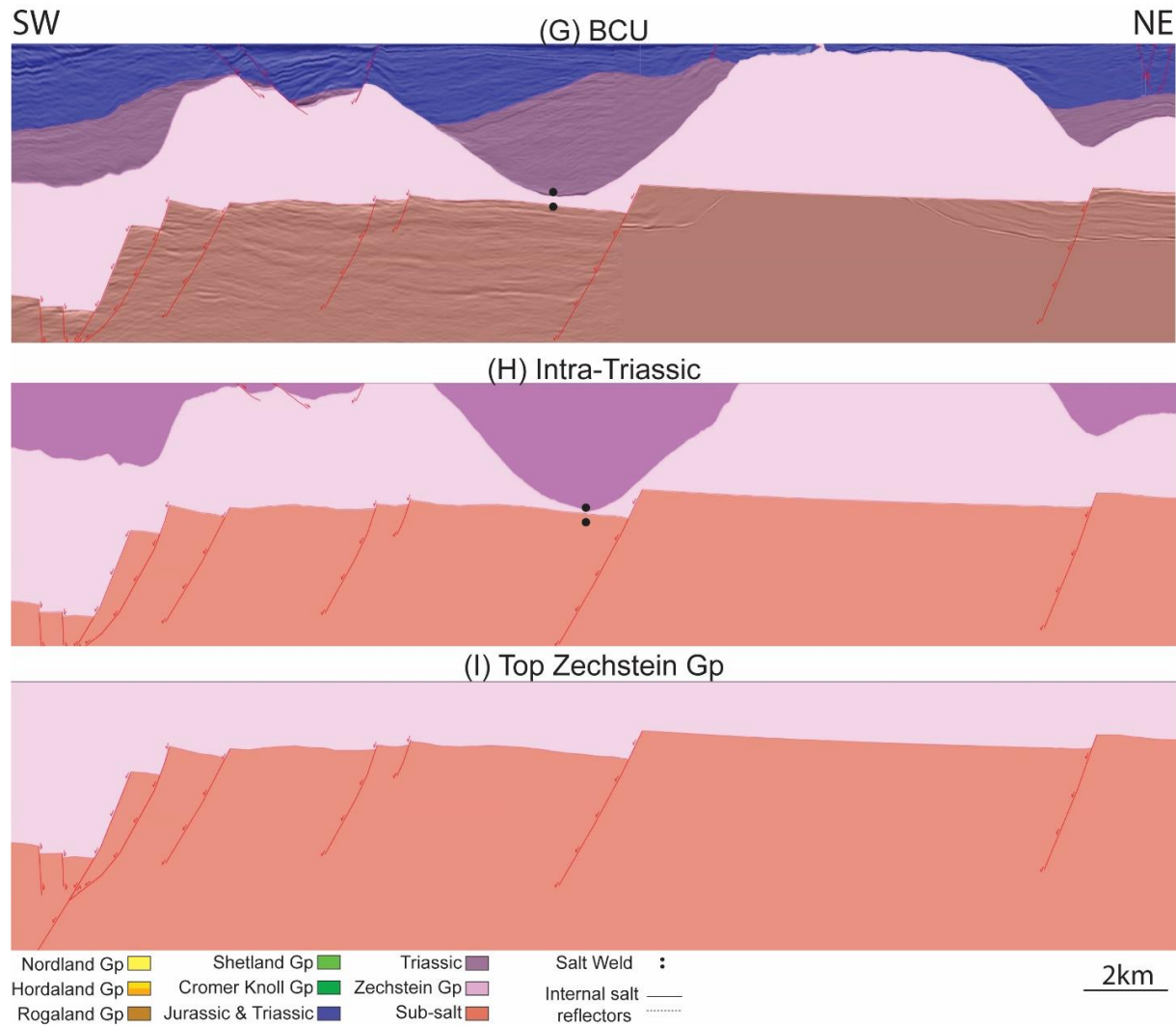
*Restored Oda structure. Supra-salt faults are restored using **elliptical fault flow**. (A) Present day geometries; and (B) Nordland group removed, underlying units are decompacted down to top Zechstein Group and flexural isostasy is accounted for.*



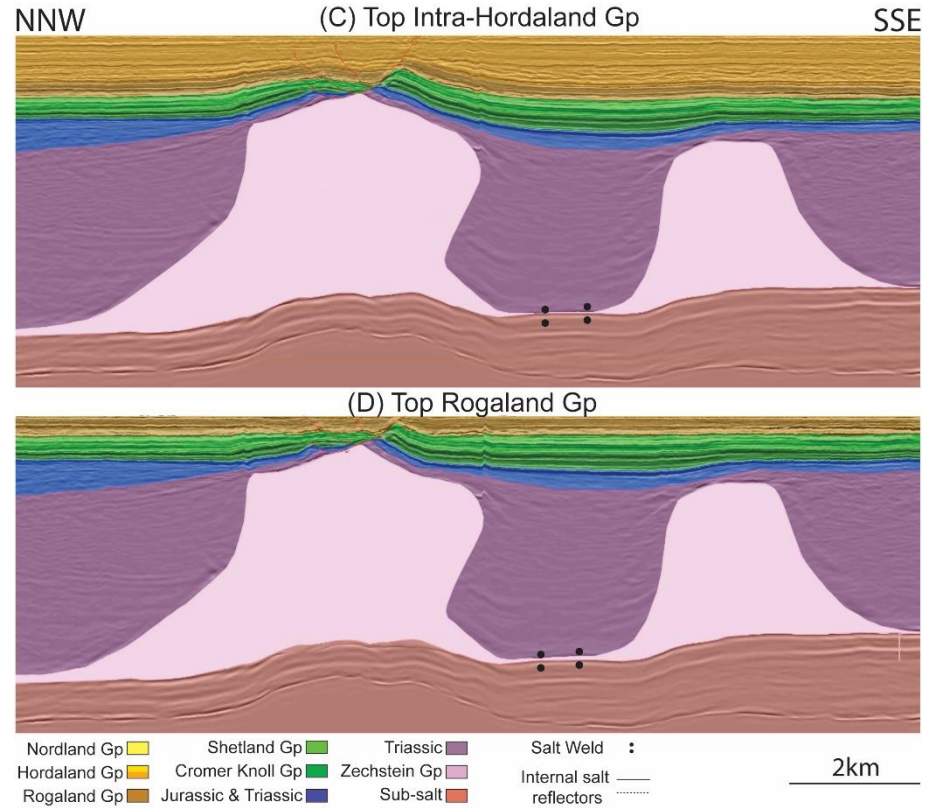
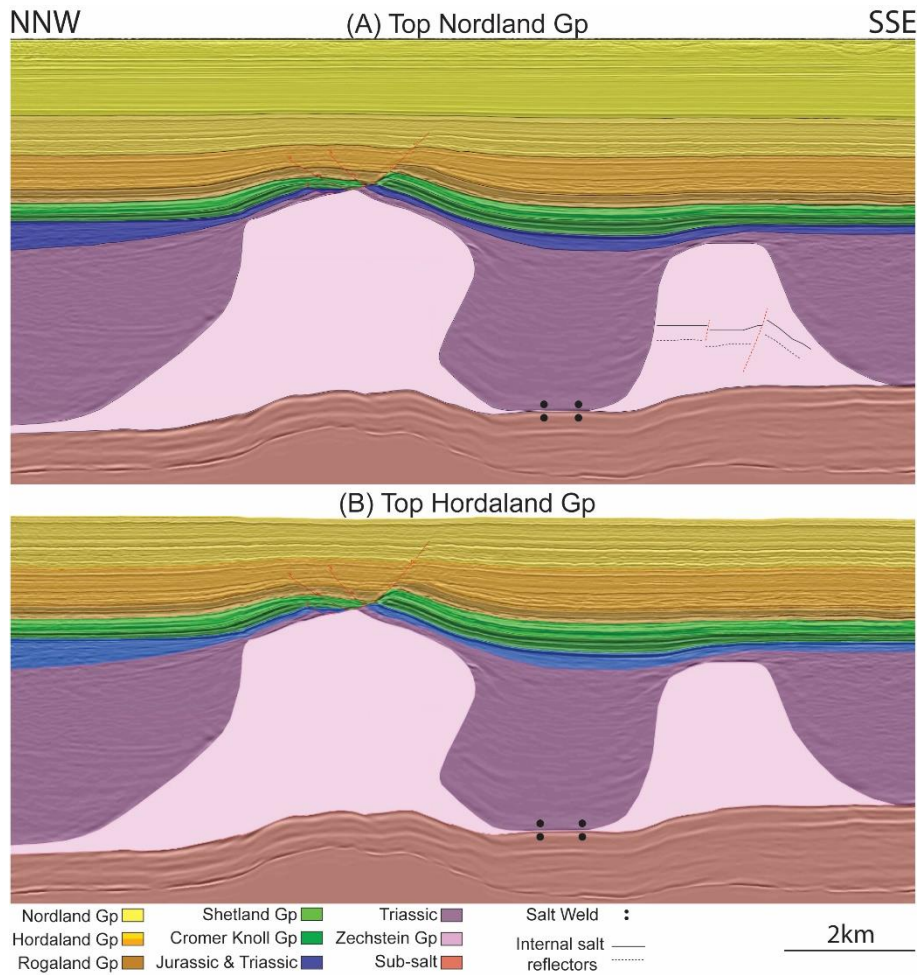
*Restored Oda structure. Supra-salt faults are restored using **elliptical fault flow**. (C) upper Hordaland Group removed, underlying units are decompacted down to top Zechstein Group, flexural isostasy is accounted for and beds are unfolded; and (D) intra-Hordaland Group removed, underlying units are decompacted down to top Zechstein Group, flexural isostasy is accounted for and beds are unfolded.*



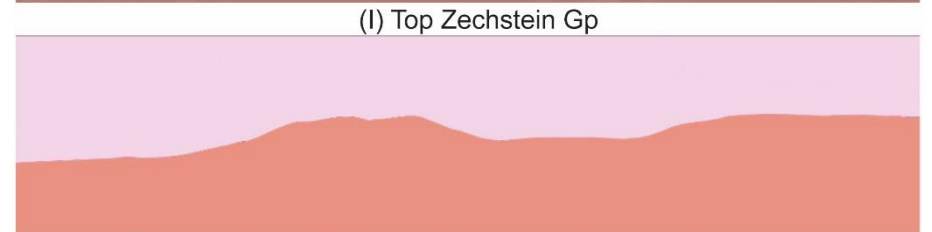
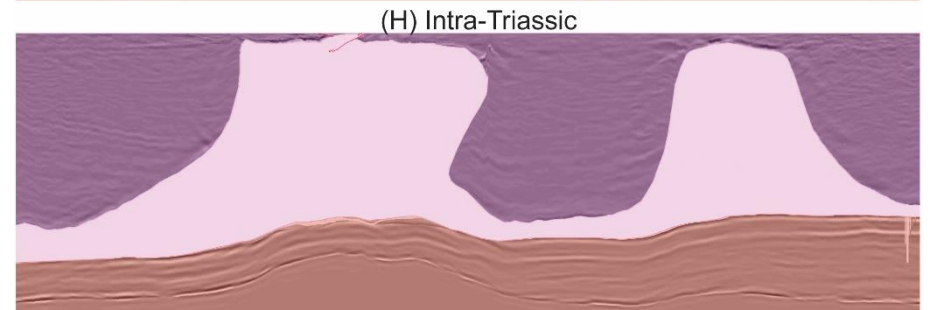
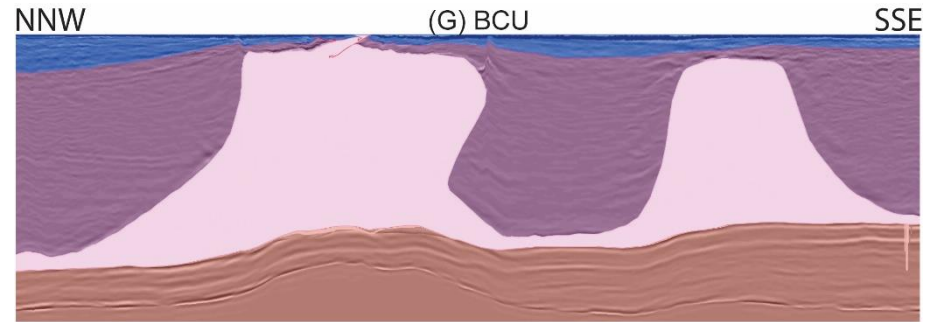
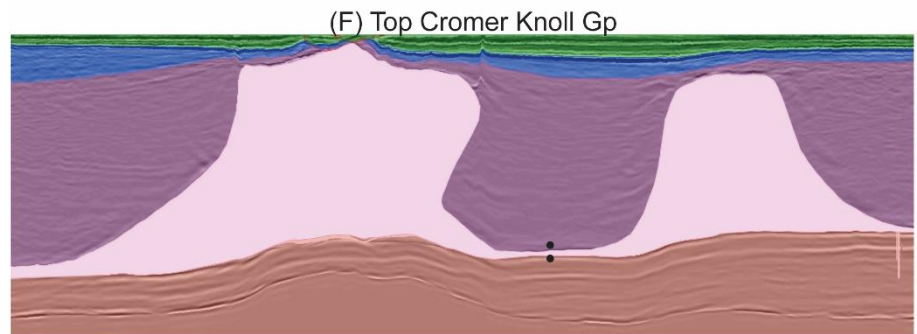
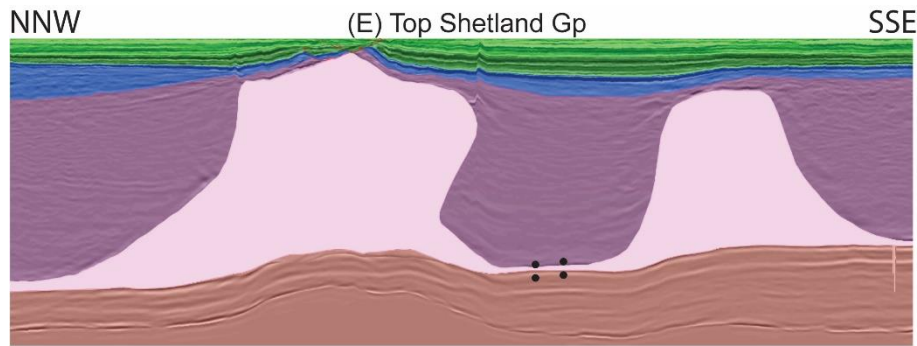
Restored Oda structure. Supra-salt faults are restored using **elliptical fault flow**. (E) Rogaland Group removed, underlying units are decompacted down to top Zechstein Group, flexural isostasy is accounted for and beds are unfolded; and (F) Shetland Group removed, underlying units are decompacted down to top Zechstein Group, flexural isostasy is accounted for and beds are unfolded.



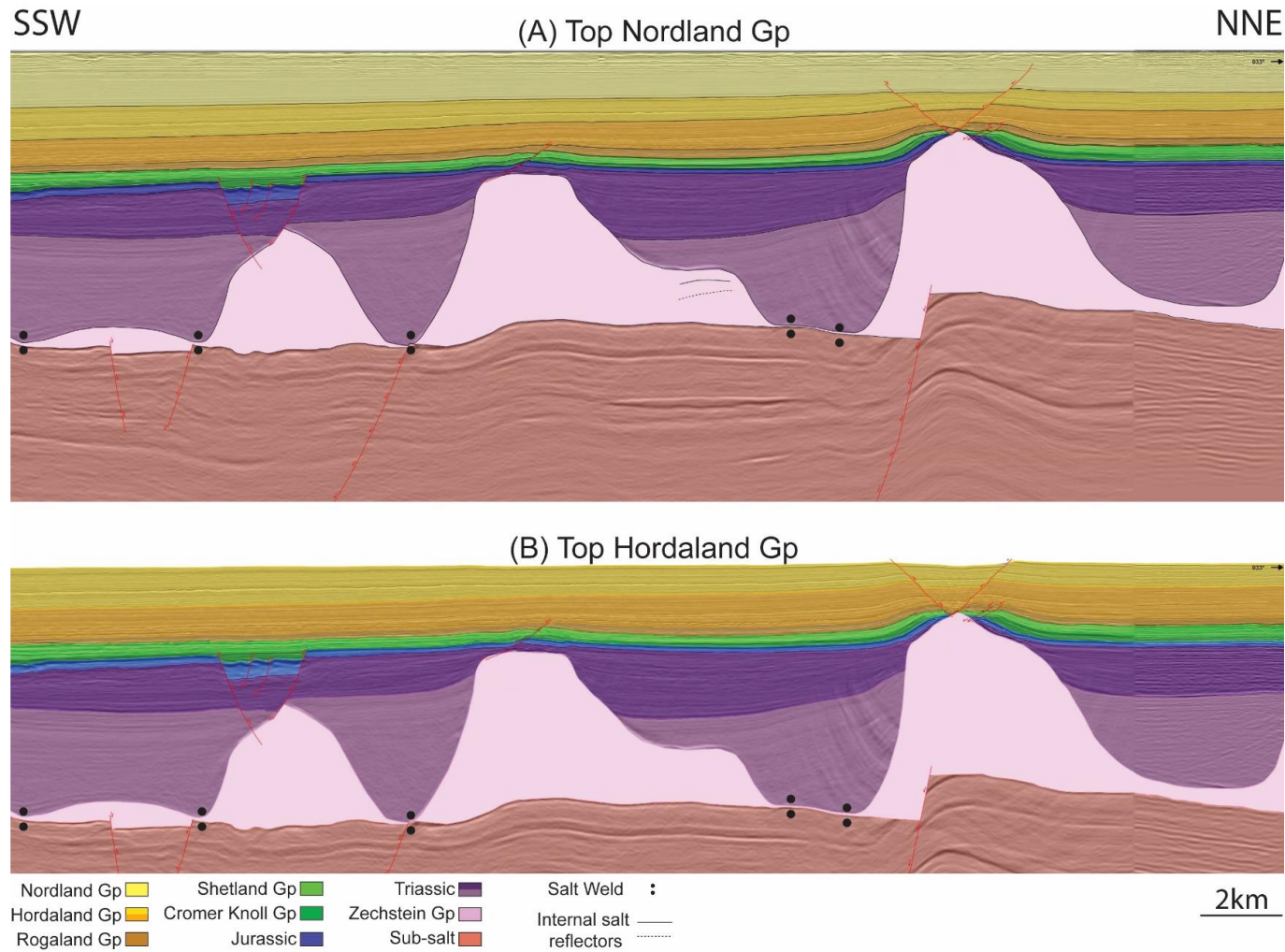
Restored Oda structure. Supra-salt faults are restored using **elliptical fault flow**. (G) Cromer Knoll Group removed, underlying units are decompacted down to top Zechstein Group, flexural isostasy is accounted for and beds are unfolded; (H) Jurassic and upper Triassic units are removed, underlying units are decompacted down to top Zechstein Group, flexural isostasy is accounted for and beds are unfolded; and (I) Lower Triassic is removed. The final section has been made for illustrational purposes, where the underlying faults are kept fixed and the top Zechstein Group is flattened to a regional level which represents a conceptual Zechstein Group thickness (i.e. less than 2 km, except for the hanging wall in the SW).



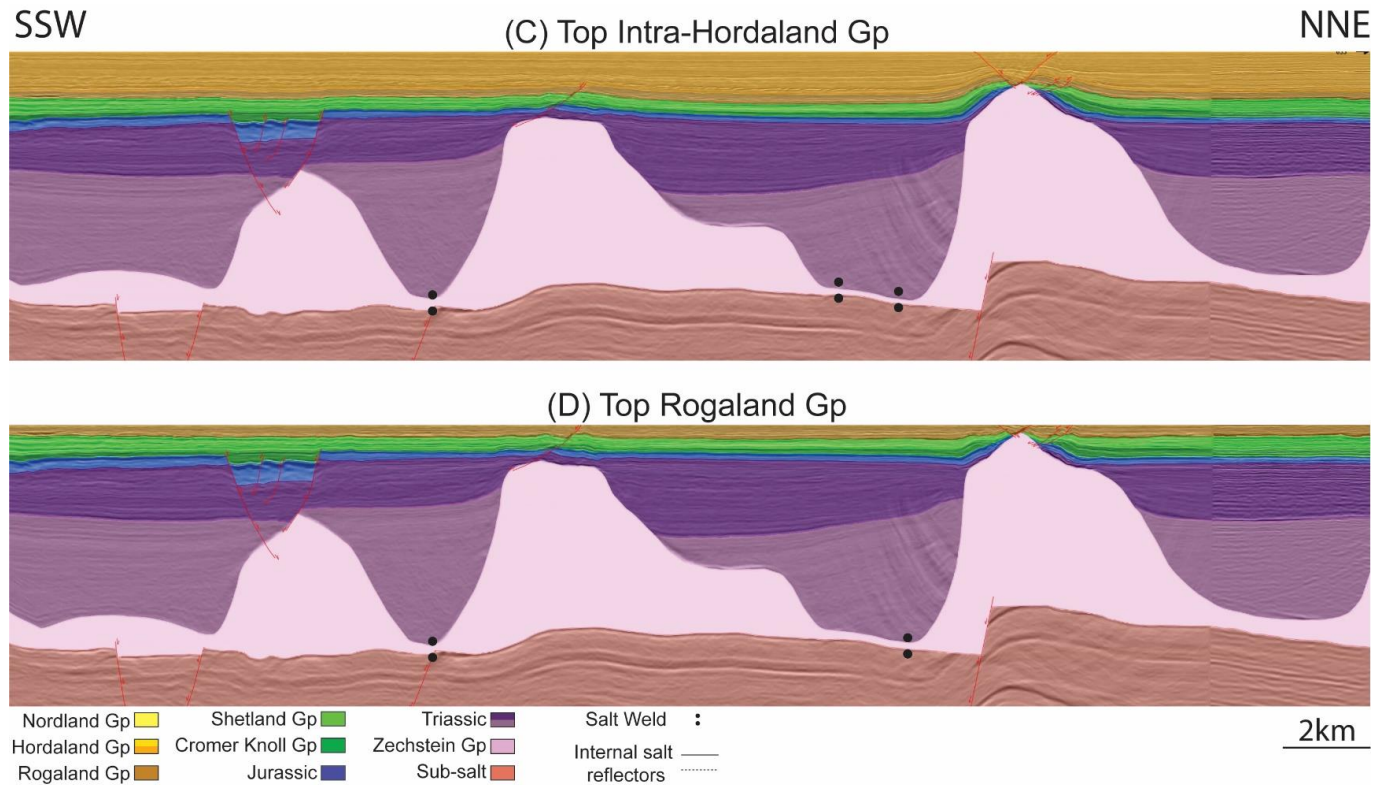
Restored NE-SW trending diapir. Supra-salt faults are restored using **elliptical fault flow**. (A) Present day geometries; (B) Nordland group removed, underlying units are decompactified down to top Zechstein Group and flexural isostasy is accounted for; (C) upper Hordaland Group removed, underlying units are decompactified down to top Zechstein Group, flexural isostasy is accounted for and beds are unfolded; and (D) intra-Hordaland Group removed, underlying units are decompactified down to top Zechstein Group, flexural isostasy is accounted for and beds are unfolded.



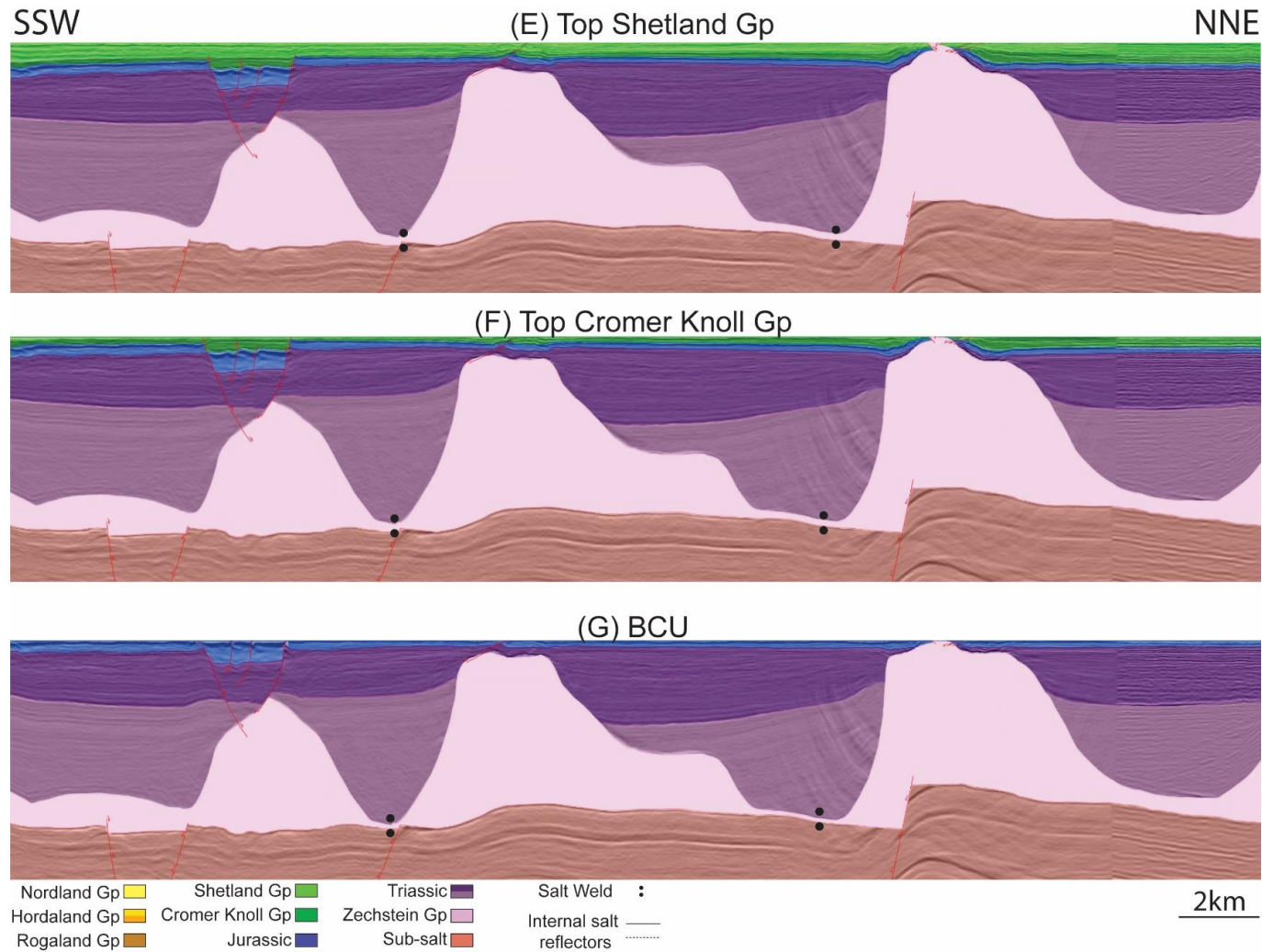
Restored NE-SW trending diapir. Supra-salt faults are restored using **elliptical fault flow**. (E) Rogaland Group removed, underlying units are decompacted down to top Zechstein Group, flexural isostasy is accounted for and beds are unfolded; (F) Shetland Group removed, underlying units are decompacted down to top Zechstein Group, flexural isostasy is accounted for and beds are unfolded; (G) Cromer Knoll Group removed, underlying units are decompacted down to top Zechstein Group, flexural isostasy is accounted for and beds are unfolded; (H) Jurassic and upper Triassic units are removed, underlying units are decompacted down to top Zechstein Group, flexural isostasy is accounted for and beds are unfolded; and (I) Lower Triassic is removed. The final section has been made for illustrational purposes, where the underlying faults are kept fixed and the top Zechstein Group is flattened to a regional level which represents a conceptual Zechstein Group thickness (i.e. less than 2 km).



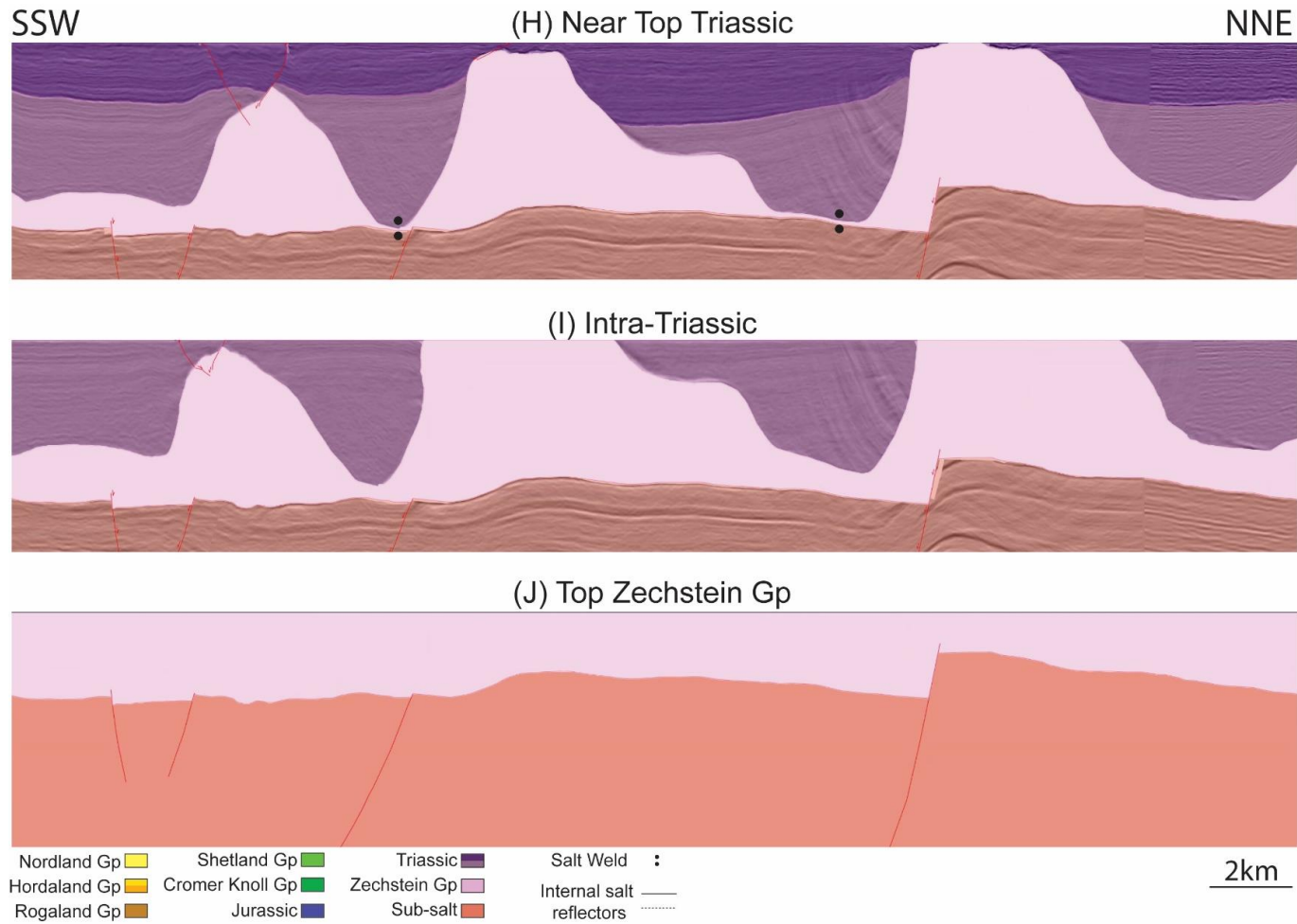
Restored NW-SE trending diapir. Supra-salt faults are restored using **elliptical fault flow**. (A) Present day geometries; and (B) Nordland group removed, underlying units are decompacted down to top Zechstein Group and flexural isostasy is accounted for.



*Restored NW-SE trending diapir. Supra-salt faults are restored using **elliptical fault flow**. (C) upper Hordaland Group removed, underlying units are decompacted down to top Zechstein Group, flexural isostasy is accounted for and beds are unfolded; and (D) intra-Hordaland Group removed, underlying units are decompacted down to top Zechstein Group, flexural isostasy is accounted for and beds are unfolded.*



Restored NW-SE trending diapir. Supra-salt faults are restored using **elliptical fault flow**. (E) Rogaland Group removed, underlying units are decompacted down to top Zechstein Group, flexural isostasy is accounted for and beds are unfolded; (F) Shetland Group removed, underlying units are decompacted down to top Zechstein Group, flexural isostasy is accounted for and beds are unfolded; and (G) Cromer Knoll Group removed, underlying units are decompacted down to top Zechstein Group, flexural isostasy is accounted for and beds are unfolded.



Restored NW-SE trending diapir. Supra-salt faults are restored using **elliptical fault flow**. (H) Jurassic unit is removed, underlying units are decompacted down to top Zechstein Group, flexural isostasy is accounted for and beds are unfolded; (I) Upper Triassic is removed, underlying units are decompacted down to top Zechstein Group, flexural isostasy is accounted for and beds are unfolded; and (J) Lower Triassic is removed. The final section has been made for illustrational purposes, where the underlying faults are kept fixed and the top Zechstein Group is flattened to a regional level which represents a conceptual Zechstein Group thickness (i.e. less than 2 km).